TW-0077
18 July 2002

HUMID AIR TURBINE CYCLE TECHNOLOGY DEVELOPMENT PROGRAM

TECHNICAL PROGRESS REPORT

FINAL REPORT

PERIOD OF PERFORMANCE: 30 SEPTEMBER 1996 THROUGH 28 FEBRUARY 2002

Prepared for
National Energy Technology Center
U.S. Department of Energy
AAD Document Control M/S 921-107
P.O. Box 10940
Pittsburgh, PA 15236

Prepared under
Contract DE-AC21-96MC33084

Prepared by
Pratt & Whitney
Advanced Engine Programs
400 Main Street
East Hartford, CT 06108

DISCLAMER NOTICE

THIS REPORT WAS PREPARED AS AN ACCOUNT OF WORK SPONSORED BY AN AGENCY OF THE U.S. GOVERNMENT. NEITHER THE U.S GOVERNMENT NOR ANY AGENCY THEREOF, NOR ANY OF THEIR EMPLOYEES, MAKES ANY WARRANTY, EXPRESS OF IMPLIED, OR ASSUMES ANY LEGAL LIABILITY OR RESPONSIBILITY FOR THE ACCURACY, COMPLETENESS, OR USEFULNESS OF ANY INFORMATION, APPARATUS, PRODUCT, OR PROCESS DISCLOSED, OR REPRESENTS THAT ITS USE WOULD NOT INFRINGE PRIVATELY-OWNED RIGHTS. REFERENCE HEREIN TO ANY SPECIFIC COMMERCIAL PRODUCT, PROCESS, OR SERVICE BY TRADE NAME, TRADEMARK, MANUFACTURER, OR OTHERWISE DOES NOT NECESSARILY CONSTITUTE OR IMPLY ITS ENDORSEMENT, RECOMMENDATION, OR FAVORING BY THE U.S. GOVERNMENT OR ANY AGENCY THEREOF. THE VIEWS AND OPINIONS OF AUTHORS EXPRESSED HEREIN DO NOT NECESSARILY STATE OR REFLECT THOSE OF THE U.S. GOVERNMENT OR ANY AGENCY THEREOF.

Published by Business Development Technical Writing

ABSTRACT

The Humid Air Turbine (HAT) Cycle Technology Development Program focused on obtaining HAT cycle combustor technology that will be the foundation of future products. The work carried out under the auspices of the HAT Program built on the extensive low emissions stationary gas turbine work performed in the past by Pratt & Whitney (P&W). This Program is an integral part of technology base development within the Advanced Turbine Systems Program at the Department of Energy (DOE) and its experiments stretched over 5 years. The goal of the project was to fill in technological data gaps in the development of the HAT cycle and identify a combustor configuration that would efficiently burn high moisture, high-pressure gaseous fuels with low emissions. The major emphasis will be on the development of kinetic data, computer modeling, and evaluations of combustor configurations.

The Program commenced during the 4th Quarter of 1996 and closed in the 4th Quarter of 2001. It teamed the National Energy Technology Laboratory (NETL) with P&W, the United Technologies Research Center (UTRC), and a subcontractor on-site at UTRC, kraftWork Systems Inc. The execution of the program started with bench-top experiments that were conducted at UTRC for extending kinetic mechanisms to HAT cycle temperature, pressure, and moisture conditions. The fundamental data generated in the bench-top experiments was incorporated into the analytical tools available at P&W to design the fuel injectors and combustors. The NETL then used the hardware to conduct combustion rig experiments to evaluate the performance of the combustion systems at elevated pressure and temperature conditions representative of the HAT cycle. The results were integrated into systems analysis done by kraftWork to verify that sufficient understanding of the technology had been achieved and that large-scale technological application and demonstration could be undertaken as follow-on activity. An optional program extended the experimental combustion evaluations to several specific technologies that can be used with HAT technology.

After 5 years of extensive research and development, P&W is pleased to report that the HAT Technology Development Program goals have been achieved. With 0 to 10 percent steam addition, emissions achieved during this program featured less than 8 ppm NO_x, less than 16 ppm CO, and unburned hydrocarbons corrected to 15 percent O_2 for an FT8 engine operating between 0° and 120°F with 65 to 100 percent power at any day.

CONTENTS

Section *Page*

ABSTRACT ii

EXECUTIVE SUMMARY xiii

1. EXPERIMENTAL 1-1

1.1 Task 101: Program Management Personnel 1-1

1.2 Task 102: Project Plan 1-2

1.3 Task 201: Kinetic Modeling and Fundamental Database Generation 1-2

1.4 Task 202: CFD Modeling of Nozzle and Combustor Performance 1-2

1.5 Task 203: NETL Combustion Evaluation Studies 1-3

1.6 Task 204: United Technologies Corporation Cost-Share Studies 1-3

1.7 Task 301: Cycle Analysis Support 1-5

1.8 Task 302: Performance Analysis of FT4000 Applications 1-5

1.9 Task 303: Performance Analysis of FT8 Applications 1-6

1.10 Task 401: Dual Fuel Nozzle 1-6

1.11 Task 402: Hybrid Combustor/Catalytic Nozzle 1-6

1.12 Task 403: Liner Evaluation 1-7

2. RESULTS AND DISCUSSION 2-1

2.1 Kinetic Modeling and Fundamental Database Generation 2-1
2.1.1 High Pressure Flat-Flame Burner Facility 2-1
2.1.2 High Pressure, High Temperature Turbulent Burner Facility 2-3
2.1.3 Solubility of Air in Water at Elevated Pressures 2-8
2.1.4 Chemical Kinetic Modeling 2-8
2.1.5 Schedule and Planned Activities 2-10

2.2 Role of Humidity and Unmixedness on NO_x Generated in a Gas Turbine 2-11
2.2.1 Modeling 2-11
2.2.2 Results 2-13

2.3 Pressure Effect on NO_x and CO Emissions in Industrial Gas Turbines 2-14
2.3.1 Experiments 2-16
2.3.2 Modeling 2-16
2.3.3 Results 2-19
2.3.4 Conclusions 2-23

2.4 An Experimental and Modeling Study of Humid Air Premixed Flames 2-23
2.4.1 Experiments 2-25
2.4.2 Modeling 2-26
2.4.3 Results and Discussion 2-27
2.4.4 Conclusions 2-31

Section ***Page***

2.5 NO_x Scaling Characteristics for Industrial Gas Turbine Fuel Injectors 2-32
2.5.1 Experimental Setup 2-33
2.5.2 Emissions Modeling 2-35
2.5.3 Results 2-35
2.5.4 Combustor Thermal Analysis 2-37
2.5.5 CONCLUSIONS 2-42
2.6 Cycle Definition: Analyses of HAT Cycle Systems 2-42
2.6.1 Summary 2-42
2.6.2 Introduction 2-42
2.6.3 HAT Cycle Basics 2-44
2.6.4 Baseline HAT Cycle 2-46
2.6.5 Alternative Configurations 2-50
2.6.6 Concluding Remarks 2-53
2.7 Humid Air NO_x Reduction Effect on Liquid Fuel Combustion 2-53
2.7.1 Experimental Technique 2-54
2.7.2 Results and Discussion 2-56
2.7.3 Conclusions 2-59
2.8 Tests of Hybrid Combustor 2-59
2.8.1 Component Design and Hardware 2-60
2.8.2 Test Description 2-62
2.8.3 Experimental Considerations 2-63
2.8.4 Flow Control 2-63
2.8.5 Results 2-64
2.8.6 Component Inspection 2-70
2.8.7 Summary 2-72
2.8.8 Recommendations 2-72
2.9 Humid Air Combustion With a Convectively-Cooled Liner 2-73
2.9.1 Experimental Technique 2-73
2.9.2 Results and Discussion 2-74
2.9.3 Conclusions 2-78

3. CONCLUSION 3-1

4. REFERENCES 4-1

FIGURES

Figure		*Page*
1-1.	Program Management Organization	1-1
1-2.	Schematic of the Tangential Air Entry Nozzle Tested in the NETL Facilities	1-4
1-3.	NO_x Emissions Levels and Pressure Pulsation Levels from Engine Testing Shown as a Function of Power Setting for the Nozzle Features Evaluated at the NETL.	1-5
2-1.	Flat Flame Burner Assembly	2-1
2-2.	Schematic of High-Pressure Flat Flame Burner Combustor	2-2
2-3.	High-Pressure Flat Flame Combustor	2-3
2-4.	Radial Temperature Profile at 5 Atm and $\phi = 1.3$	2-3
2-5.	Radial Temperature Profiles in Flat Flame Burner at Various Pressures	2-3
2-6.	Schematic of High Temperature, High Pressure Combustion Apparatus	2-4
2-7.	Photograph of the High-Temperature Combustion Facility	2-5
2-8.	Schematic of Partially Premixed Burner System	2-5
2-9.	Burner Configuration Used in High-Pressure Combustion Facility	2-5
2-10.	NO_x Emissions as a Function of Flame Temperature at 10 Atm	2-6
2-11.	NO_x Emissions as a Function of Flame Temperature at 20 Atm	2-6
2-12.	NO_x Emission as a Function of Flame Temperature at 30 Atm	2-6
2-13.	NO_x Emissions as a Function of Flame Temperature at 20 Atm	2-7
2-14.	Effect of Premixing on NO_x Levels at 20 Atm	2-7
2-15.	NO_x Production in PSR at 20 Atm (GRI-MECH 2.11)	2-7
2-16.	NO_x Predictions in PSR and Data Versus Flame Temperature	2-7
2-17.	Solubility of Nitrogen in Water at High Pressure	2-8
2-18.	PSR Temperature as a Function of τ	2 9
2-19.	Corrected NOx as a Function of τ	2 9
2-20.	Corrected CO as a Function of τ	2 9
2-21.	Task 201 Spending Plan	2-10
2-22.	Task 201 Program Plan Schedule	2-10
2-23.	A Schematic of the Single PSR, a PSR Followed By 25 Smaller PSR, and a PSR Reactor Network Used to Model the Flame	2-12
2-24.	Predicted NO_x Emissions as a Function of ϕ and a Gaussian Distribution About $\phi = 0.6$ at Different Standard Deviation (σ)	2-13
2-25.	Comparison of the NO_x Formation With a Single PSR and Network PSR Under Dry and Humid Conditions	2-13

Figure ***Page***

2-26. Comparison of the NO_x Formation at Different Levels of Unmixedness for Dry and Humid Flames at 1 Atm and 13.6 Atm and at a T_{adb} of 1820K 2-13

2-27. Comparison of the NO_x Formation in the Network PSR at Different Unmixedness Number (U) for Flames at 13.6 Atm, T_3 = 730K, T_{adb} of 1820K, and Different Moisture Conditions 2-14

2-28. Comparison of the NO_x Formation in the Network PSR at Different Levels of Unmixedness for Flames at 13.6 Atm, T_3 = 730K, and Different Moisture Contents 2-14

2-29. Schematic of an Earlier Aerodynamic Nozzle 2-16

2-30. Modified Centerbody for the Tangential Entry Nozzle 2-16

2-31. Schematic of the Centerbody End Detail for the Axial Nozzles 2-16

2-32. A Schematic of the Experimental Setup 2-17

2-33. NO_x Emissions at Different Psi Levels 2-17

2-34. Effect of Pressure on NO_x Emissions as a Function of Equivalence Ratio 2-17

2-35. NOx Predictions at Different Pressures Using a Single PSR 2-18

2-36. Schematic of the PSR Reactor Network Used To Model the Flow Distribution Varied With Pressure 2-18

2-37. Schematic of the PSR Reactor Network Used To Predict NOx Emissions at Different Pressures 2-18

2-38. NO_x Predictions for a Tangential Entry Nozzle 2-21

2-39. NO_x Model Predictions for an Axial Nozzle Using the Modified Version of the PSR Network Shown in Figure 2-37 2-21

2-40. Effect of Pressure on the Different NO_x Formation Pathways 2-22

2-41. CO Predictions (Lines) Versus Experimental Data (Symbols) for the Tangential Entry Nozzle 2-22

2-42. CO Predictions (Lines) Versus Experimental Data (Symbols) for the Axial Nozzle 2-22

2-43. A Schematic of the HAT Cycle 2-24

2-44. A Schematic of the Experimental Setup 2-25

2-45. A Schematic of the PSR Reactor Network Used To Model the Flame 2-26

2-46. Comparison Between Measured and Computed NO_x at 200 Psi at Different Pilot Levels 2-27

2-47. Comparison Between Measured and Computed CO at 200 Psi at Different Pilot Levels 2-27

2-48. Comparison Between Measured and Computed NO_x for a 5 Percent Side Pilot Flame at 200 Psi for Different Steam Loading 2-28

2-49. Comparison Between Measured and Computed CO for a 5 Percent Side Pilot Flame at 200 Psi for Different Steam Loading 2-28

2-50. Comparison Between Measured and Computed NO_x for a 5 Percent Side Pilot Flame at 200 Psi for Different Steam Loading 2-29

2-51. Comparison Between Measured and Computed CO for a 5 Percent Side Pilot Flame at 200 Psi for Different Steam Loading 2-29

Figure ***Page***

2-52. Influence of Different Pathways on NO_x Formation for a Flame With a 0 Percent Side Pilot and 0 Percent Steam 2-30

2-53. Influence of Different Pathways on NO_x Formation for a Flame With a 0 Percent Side Pilot and 15 Percent Steam 2-30

2-54. Influence of Different Pathways on NO_x Formation for a Flame With a 5 Percent Side Pilot and 0 Percent Steam 2-31

2-55. Influence of Different Pathways on NO_x Formation for a Flame With a 5 Percent Side Pilot and 15 Percent Steam 2-31

2-56. Schematic of an Earlier Aerodynamic Nozzle 2-33

2-57. Schematic of the Centerbody End Detail 2-34

2-58. Schematic of the Combustion Test Facility 2-34

2-59. NO_x Versus Flame Temperature Under Nonpiloting Conditions 2-36

2-60. NO_x Versus Flame Temperature Under Piloting Conditions 2-36

2-61. Nozzle Tip Temperature Versus Flame Temperature 2-37

2-62. T_{tip} Predictions from Combustion Flame Temperature Increases 2-38

2-63. CO Emissions for Nonpiloting Data and Expected Trends Under the Flame Temperature Increases 2-38

2-64. Initial PSR Network for Combustor Modeling 2-40

2-65. Final PSR Network To Assess Mixing Nonuniformity 2-40

2-66. Final PSR Network Modeling Comparison With Nonpiloting Experimental Data 2-41

2-67. Final PSR Network Modeling Comparison With Piloting Experimental Data 2-41

2-68. Effects of the Three Mechanisms 2-42

2-69. Simplified HAT Cycle Schematic 2-44

2-70. Combined Cycle 2-44

2-71. Intercooled Gas Turbine 2-45

2-72. Recuperated Gas Turbine 2-45

2-73. Detailed HAT Cycle Schematic 2-45

2-74. Parametric Performance Analysis of FT4000 I/C HAT Cycle 2-47

2-75. Efficiency as a Function of Moisture Addition 2-48

2-76. Specific Power as a Function of Moisture Added 2-48

2-77. Efficiency as a Function of Combustor Exit Temperature 2-48

2-78. Output Power Versus Moisture Addition 2-48

2-79. Sketch of Proposed Convectively Cooled Canted Combustor 2-49

2-80. Limitation Set By Gas Turbine Area 2-49

2-81. Effect of Errors in Turbine Cooling Flow on Performance 2-49

Figure *Page*

2-82. Predicted NO_x Emission for 15 Percent Moisture Fraction 2-50
2-83. Simple Cycle HAT 2-51
2-84. FT4000 Simple Cycle HAT Parametric Performance 2-51
2-85. FT8 Simple Cycle HAT Performance 2-52
2-86. FT8 I/C HAT Performance 2-52
2-87. FT8 HAT Efficiency as a Function of Added Moisture 2-52
2-88. FT8 HAT Specific Power as a Function of Added Moisture 2-52
2-89. A Typical Diagram of the HAT Cycle 2-53
2-90. Diagram of Axial Swirler Dual Fuel Nozzle 2-55
2-91. Macrolaminate Multipoint Liquid Fuel Injector 2-55
2-92. Comparison of Measured NO_x and CO of Diesel Fuel Combustion Between 50 Psia and 100 Psia Dry Cases (T_{air} 860ºF and 4 Percent Centerbody Gas Fuel) 2-56
2-93. Comparison of Measured NO_x and CO of Diesel Fuel Combustion at Different Equivalence Ratios Between Dry and 10 Percent Steam Cases at 100 Psia 2-57
2-94. Adiabatic Flame Temperature (ºF) 2-58
2-95. Schematic of Hybrid Combustion Integrated in a Gas Turbine 2-60
2-96. Cut-Away Isometric View of the Hybrid Combustor Installed as a Pilot in the TEN Burner 2-60
2-97. Schematic Side View of Catalytic Reactor/Heat Exchanger With Thermocouple Locations Denoted 2-61
2-98. Photograph of Hollow Nosecone and Components of Hybrid Burner 2-61
2-99. Separated Components of the Hybrid Burner 2-62
2-100. Separated Components of the Hybrid Burner 2-62
2-101. Exit View of the CRHX 2-62
2-102. Entrance View of the CRHX 2-62
2-103. Initial Catalyst Lightoff 2-64
2-104. Blowup of Initial Catalyst Lightoff 2-65
2-105. Effect of Pilot Level and Catalyst on NO_x Emissions 2-66
2-106. Effect of Catalyst Pilot Level on NO_x and CO Emissions and Catalyst Temperature 2-67
2-107. Incremental NO_x Emissions from the Pilot 2-67
2-108. Effect of Pilot Level and Catalyst on NO_x Emissions 2-68
2-109. Effect of Catalyst, Pilot Level, and Steam on NO_x Emissions 2-68
2-110. Effect of Pressure on NO_x Emissions With and Without the Pilot 2-68
2-111. Effect of Catalyst and Pilot Level on CO Emissions 2-68
2-112. Effect of Pilot Level and Catalyst on CO Emissions 2-69
2-113. Effect of Pilot Level and Catalyst on CO Emissions 2-69

Figure ***Page***

2-114. Effect of Pressure and Piloting on CO Emissions 2-69
2-115. Effect of Catalyst, Pilot Level, and Steam on NO_x Emissions 2-70
2-116. Effect of Catalyst, Pilot Level, and Steam on CO Emissions 2-70
2-117. Effect of Steam Addition and Piloting on NO_x Emissions 2-70
2-118. Effect of Steam Addition and Piloting on CO Emissions 2-70
2-119. Photograph of Nosecone After Testing 2-71
2-120. Thermal Stress Observed at TC Welds (Endcap) 2-71
2-121. Thermal Stress Observed at TC Welds (Sidewalls) 2-71
2-122. Discolored CRHX After Tests 2-71
2-123. Discolored CRHX After Tests 2-71
2-124. Test-Warped Plates 2-72
2-125. A Diagram of the Convectively-Cooled Liner 2-73
2-126. Cooled Liner Versus Refractory Liner for the Axial Nozzle 2-74
2-127. Cooled Liner Versus Refractory Liner for the TEN 2-75
2-128. Axial Nozzle Versus TEN for the Convectively-Cooled Liner 2-75
2-129. Inlet Air Temperature Effect for Convectively-Cooled Liner With TEN 2-76
2-130. Inlet Air Temperature Effect for Convectively-Cooled Liner With TEN 2-76
2-131. Pressure Effect for Convectively-Cooled Liner With Axial Nozzle 2-76
2-132. Pilot Effect for Convectively-Cooled Liner With Axial Nozzle 2-76
2-133. Steam Effect for Convectively-Cooled Liner With Axial Nozzle 2-77
2-134. Steam Effect for Convectively-Cooled Liner With Axial Nozzle 2-77

TABLES

Table *Page*

2-2. Distribution of Fuel in Reactors 1 to 5 in the Network Shown in Figure 2-37 2-19
2-1. Distribution of Fuel and Air in the Network for the Two Nozzles Shown in Figure 2-36 2-19
2-3. Nozzle/Combustor Configurations 2-34
2-4. Operating Conditions 2-35
2-5. Initial PSR Network Fuel and Air Distributions 2-39
2-6. Final PSR Modeling Fuel Distributions 2-40
2-7. FT4000 Intercooler Characteristics 2-46
2-8. Baseline HAT FT4000 Intercooler 2-47
2-9. Performance of the 3100°F HAT 2-50
2-10. Performance of the Simple Cycle HAT 2-51
2-11. Performance of FT8-Based Systems 2-52
2-12. Fractional Mass Flow Splits for Air 2-64

Acronyms

Numerics

3-D	Three-Dimensional

A

ASME	American Society of Mechanical Engineers
ATS	Advanced Turbine System

C

CFD	Computational Fluid Dynamics
CRHX	Catalytic Reactor/Heat Exchanger

D

DOE	Department of Energy

G

GRI	Gas Research Institute

H

HAT	Humid Air Turbine
HRSG	Heat Recovery Steam Generator

I

I/C	Intercooler
ICAD	Intercooler Aeroderivative

L

LECTR	Low Emissions Combustor Test and Research
LHV	Lower Heating Value

N

NETL	National Energy Technology Laboratory
NIST	National Institute of Standards and Technology

O

OPR	Overall Pressure Ratio

Acronyms

P

P&W	Pratt & Whitney
PFR	Plug Flow Reactor
PSR	Perfectly Stirred Reaction

S

SLA	Stereolithographic
SOAPP	State-of-the-Art Performance Program

T

TC	Thermocouple Bead
TEN	Tangential Entry Nozzle
Tflame	Flame Temperature

U

UHC	Unburned Hydrocarbons
UTC	United Technologies Corporation
UTRC	United Technologies Research Center

EXECUTIVE SUMMARY

The HAT Cycle Technology Development Program focused on obtaining HAT cycle combustor technology that will be the foundation of future products. The work carried out under the auspices of the HAT Program built on the extensive low emissions stationary gas turbine performed in the past by P&W. This Program is an integral part of technology base development within the Advanced Turbine Systems Program at the Department of Energy (DOE) and its experiments stretched over 5 years. The goal of the project is to fill in technological data gaps in the development of the HAT cycle and to identify a combustor configuration that will efficiently burn high moisture, high-pressure gaseous fuels with low emissions.The major emphasis will be on the development of kinetic data, computer modeling, and evaluations of combustor configurations.

The HAT Cycle Program commenced in the 4th Quarter of 1996 and finished in the 4th Quarter of 2001. It teamed the NETL with P&W, UTRC, and a subcontractor on-site at UTRC, kraftWork Systems Inc. The execution of the program started with bench-top experiments conducted at UTRC to extend kinetic mechanisms to the HAT cycle temperature, pressure, and moisture conditions. The fundamental data generated in the bench-top experiments were incorporated into the analytical tools available at P&W to design the fuel injectors and combustors. The NETL then used the hardware to conduct combustion rig experiments to evaluate the performance of the combustion systems at elevated pressure and temperature conditions representative of the HAT cycle. The results were integrated into systems analysis done by kraftWork to verify that sufficient understanding of the technology had been achieved and that large-scale technological application and demonstration could be undertaken as follow-on activity. An optional program extended the experimental combustion evaluations to several specific technologies that can be used with HAT technology.

After 5 years of extensive research and development, P&W can report that HAT Cycle Technology Development Program goals have been achieved. With 0 to 10 percent steam addition, emissions achieved during this program featured less than 8 ppm NO_x, less than 16 ppm CO, and unburned hydrocarbons corrected to 15 percent O_2 for an FT8 engine operating between 0° and 120°F with 65 to 100 percent power at any day.

1. EXPERIMENTAL

1.1 TASK 101: PROGRAM MANAGEMENT PERSONNEL

This task encompassed the overall management of the HAT Cycle Development contract. Dr. William H. Day had primary responsibility for this task. The day-to-day management of this task was carried out by Marc C. Lamoureux using input from Technical Task Managers A. J. DeMarco (Business Manager), and Leigh Fournier (Contract Administrator). The organization of the Program Management is shown below in Figure 1-1.

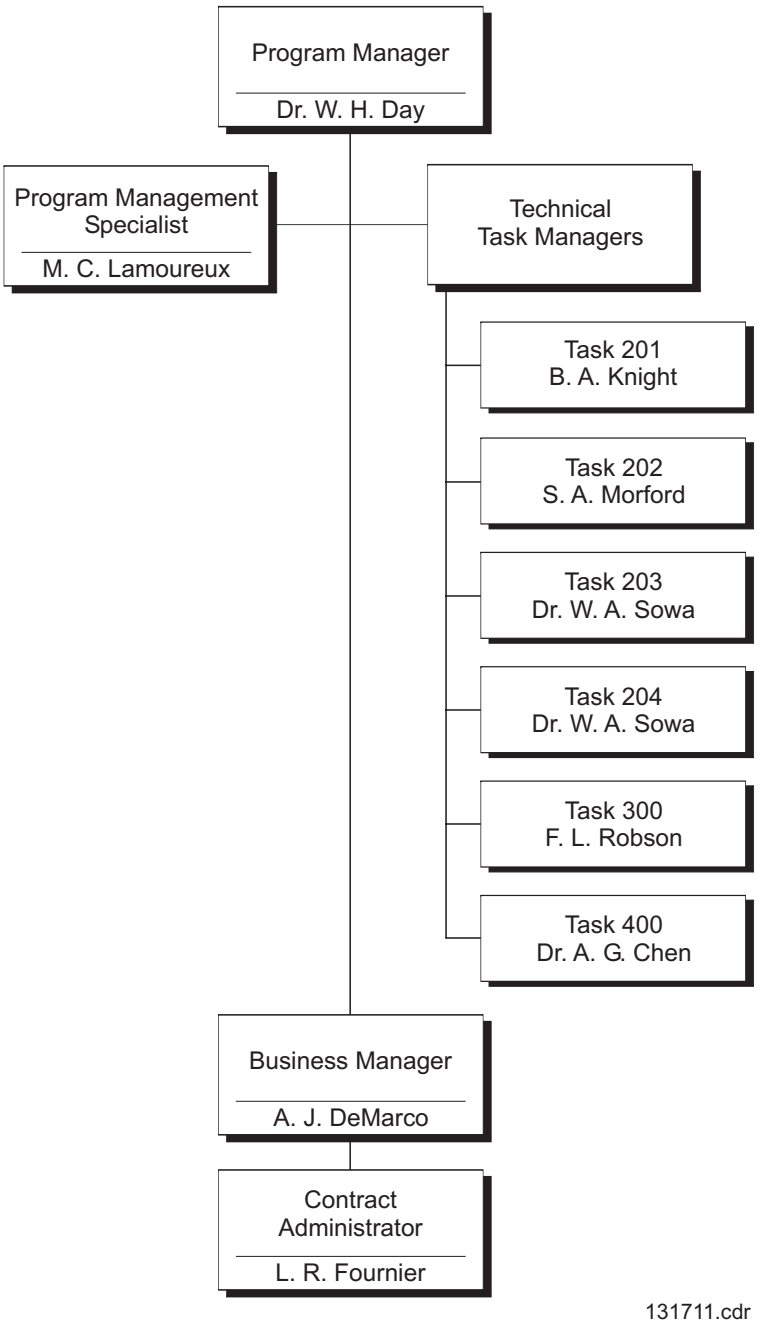

Figure 1-1. Program Management Organization

1.2 TASK 102: PROJECT PLAN

The submittal of a project plan was required by the HAT Program contract first, as a part of the proposal, and later, as an update after the program award. This requirement was fulfilled and supported by the same Program Management organization featured in Figure 1-1.

1.3 TASK 201: KINETIC MODELING AND FUNDAMENTAL DATABASE GENERATION

The objectives of Task 201 were to conduct bench top experiments and undertake kinetic modeling studies to define the effects of high water vapor content in air on the flame stability and emissions in HAT cycle combustion systems burning natural gas. The effects of temperature, pressure, fuel composition, and H_2O content on CO, NO_x, and UHC production, flame stability, and ignition were to be defined. Kinetic mechanisms were to be evaluated and modified as necessary to accurately describe the experimental results. Validated kinetic mechanisms were to be evolved into reduced reaction sets for integration into computational fluid dynamics (CFD) codes. Ultimately, the results of the small-scale combustion experiments and kinetic modeling were to be used to guide the design of a full-scale nozzle and combustor.

This task was conducted under the supervision of Brian Knight and was successfully completed by September 1998. As a result of this task, publications were submitted to the American Society of Mechanical Engineers (ASME) and the joint meeting of the U.S. section of the Combustion Institute.

Brief conclusions from the experiments include:

1. Excellent agreement between the measured and modeled NO_x (5 to 10 percent) was obtained. Trends of added moisture reducing NO_x and the effects of equivalence ratio and piloting level were well predicted.
2. The CO predictions were higher by about 30 to 50 percent. The CO discrepancies are attributed to in-probe oxidation.
3. The agreement between the data and model predictions over a wide range of conditions indicate the consistency and reliability of the measured data and usefulness of the modeling approach.
4. An analysis of NO_x formation revealed that, at constant temperatures, the presence of steam leads to lower O-atom concentration, which reduces *Zeldovich and* N_2O NO_x while higher OH-atom concentration reduces *Fenimore* NO_x.

1.4 TASK 202: CFD MODELING OF NOZZLE AND COMBUSTOR PERFORMANCE

The objectives of Task 202 were to conduct CFD simulations with combustion to model the nozzle and liner concepts, to guide fuel injector and combustion liner design, and to aid understanding of the NETL combustion system testing carried out in Task 203.

This task was conducted under the supervision of Stephen Morford. The P&W code, CORSAIR, was used for all simulations. The task was successfully completed by September 1998.

First, CFD calculations were performed for the full-scale premixing fuel injector in a simulated NETL single nozzle combustion rig. Three-dimensional (3-D) calculations were performed to identify aerodynamic differences between swirl vane geometries and to examine gross flowfield structure. The CFD predictions have identified a relationship between swirl vane chord-to-gap ratio and radial distribution of axial velocity at the discharge plane of the injector. Furthermore, the CFD calculations indicate that a *Coanda* or *wall jet* flow structure exists within the simulated combustor test section, independent of swirler vane geometry. These predictions have been confirmed by measurements made with pilot static probes traversed radially across the fuel injector discharge plane and across a simulated combustor exit.

Following this, the development of a preferred method for fuel preparation was explored to optimize premixed combustion. Methods to eliminate the *Coanda* flow field were identified. Flow separation regions inside of the

nozzle were also identified and corrected. This led to preparation of stereolithographic (SLA) hardware used for fuel/air mixing validation studies.

Additionally, the development of a preferred method for fuel preparation was explored experimentally to optimize premixed combustion. The fuel/air mixing of the nozzle was assessed using CO_2 as a fuel simulator. Spatial uniformity of CO_2 concentration was measured across the exit plane of the fuel injector. A statistical analysis of the mixing data indicated a spatial non-uniformity of 4.3 percent standard deviation over mean was achieved.

1.5 TASK 203: NETL COMBUSTION EVALUATION STUDIES

The objectives of Task 203 were to conduct tests in the low emissions combustor test and research facility at NETL. Specifically, these tests were to demonstrate and verify aerothermal design methodology to scale existing fuel injector hardware to a size consistent with NETL facility capabilities, to evaluate emissions performance under dry air operating conditions, to measure dynamic pressure response of the combustion system, and to evaluate combustion performance under humid air conditions.

This task was conducted under the supervision of Dr. William Sowa and was successfully completed by the end of 1999.

UTC staff designed and fabricated nozzle and liner hardware for the tests and assisted off-site, as well as on-site, while NETL staff conducts the experiments. As a result of this task, publications were made to ASME and the Eastern States section of Combustion Institute.

Brief conclusions from the experiments include:

1. The tangential entry nozzle (TEN), at lower pressures, has lower NO_x emissions than the axial nozzle, but at higher pressures, lower NO_x emissions were measured in the axial nozzle.
2. NO_x emissions go up with pressure in both tangential and axial nozzles; CO emissions go down with pressure.
3. Moisture loading of 15 percent in the air reduces NO_x emissions by as much as a factor of 3 to 8 (depending on the T_{eq}) at the same T_{eq} as a dry flame.[1] This reduction is attributed to the decrease in O-atom concentration.
4. NO_x levels increased with nozzle scale and increased at a greater rate when diffusion piloting was added.
5. With 15 percent added humidity, less than 2 ppm NO_x, less than 4 ppm CO and unburned hydrocarbons corrected to 15 percent O_2 have been achieved.

1.6 TASK 204: UNITED TECHNOLOGIES CORPORATION COST-SHARE STUDIES

The objective of Task 204 was to conduct engine tests of different fuel nozzle hardware by United Technologies Corporation (UTC), to select hardware concepts, and to provide a database to compare data obtained at the NETL. This task was conducted under the supervision of Dr. William Sowa and was successfully completed by March 1998.

[1] T_{eq} is defined as the equilibrium adiabatic flame temperature.

An FT8 baseline engine incorporating dry low NO_x features was used for this task. The cost-share studies that are part of this program were completed during the 4th Quarter of 1997. During these engine tests the viability of several different designs was evaluated. These designs represented variations on the nozzle design presented in Figure 1-2, which illustrates a tangential air entry nozzle as installed in the NETL test facilities. Air enters the nozzle through slots that cause the air to swirl through the main fuel/air mixing chamber. Fuel is added to the air at the entrance to each slot. A centerbody is provided to control the back flow region in the nozzle. The centerbody is fed with pilot fuel that can be either introduced internal to the centerbody or at the end of the centerbody, depending on the amount of premixing of the pilot fuel that is desired before combustion. The centerbody pilot provides flame stability control at different operating conditions in the engine cycle. The general design and operation of the nozzle has been described in different public domain references.[1] A second diffusion pilot is provided in the sidewall of the combustor liner. This pilot was used for initial lightoff and for transient operation.

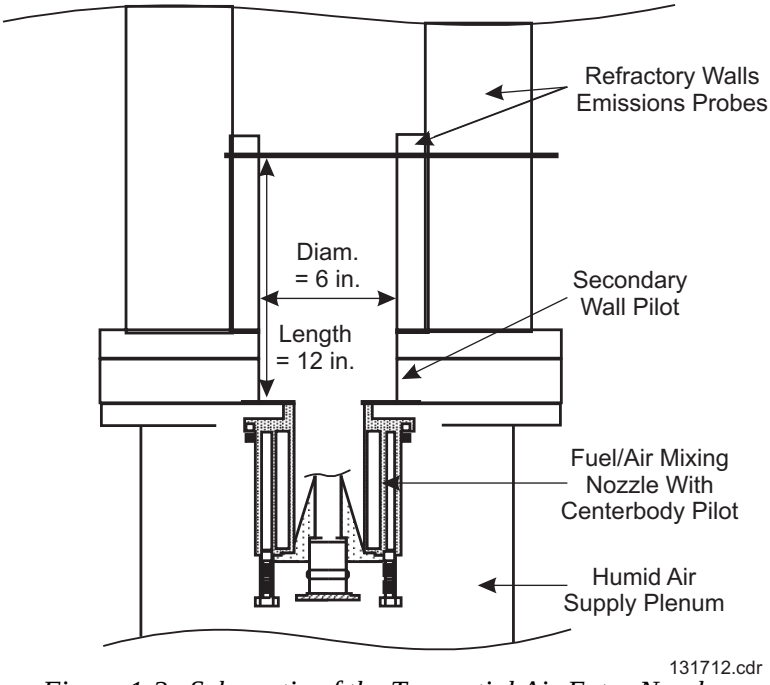

Figure 1-2. Schematic of the Tangential Air Entry Nozzle Tested in the NETL Facilities

The engine testing was used to evaluate the performance of different variations of nozzle designs and how it affects overall engine performance. Design changes included different strategies for centerbody piloting, as well as evaluation of different internal fuel/air mixing strategies. Several different ambient-day conditions were used to evaluate design performance. On each different day, both low power and high power nozzle performance were evaluated. Attractive design features identified during the engine tests were incorporated into the initial sets of nozzles tested as part of the NETL program.

Unlike the relatively idealized testing that occurs at the NETL facility, the engine provided realistic boundary conditions that put additional constraints on nozzle acceptability. Significant differences in boundary conditions between the NETL facility and engine tests include the following:

1. Diffuser air feed to the nozzle that is not as *clean* as a plenum feed
2. Active air addition through liner walls for liner cooling and turbine profile maintenance
3. Nozzle-nozzle interaction
4. Near-choked combustor exit conditions for the flow as it exits the combustion chamber.

Figure 1-3 shows representative data from the cost share studies for the nozzle design features to be evaluated during the NETL tests. The data indicate that the engine operating at baseload had pressure pulsation levels safely within the design-allowable levels while obtaining the desired dry low NO_x levels.

[1] Snyder, T.S., Rosfjord, T.J., McVey, J.B. and Chiappetta, L.M., "Comparison of Liquid Fuel/Air Mixing and NO_x Emissions For a Tangential Entry Nozzle," *International Gas Turbine and Aeroengine Congress and Exposition*, The Hague, Netherlands, June 13-16, Paper No. 94-GT-283, 1994; and Snyder, T.S., Rosfjord, T.J., McVey, J.B., Hu, A.S., and Schlein, B.C., "Emission and Performance of a Lean-Premixed Gas Fuel Injection System for Aeroderivative Gas Turbine Engines," Transactions of the ASME, Vol. 118, pp. 38-45, January 1996.

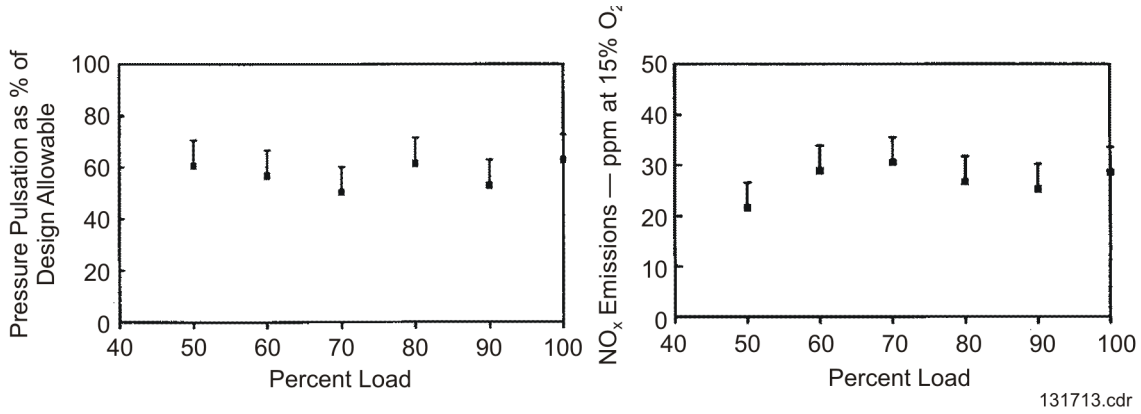

Figure 1-3. NO_x Emissions Levels and Pressure Pulsation Levels from Engine Testing Shown as a Function of Power Setting for the Nozzle Features Evaluated at the NETL

The cost-share activity provides a strong link between the NETL facility testing and engine application. Definition of engine constraints and the development of correlations between the NETL results and the engine results will facilitate the transition of NETL study results to engine compatible hardware. These comparisons (between rig and engine) provide understanding of the influence of boundary conditions on performance in the different test environments.

1.7 TASK 301: CYCLE ANALYSIS SUPPORT

The objective of Task 301 was to support the HAT Cycle Program by providing a matrix of operating conditions for advanced HAT cycles on natural gas. This task was conducted under the supervision of Fred Robson and was completed successfully by September 2000.

The UTC-proprietary State-of-the-Art Performance Program (SOAPP) was used to do the analysis. The model includes changes in saturator, combustor, fuel, and turbine cooling that have been identified by P&W and others during ongoing programs.

In the HAT cycle, the compressor discharge is humidified in a saturator that uses heat recovered from within the gas turbine cycle. This mixture is then recuperated against the gas turbine exhaust. This increases both the output and efficiency of the gas turbine. A variety of engine configurations including simple and intercooled cycles and cycles using reheat were analyzed. Intercooled engines operating at pressure ratios of 40 and greater offered the best performance. A matrix of operating conditions for advanced HAT cycles on natural gas had been defined.

1.8 TASK 302: PERFORMANCE ANALYSIS OF FT4000 APPLICATIONS

The objective of Task 302 was to estimate the performance of the baseline version of the FT4000 and FT4000 IC. This task was conducted under the supervision of Fred Robson was successfully completed by September 2000.

The output of the baseline FT 4000 IC engine was estimated to be 147.5 MW at an efficiency of 47.5 percent lower heating value (LHV). This engine operated with a combustor exit temperature of 2715°F and an overall pressure ration (OPR) of 56.4. This temperature was dictated by NO_x production. In the HAT cycle configuration, the output increased to nearly 248.4 MW and the efficiency increased to 58.7 percent (LHV) at the same operating conditions. Because the humidified air significantly reduces NO_x formation, higher temperature versions were investigated. At a combustor exit temperature of 3100°F, which is projected to have NO_x emissions of under 9 ppm, the output was 329.2 MW at an estimated efficiency of 61.2 percent (LHV).

The simple cycle version of the FT4000 had an output of 48 MW at an efficiency of 37.4 percent. In HAT configuration, the output was estimated to be 106.5 MW at an efficiency of 51.8 percent. Both configurations had an operating temperature of 2476°F.

1.9 TASK 303: PERFORMANCE ANALYSIS OF FT8 APPLICATIONS

The objective of Task 303 was to estimate the performance of the baseline version of the FT8. This task was conducted under the supervision of Fred Robson and was successfully completed by September 2000.

Several variations of the PWPS FT8 were analyzed. The baseline engine is a simple cycle operating at an OPR of 19.8 and a combustor exit temperature of 2208°F. Its output is 25.2 MW at an efficiency of 38.2 percent (LHV). In HAT configuration, the output was estimated to be 44.3 MW at an efficiency of 47 percent (LHV). An intercooled version was also investigated. This engine had a baseline output of 57.8 MW at an efficiency of 38.9 percent (LHV) and operated with an OPR of 24.2 at a combustor exit temperature of 2462°F. In HAT configuration, the output was estimated to be 83.7 MW at an efficiency of 53.3 percent (LHV).

1.10 TASK 401: DUAL FUEL NOZZLE

The objective of Task 401 was to investigate experimentally the effects of operating pressure, moisture content, and flame temperature on combustor emissions and dynamic pressure levels with the dual fuel nozzle. The emphasis is on the liquid fuel combustion rather than the natural gas combustion, since the latter has been investigated thoroughly in Task 203. This task, conducted under the supervision of Dr. Alexander Chen, was successfully completed by April 2001. As a result of this task, a paper was submitted to ASME for publication.

The axial spray liquid module was chosen for the initial tests and yielded unstable combustion with high CO and NO_x emissions and high nozzle centerbody tip temperature. The unstable combustion was caused by the lack of fuel in the outer recirculation zone of the combustor due to the axial liquid injection direction. The high nozzle tip temperature was caused by insufficient cooling and concentration of fuel just downstream to the nozzle centerbody. UTRC modified the nozzle accordingly. The new nozzle uses a 60°F liquid module to send more fuel to the outer recirculation zone and increases centerbody tip cooling air by 15 percent. Testing of this improved nozzle was successfully completed in April 2001 at the NETL in Morgantown, West Virginia.

Brief conclusions of this task were the following:

1. Stable combustion with the 60°F injection dual fuel axial swirler nozzle was achieved for both natural gas and No. 2 diesel fuel, with and without steam
2. With 10 percent steam addition, more than 90 percent reduction of NO_x relative to the dry case for the same flame temperature was achieved for diesel fuel at 100-psi pressure
3. RMS pressures were below 0.21 psi for diesel fuel, with and without 10 percent steam addition, throughout the entire tested flame temperature range of 2440° to 3090°F.

Details are summarized in:

1.11 TASK 402: HYBRID COMBUSTOR/CATALYTIC NOZZLE

The objective of Task 402 was to investigate the performance of a hybrid burner combining a catalyst with a heat exchanger under practical dry and humid air engine operating conditions. This task was conducted under the supervision of Meredith Colket and was successfully completed by March 2001.

A hybrid pilot consisting of a catalytic system imbedded in the tangential entry nozzle was designed and constructed. In March 2001, this system was tested at the NETL.

Brief conclusions from the experiments include the following:

1. Autoignition of fuel/air mixture with the catalyst was achieved

2. The catalyst reactor/heat exchanger/mixer performed as designed and was intact after the initial tests
3. Both NO_x and CO levels were reduced when the catalyst lit the fuel/air mixture, consistent with laboratory demonstrations
4. RMS pressures were reduced when the catalyst lit the mixture, suggesting more stable combustion.

1.12 TASK 403: LINER EVALUATION

The objective of Task 403 was to investigate humid air combustion and combustor liner durability under realistic combustor geometry and acoustic boundary conditions. The tests of this task were done under the supervision of Dr. William Sowa. The final stage of the task was conducted under the supervision of Dr. Alexander Chen. The task was successfully completed by September 2001.

Testing with the new liner commenced in late March 1999, but was delayed several times due to air leakage problems caused by damaged grafoil seals, as well as high dynamic pressure. After the sealing issues were resolved in late April 1999, testing was continued. The final test of this task was completed in February 2000.

Experimental data was obtained for natural gas premixed combustion in dry and humid air in a convectively cooled liner with near-choke exit at different pressures over a wide range of equivalence ratios. The effect of liner, nozzle, inlet temperature, inlet pressure, pilot level, humidity, and equivalence ratio on NO_x and CO emissions and dynamic pressure was evaluated based on the data.

Brief conclusions from the experiments include the following:

1. The RMS pressure reached as high as 8 psi in the cooled liner combustor with exit choke, significantly larger than that in the refractory liner combustor without exit choke.
2. For the same equivalence ratios, the NO_x in the cooled liner combustor was similar to that in the refractory liner.
3. Introduction of 5 percent steam in air suppressed NO_x production by more than 40 to 50 percent for the same flame temperature.

2. RESULTS AND DISCUSSION

2.1 KINETIC MODELING AND FUNDAMENTAL DATABASE GENERATION

The objectives of this task were to conduct laboratory experiments and undertake kinetic modeling studies to define the effects of high water vapor content in air on the flame stability and emissions in HAT cycle combustion systems burning natural gas.The effects of temperature, pressure, fuel composition, and H_2O content on CO, NO_x, and UHC production, flame stability, and ignition will be defined. Kinetic mechanisms will be evaluated and modified as necessary to accurately describe the experimental results. Validated kinetic mechanisms will be evolved into reduced reaction sets for integration into CFD codes. Ultimately, the results of the small-scale combustion experiments and kinetic modeling will be used to guide in the design of a full-scale nozzle and combustor.

A definition of experiments, performed in the small-scale combustor evaluation program, are divided into the following phases:

- Modify test combustor facility and flow systems to accommodate steam injection
- Perform baseline combustion tests to determine operating limits of HAT cycle combustor with existing facility design
- Design laminar premixed or partially premixed turbulent burner to provide optimum flame stability and minimized emissions under HAT cycle conditions
- Perform extensive combustion tests to determine in detail the effects of temperature, pressure, fuel composition, and H_2O content on emissions and operability limits of HAT cycle combustor
- Perform data analysis and develop design criteria for subscale combustor testing in sector rig.

Part of Task 201 is devoted to examining the chemical kinetics of NO_x production, CO burnout, and unburned hydrocarbon emissions. For this program, UTRC is employing computer codes for chemical kinetic predictions based principally upon CHEMKIN II, one of the best chemical kinetic tools for examining this problem since the code readily treats pressure-dependent variations in reaction rates. Conditions up to 60 atm of pressure are of interest to this program and existing reaction sets will necessarily have to be extrapolated well outside of their validated regimes; hence, the pressure dependent features of CHEMKIN II should minimize related uncertainties. Several kinetic codes interacting with the CHEMKIN II software have been developed at UTRC including a parallel/series network of perfectly stirred reactors for simulation of combustors and predictions of emissions.

2.1.1 High Pressure Flat-Flame Burner Facility

Preliminary tests were performed as part of an evaluation of the applicability of the high pressure flat-flame combustor to this program. This combustor presently is configured to operate with a fully premixed burner at pressures up to 63 atm and inlet temperatures up to 670K (1210°R). Tests were performed at a constant inlet equivalence ratio to determine the radial temperature and species profiles at elevated pressures with ambient temperature inlet gas. These tests were to confirm the one-dimensional behavior of the premixed flat-flame burner, shown in Figure 2-1. The probe for obtaining gas samples or thermocouple measurements can be moved radially and the burner translated axially to obtain radial or axial temperature and species measurements. The schematic diagram of the combustion facility showing probe locations is shown in Figure 2-2.

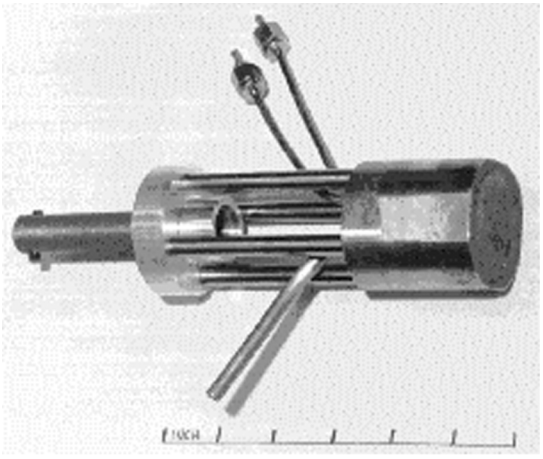

131714.cdr

Figure 2-1. Flat Flame Burner Assembly

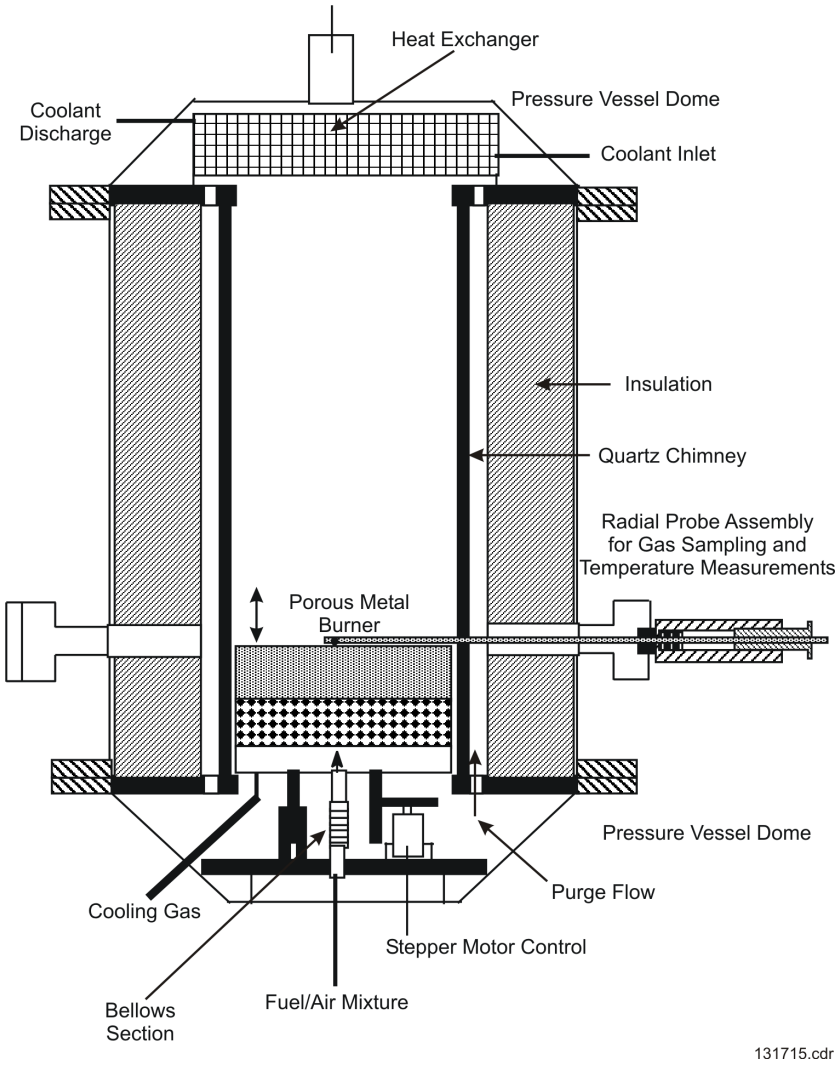

Figure 2-2. Schematic of High-Pressure Flat Flame Burner Combustor

A photograph of the flat flame combustor is shown in Figure 2-3. The vessel is rated for operation at 63-atm pressure with an inlet temperature of 673K. For the flat-flame combustor evaluation tests, a beryllium/yttrium oxide coated fine wire Type R thermocouple was used to measure the axial (downstream) profile on the burner centerline as a function of vessel pressure. Radial profiles were also acquired at 5 and 10 atm and 5.6 mm above the burner surface (the location chosen as well downstream of the flame zone where high gradients would exist in species and temperature). Temperature measurements were also made, where $\phi = 0.98$ and $\phi = 1.3$. A plot of the radiation corrected radial temperatures at 5 atm are shown in Figure 2-4 (zero being the midpoint of the burner).

This data confirmed the one-dimensional nature of the flat-flame burner which is critical for modeling of this flame structure. However, the laminar flat-flame burner used in this evaluation was not conducive to detailed flame probing at adiabatic conditions. The delicate balance between flame speed and approach velocity to the burner surface in order to position the flame front at precisely the same standoff distance from the burner was very difficult to maintain. Although data was acquired up to 60-atmosphere pressure at an equivalence ratio of 0.95, the radial and

axial temperature profiles indicated that the heat loss to the water-cooled centered metal burner varied with pressure. This is shown in Figure 2-5 where it is seen that as the pressure increased, the heat loss to the burner and chimney walls increased. Attempts to lift the flame off of the burner surface to reduce the heat loss only resulted in loss of the flame (liftoff). For this reason, it was decided to concentrate the data acquisition in the high pressure, high temperature turbulent partially-premixed flame facility.

2.1.2 High Pressure, High Temperature Turbulent Burner Facility

The high pressure experimental apparatus designed for this program is composed of five subsystems:

1. Gas flow control
2. Gas and facility thermal control (heaters)
3. Fuel/air mixing section
4. Combustor section
5. Gas analysis system.

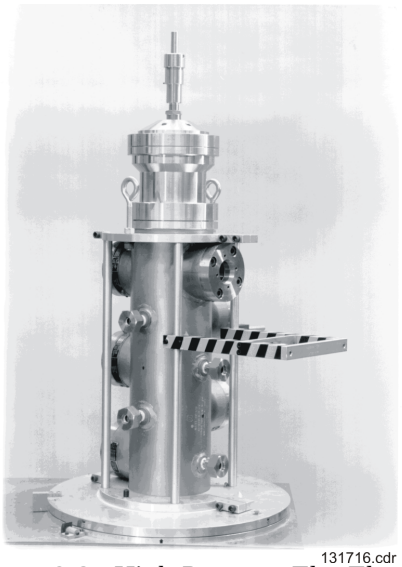

Figure 2-3. High-Pressure Flat Flame Combustor

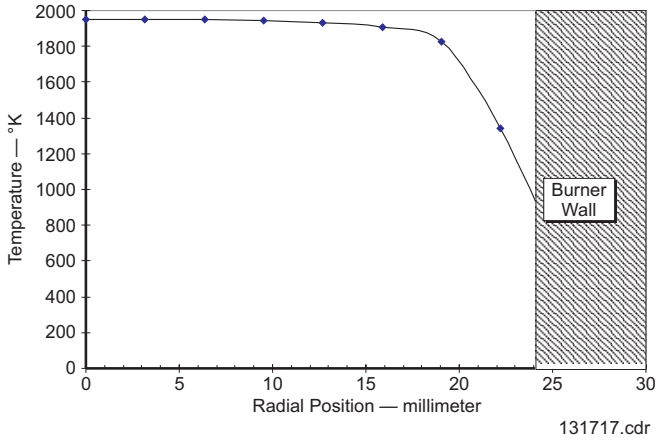

Figure 2-4. Radial Temperature Profile at 5 Atm and ϕ = 1.3

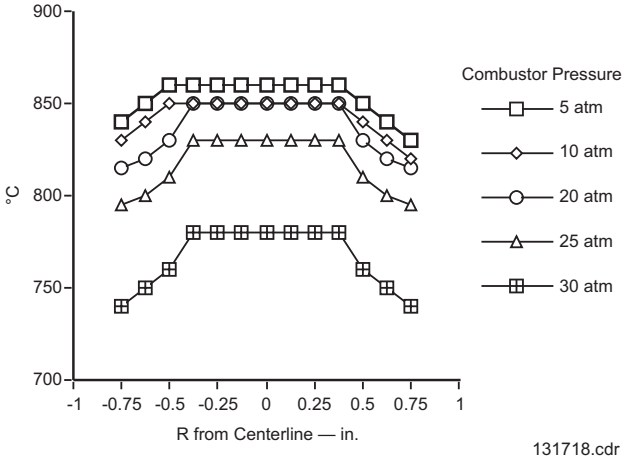

Figure 2-5. Radial Temperature Profiles in Flat Flame Burner at Various Pressures

The fuel/air/water mixture is burned in a combustor where the flame is stabilized by either a porous steel disk or a partially premixed burner configuration. The combustor schematic is shown in Figure 2-6. The flameholder is designed to minimize quenching due to heat loss, and yet provide a stable flame over a wide range of operating conditions, such as velocity, equivalence ratio, pressure, and temperature. Testing at conditions expected in a land-based gas turbine enables a comparison to be made between the emissions and flame stability of methane flames with and without water addition.

Initial experiments have been performed at a maximum inlet pressure of 426 psig. All gases for the experiment, as well as the inlet section to the combustor are electrically heated to the specified operating temperatures using ceramic lined heating furnaces powered by microprocessor-based thermal controllers. The gases were supplied from compressed gas cylinders, monitored and controlled by digital electronic flowmeters, and pressure in the reactor controlled with a pneumatically-operated back-pressure regulator. A pressure relief vent was incorporated in the design to prevent rig pressure from exceeding the design value of the pressure vessel. Stress analysis has been performed on each component of the system and the reactor components pressure tested by the manufacturer to comply with standard pressure vessel codes for operation at the design temperature and pressure.

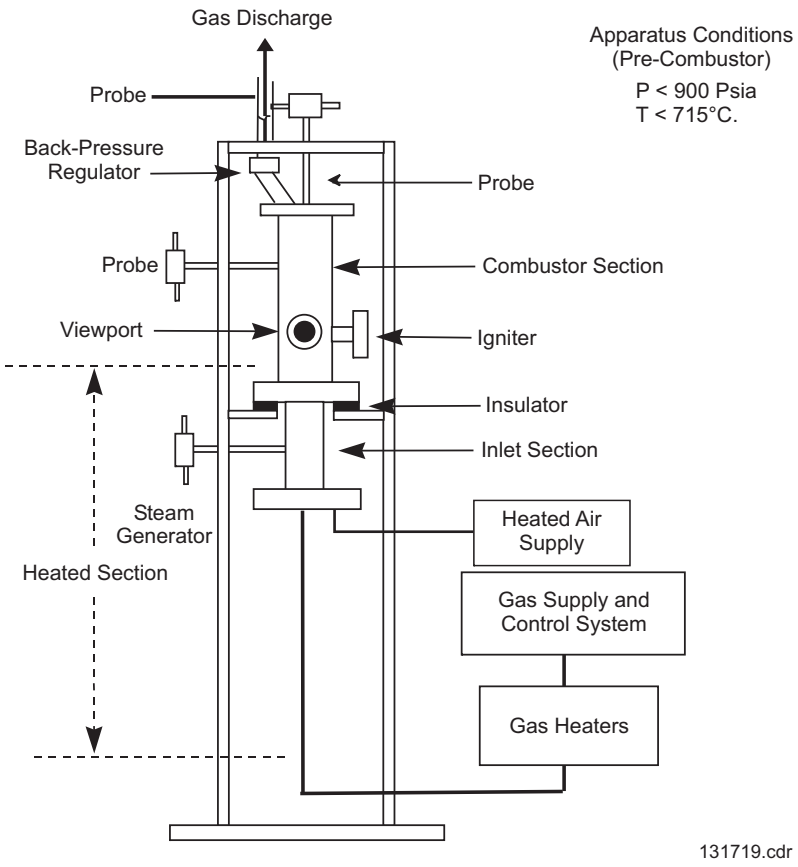

Figure 2-6. Schematic of High Temperature, High Pressure Combustion Apparatus

Gas sampling can be accomplished through the use of three probes: One located just downstream of the mixing zone, one fixed probe located in the combustor exhaust stream, and one axially-oriented probe that can be positioned along the axis of the combustor. The data presented below was obtained from the fixed sample port located in the combustor exhaust. The traversing probes are cooled with water heated to 125°C to prevent internal water condensation. The position is adjustable on the traversing probes by rotating a threaded collar that retains the probe in a fixed mount and which, in turn, is threaded into the desired probe location in the apparatus. The gas sample is conducted to the analyzers through a heated sample line and water trap, as required. Temperature is monitored at six locations in the apparatus with chromel-alumel thermocouples whose outputs are displayed on digital panel meters. In the combustor, the temperatures are monitored by two Type B thermocouples (platinum/30 percent rhodium versus platinum/6 percent rhodium). The viewport is monitored by a video camera so that personnel are not positioned in direct line-of-sight with the viewport. The viewport is located at the flame-holder in the combustor section, 90 deg from the position of the hot surface platinum wire ignition source. The gas sampling system includes two NDIR CO and one NDIR CO_2 analyzer, a paramagnetic O_2 analyzer, and a thermoelectron $NO\text{-}NO_2\text{-}NO_X$ analyzer. The gas sample is transported to the emissions instrument rack through a metal-bellows sample pump. Integrity of the sampling system is checked regularly by flowing nitrogen through the test apparatus at atmospheric pressure; oxygen concentration is monitored to determine if the sampling system is leak-free. All gases used for calibration of the analyzers were gravimetrically made by Scott Analytical Gases and are traceable to National Institute of Standards and Technology (NIST) standards. Gas samples can also be analyzed with a gas chromatograph.

The high inlet temperature apparatus has been modified to incorporate steam injection into the combustion airflow. A high precision water flow measuring system has been acquired that is capable of operation at pressures up to 1,000 psia and able to measure the low flowrates of water that will be used in this experiment. The water is fed into a steam vaporizer through stainless steel pressurized cylinders equipped with sight tubes so that the flow can be continuously monitored. The electronic flowmeter for the water flow measurement has a precision of a quarter percent of full scale, with an operating range of 0.001 to 0.08 gpm. The water flowmeter has been factory calibrated, and this calibration has been checked at UTRC under our proposed operating conditions. The pressurized water cylinders are in place, and all necessary plumbing modifications made to the combustor for steam injection. Several versions of the steam generator and injection system have been built and tested and a design that provides steady steam flow at very low mass flow has been incorporated in the facility (shown in Figure 2-7).

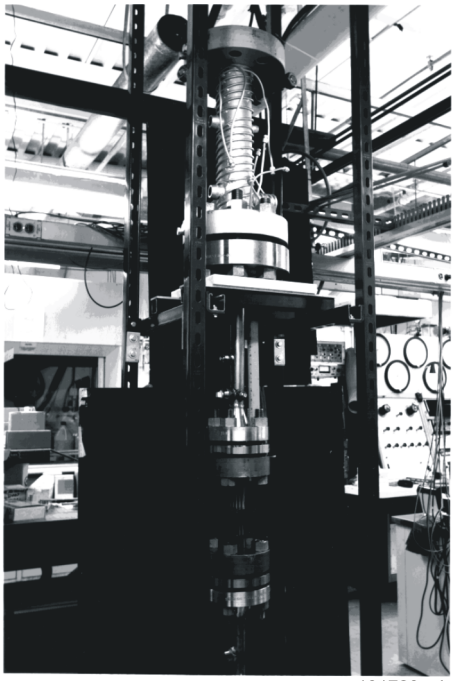

Figure 2-7. Photograph of the High-Temperature Combustion Facility

A suitable, robust burner applicable for investigating the characteristics of premixed flames, specifically with regard to NO_x generation has been selected based upon prior, UTRC-funded activities. A schematic of this burner, with a representation of a turbulent flame above the burner is provided in Figure 2-8 and Figure 2-9. Such a configuration was selected over the more conventional laminar premixed flames due to difficulties of making such a flame nearly adiabatic (or with controlled/measured heat loss). Such a task is difficult at ambient conditions and is virtually impossible at the elevated inlet pressures and temperatures of interest in this program. In addition, turbulent flames have more practical interest. Hence, the geometry depicted in Figure 2-8 and Figure 2-9**,** with a turbulent, high mass flow rate flame, was selected for study in this program. This burner has several flowpaths available for control. In the central tube, the fuel is partially premixed (typically, to fuel-rich conditions). The mixture exits at the top of a mixing chamber where it flows, along with the remaining *premixing* air through a narrow annular region. The flow then exits out the top and the mixture burns in a turbulent, premixed flame.

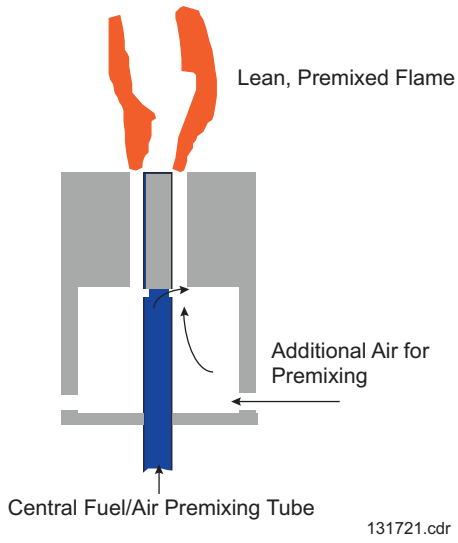

Figure 2-8. Schematic of Partially Premixed Burner System

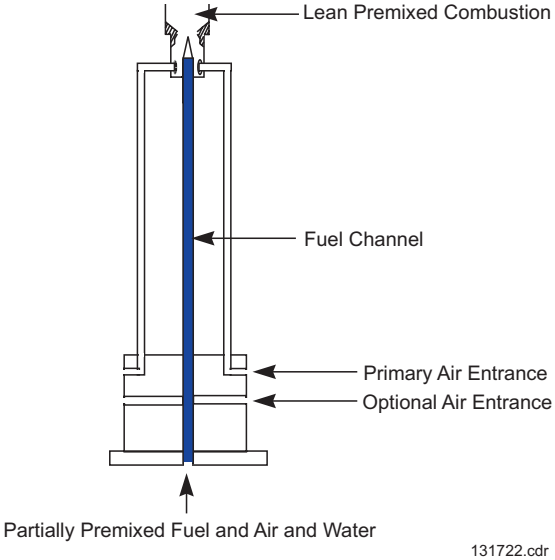

Figure 2-9. Burner Configuration Used in High-Pressure Combustion Facility

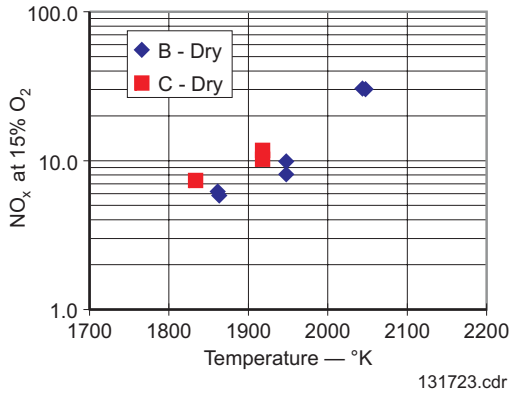

Figure 2-10. NO_x Emissions as a Function of Flame Temperature at 10 Atm

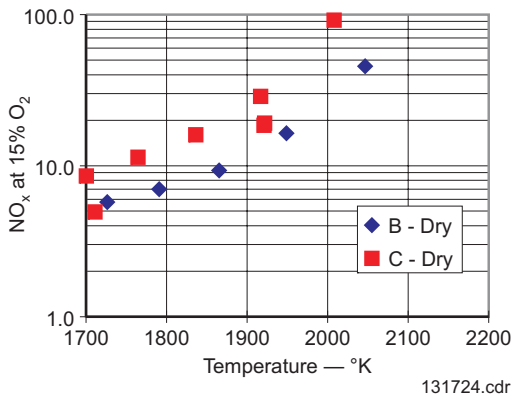

Figure 2-11. NO_x Emissions as a Function of Flame Temperature at 20 Atm

Initially, we attempted to characterize the performance of the burner under different flow conditions. Tests were performed at 10 atm, 20 atm, and 30 atm and with the air preheated to 700K (800°F). In one sequence of tests, at 30 atm and at 725K (845°F) preheat, the flame flashed into the premixing chamber and destroyed the burner. This learning experience helped to redefine desired operating conditions for this burner, which had been proven to be quite robust for all prior studies at pressures of 20 atm and below. Specifically, minimal flow velocities are desired (not always achievable due to startup transients, etc.) and lower levels of preheat desired. The latter is not perceived to be a problem since applicable T_3 temperatures for the advanced cycles are expected to be in the neighborhood of 590K to 650K (600° to 700°F) due to intercooling, and flashback should be further inhibited due to the presence of water. To enable higher flow velocities that will also inhibit flashbacks, a new, larger air flowmeter for the early premixing core flow was calibrated and installed. Low initial air temperatures may have to be the principal tool for inhibiting flashback under such very high-pressure conditions, until yet higher mass flows can be attained.

Plots of NO_x emissions as a function of the calculated equilibrium flame temperature based on input flow rates for 10 atm, 20 atm, and 30 atm as measured in this burner are shown in Figure 2-10, Figure 2-11, and Figure 2-12. A cursory examination of this data clearly indicates that the scatter is significantly larger than desirable for the intended purposes. Upon careful examination of the data obtained at 10 atm, it was shown that the four lowest NO_x levels of the series (B) data set with flame temperatures between 1850K and 1950K (2870° to 3050°F) were obtained with higher flow rates of air in the central premixing tube. These four run points presumably allowed for a greater level of premixing prior to the flame front. The separation of the data in Figure 2-11 at 20 atm is consistent with this interpretation. Hence, a series of tests were performed in which the flame temperature was held approximately constant while varying the split in the air mass flows between the central tube (for partial premixing NO_x emissions for these data are added to the points from Figure 2-11 and are replotted in Figure 2-13) and the larger premixing chamber.

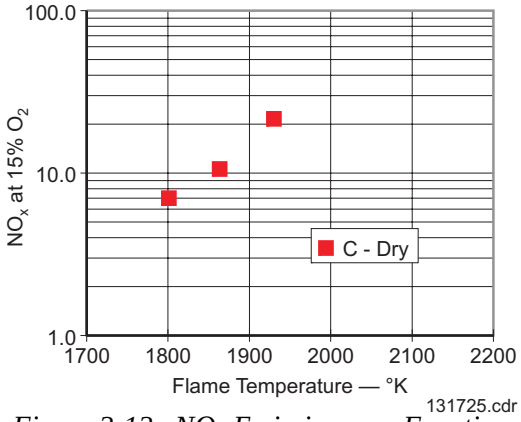

Figure 2-12. NO_x Emission as a Function of Flame Temperature at 30 Atm

The significant variation with changes in the airflow split is quite noticeable. This latter set of NO_x data at the flame temperature of 1840K (2853°F) is also plotted in Figure 2-14 as a function of the fraction of air flow that is directed through the central tube and used in the partial premixing. NO_x production should decrease as premixing is increased. Figure 2-14 demonstrates the dramatic decrease in NO_x with an increasing level of premixing, although the asymptotic value was only approached in this series of runs.

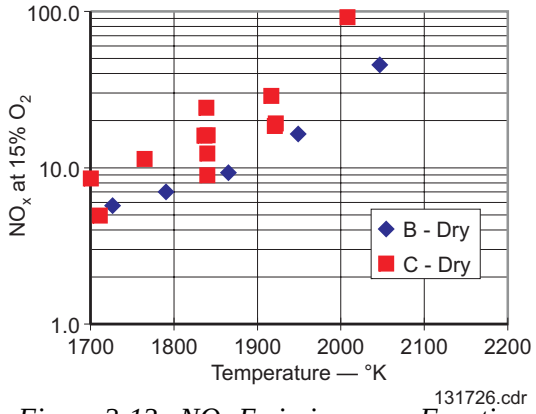

Figure 2-13. NO_x Emissions as a Function of Flame Temperature at 20 Atm

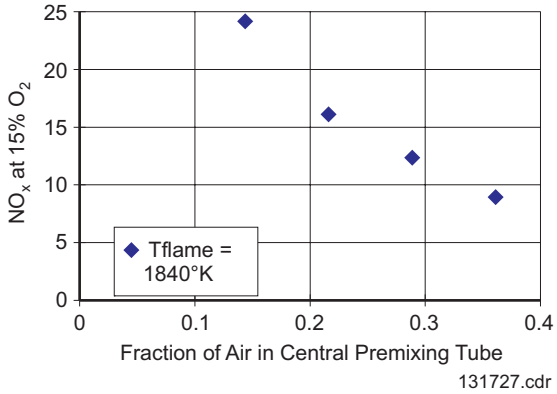

Figure 2-14. Effect of Premixing on NO_x Levels at 20 Atm

This asymptotic value (approximately 5 to 7 ppm) can be compared to predictions from a perfectly stirred reactor (PSR) and to experimental values reported by Leonard and Stegmaier[1] for a perfect premixer. In Figure 2-15, predictions made using GRI-MECH 2.11 and its associated thermodynamics file are plotted as a function of residence time in a single PSR (CHEMKIN II) as a function of residence time for five different equivalence ratios, and, hence, different flame temperatures. The equivalence ratios and equilibrium flame temperatures are reported in the insert. Initial conditions were assumed to be at 20 atm with an air temperature of 725K (845°F) and a fuel temperature (pure methane) of 350K (170°F). The predictions at 0.98, 1.95, and 3.9 msec are also plotted in Figure 2-16 as a function of equilibrium flame temperature (kinetic calculations indicate that the PSR approaches within 10K to 15K (18° to 27°R) of the equilibrium temperature after one millisecond for these conditions and within 3K to 5K (5° to 9°R) after 4 msec. Also in Figure 2-16 is the curve for experimental NO_x levels from a perfect premixer, as described by Leonard and Stegmaier. For reference, the approximate asymptotic value of the recent UTRC experiments (shown in Figure 2-14) of 5 to 7 ppm is also shown in Figure 2-16.

The procedure of varying the air flow split to evaluate the effects of unmixedness and to ensure the approach to a near perfect level of premixedness can be followed to attain related data over a range of pressure and temperature conditions. This data can be used for comparison to the previous (literature) data, as well as to validate GRI-MECH 2.11 under gas turbine conditions. Furthermore, the same or slightly modified procedure can be used for the case of steam addition to the air. Such experiments along with modeling validation will be a main focus of the remainder of this task.

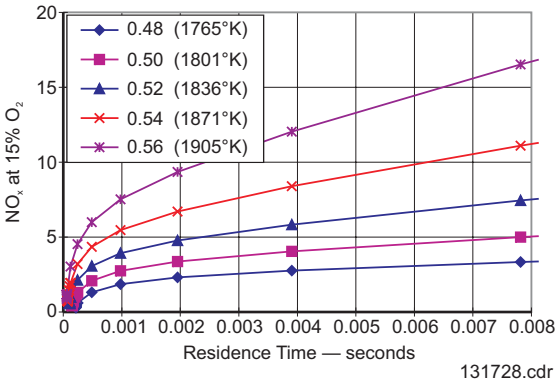

Figure 2-15. NO_x Production in PSR at 20 Atm (GRI-MECH 2.11)

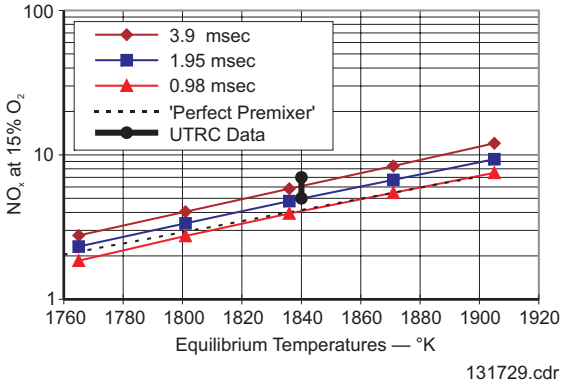

Figure 2-16. NO_x Predictions in PSR and Data Versus Flame Temperature

[1] Leonard and Stegmaier, "Development of an Aeroderivative Gas Turbine Dry Low Emissions Combustion System," Transactions of the ASME, Vol. 116, p. 542, July 1994.

2.1.3 Solubility of Air in Water at Elevated Pressures

In our laboratory studies of combustion under simulated HAT-cycle conditions, water is pressurized up to 60 atm with air. Finite solubilities of air in water at these pressures raises fear that air carried in the vaporized water stream may affect the equivalence ratio during combustion. Therefore, a calculation was performed in order to determine the mole fraction of air that can be present in water. This calculation can be performed in two different ways: A rough calculation assuming ideal solubility (gives solubility within an order of magnitude) and a more accurate and reliable calculation based on experimental data (with some engineering approximations). The ideal solubility calculation is independent of the solution and is proportional to pressure,

$$x = \frac{y_2 P}{P_{vp2}}$$

where y_2 is the mole fraction of the component in the vapor phase, P is the system pressure and P_{vp2} is the vapor pressure of the solute. This calculation gives higher solubilities than seen experimentally (a mole fraction of 10 to 3 for N_2 in H_2O at 25°C and 1 bar pressure).

In a more practical approach, the Krichevksy-Kasarnovsky equation was used to predict the solubility of nitrogen in water at elevated pressures:[1]

$$\ln\left(\frac{f}{x}\right)_2 = \ln\left(\frac{\varphi y P}{x}\right)_2 = \ln H_2 + \frac{V_2^{\infty} P}{RT}$$

Where f is the fugacity of the gas, φ is the fugacity coefficient of the gas, x is the mole fraction of the gas in solution, H_2 is the Henry's Constant, P is the system pressure, and V_2^{∞} is the partial molar volume of the gas at infinite dilution in the liquid phase. This equation predicts the experimental solubilities remarkably well up to about 650 bars.

The assumptions made in this approach are that the composition of air is assumed to be 100 percent nitrogen (oxygen and nitrogen have very similar solubilities in water, with oxygen being slightly higher), and that the fugacity coefficient φ follows the Lewis Rule and remains constant in the 1 to 100 bar pressure range (the precise value of j can be calculated from different equations of state). The experimental value of solubility at 1 bar and 25°C (the approximate storage temperature in our high-pressure vessels) was used to calculate the value of φ. The value for Henry's Constant and V_2^{∞} were evaluated from experimental data.[2] The results from this calculation are shown in Figure 2-17.

This curve indicates that water pressurized by air up to 60 atm would attain only 0.001 mole fraction of nitrogen. A similar result could be obtained for oxygen. Since the mole fraction of water vapor in air in a HAT cycle can be expected to be 0.2 to 0.3, the added air from the water vapor amounts to only about 0.0003 mole fraction in the mixture. Hence, these calculations demonstrate that the dissolved air carried with the water can be neglected.

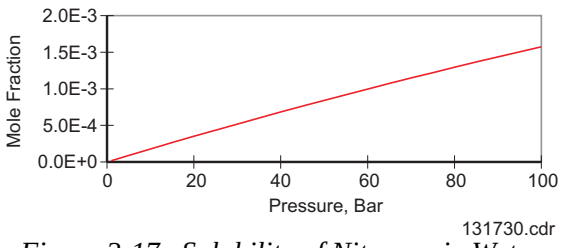

Figure 2-17. Solubility of Nitrogen in Water at High Pressure

2.1.4 Chemical Kinetic Modeling

As an example of the type of calculations that have been performed, compare the combustion of three fuels, all at 20 atm and at inlet air, fuel (natural gas) and steam temperatures of 700K (800°F). The first fuel is natural gas,

[1] Reid, Prausnitz, and Poling, *The Properties of Gases and Liquids*, 1986.

[2] Prausnitz, Lichtenthaler, and Azevedo, *Molecular Thermodynamics of Fluid-Phase Equilibria*, 1982.

assumed to be at 700K. The second is a mixture of fuel and steam at 700K (800°F), with an effective steam/air mass ratio of 0.0915. The third fuel is a *reformed* fuel mixture of methane, steam, and air (mass fractions of 0.233, 0.612, and 0.155, respectively) initially at 700K (800°F), but once reacted attains the temperature of 762K (912°F). This fuel *processing* is comparable to the autothermal reaction system proposed for gas turbine systems. The mass fraction of water in the total air stream for this autothermal case is the same as in case 2. All three are fueled at a rate to produce an (equilibrium) flame temperature of 1811K (2800°F). A series of calculations were performed for each mixture using a modified PSR code and the GRI-MECH 2.11 chemical kinetic reaction set.[1] In each case, the residence time in the PSR was reduced sequentially until the mixture could no longer support combustion. This limiting residence time has been shown to provide a measure of overall flame stability.[2] As the PSR residence time, or τ, is reduced, the reaction chemistry is no longer fast enough to provide heat release sufficient to sustain combustion and reaction temperatures are suppressed. In Figure 2-18, the PSR temperatures are plotted for each of the three fuels as a function of PSR residence time.

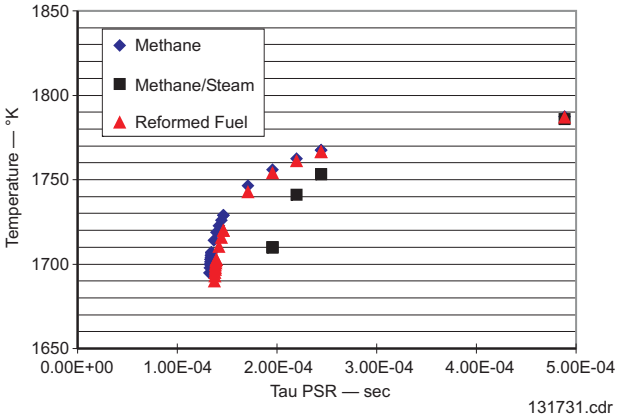

Figure 2-18. PSR Temperature as a Function of τ

As can be seen, the methane/steam system suffers from a greater level of instability relative to the other flames and suggests that any combustion device must require a greater volume or otherwise enhanced stabilization features to ensure a robust combustion system. Figure 2-18 also shows the fact that with the same incoming enthalpy, steam and methane, air flows, an autothermal reactor can *reform* the fuel into a more reactive condition such that minimal penalty is sustained in combustion stability despite the substantial addition of steam to the system. Further advantages of the steam addition and particularly the autothermal approach can be found by examining the predicted emissions (corrected CO and NO_x) in Figure 2-19 and Figure 2-20 for these same conditions.

Figure 2-19 shows how steam (unreacted or reacted with the fuel) can lead to a substantial decrease in NO_x production rates. An analysis indicates the reduction in NO_x production due to the presence of high concentrations of water is due to the dilution effect of the steam and to the suppression of the O-atom concentration, a key intermediate in the production of flame-generated NO_x. As can be seen in Figure 2-20, CO benefits are also possible with the use of the *reformed* fuel. It will be an objective of the combined experimental and modeling efforts to verify the validity of predictions such as these.

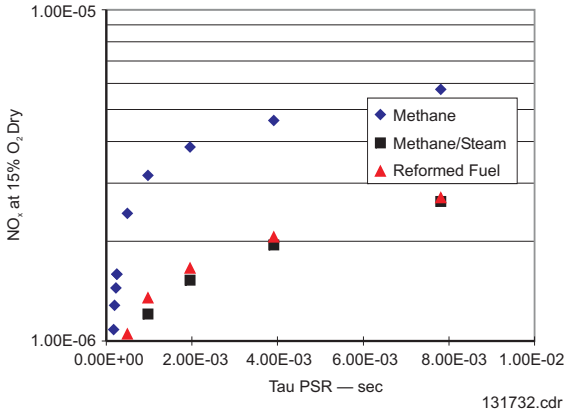

Figure 2-19. Corrected NOx as a Function of τ

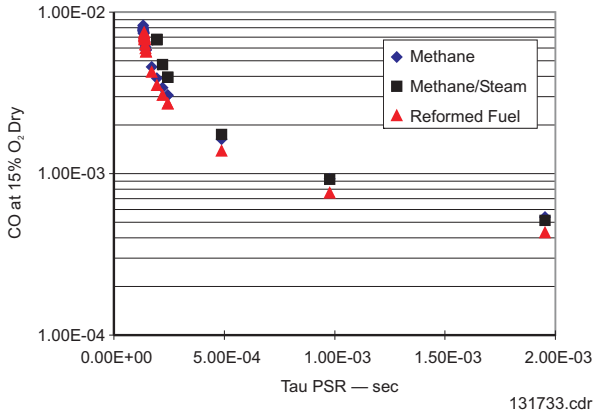

Figure 2-20. Corrected CO as a Function of τ

[1] Glarborg, P., Kee, R.J., Grcar, J.F., and Miller, J.A., "PSR: A Fortran Program for Modeling Well-Stirred Reactors," *Sandia National Laboratories Report*, SAND86-8209, February 1986.

[2] Hoffman, S., Habisreuther, P., and Lenze, B., "Development and Assessment of Correlations for Predicting Stability Limits of Swirling Flames," *Chemical and Engineering Processing*, 33, pp. 393-400, 1992.

These chemical kinetic tools will be used also to develop reduced reaction sets for use in CFD codes. CFD models, such as FLUENT®, which is licensed for use at UTRC, or CORSAIR can only accept limited reaction sets (for example, less than 10 species). The complex flow field that will be present in a proposed burner design can be examined analytically using such codes to examine residence times, flow velocities, areas of recirculation, regions of incomplete CO oxidation and general flow characteristics that may aid in screening burner concepts prior to testing in the small scale combustor. The modeling effort will be used to predict the performance of burner configurations in the full-scale combustor.

2.1.5 Schedule and Planned Activities

Figure 2-22 illustrates the program plan and schedule for Task 201. Upon examination of this previously presented schedule, activities under this task are on target with respect to the overall program timeline. In the near future, testing will be performed in the high-pressure combustor with water addition. A focus area in the fundamental database generation task will be varying the air flow split to evaluate the effects of unmixedness and to ensure the approach to a near perfect level of premixedness. This data can be used for comparison to the previous (literature) data as well as to validate GRI-MECH 2.11 under gas turbine conditions. Furthermore, the same or slightly modified procedure can be used for the case of steam addition to the air. Development of a more fully premixed burner that will operate robustly at high pressure will proceed based upon the results of the effects of premixing, as presented in Figure 2-14.

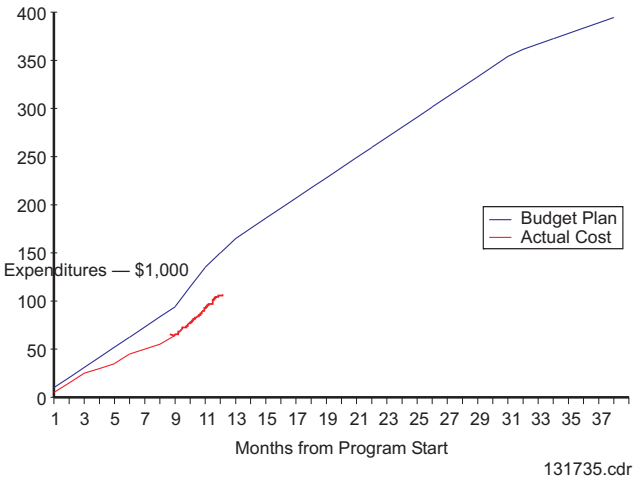

Figure 2-21. Task 201 Spending Plan

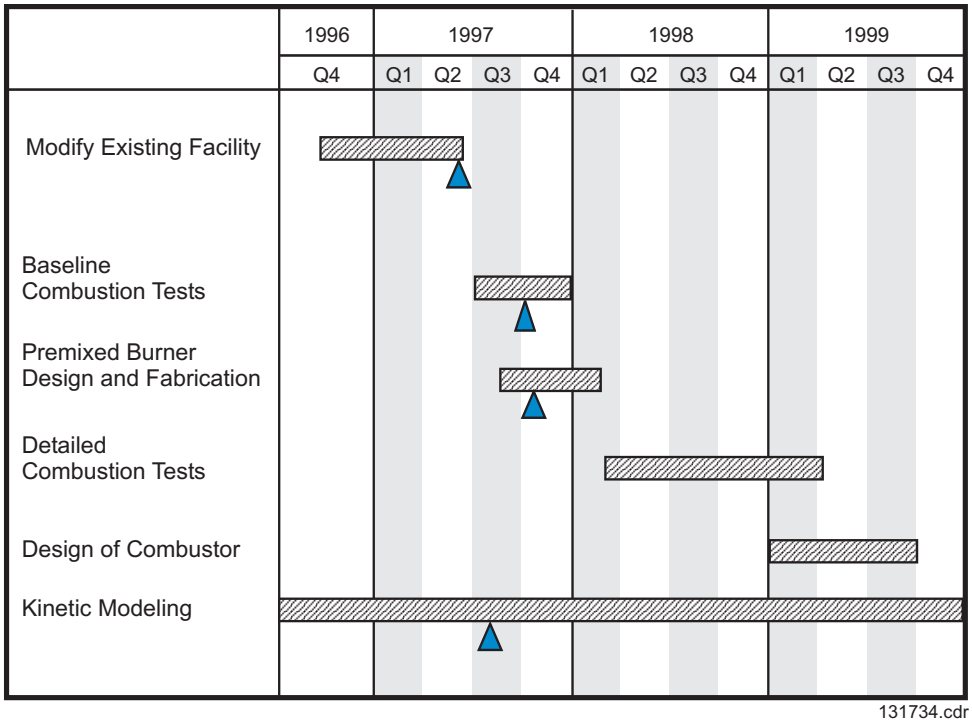

Figure 2-22. Task 201 Program Plan Schedule

2.2 ROLE OF HUMIDITY AND UNMIXEDNESS ON NO_X GENERATED IN A GAS TURBINE

Mitigation of the effect of unmixedness on NO_x emissions due to added moisture in a lean premixed flame has been studied. Calculations were performed at different equivalence ratios, pressures, inlet gas temperatures, and moisture levels. Modeling of unmixedness, or incomplete mixing, was performed by assuming a Gaussian distribution of fuel/air ratio, *f* in a network PSR or single PSR. Modeled data for dry flames compared well with the literature. A well-premixed flame formed the least amount of NO_x and the increased level of unmixedness led to higher NO_x emissions. Moisture levels not only led to a dramatic reduction in NO_x emissions, but also reduced significantly the effect of unmixedness on NO_x emissions

In recent years, much research has been directed towards the identification of gas turbine-based power systems that reduce the cost of generating electricity while increasing gas turbine efficiency and lowering emissions. One engine cycle under study is the advanced-cycle HAT. This cycle uses low temperature gas turbine exhaust heat, as well as heat from within the cycle (intercooler and aftercooler), to supply heated water to a saturator. Here, the compressor discharge is humidified and then the water-vapor laden air passes through a recuperator and combustor and then to the turbine. Both the increased mass flow of the humid air and the higher specific work of the mixture provide additional power, but require no additional compression work, resulting in efficiency and power output gains.

Moisture addition into air reduces NO_x emissions in premixed systems. Initial investigation of premixed systems revealed several different causes for the drastic reduction in NO_x emissions when moisture is increased.[1] Reduction in equilibrium temperature (T_{eq}), equivalence ratio change, dilution effect, O-atom suppression, heat release rate reduction, lowering peak temperatures and super-equilibrium O-atom are some of the mechanisms that may lead to lower NO_x. Besides reducing NO_x by the above-mentioned mechanisms, moisture may also mitigate the effect of unmixedness. Well-premixed systems form minimum NO_x and, as unmixedness increases, NO_x emissions also rise. Due to engineering design constraints, most practical combustion systems inherently have some level of unmixedness and, therefore, a NO_x penalty is realized. Variations (due to unmixedness) in the concentration profile lead to locally richer and leaner pockets in the mixture.[2]

In this paper, the effect of unmixedness on lean premixed flames has been studied computationally. The range of unmixedness numbers (*U*), for which the numerical calculations have been performed, are lower than compared to Mongia *et al.*[3] and Rutar *et al*.[4] For high *U*, some equivalence ratios in the analysis can exceed one, causing the results to be misleading due to the downward slope of NO_x formed in fuel rich zones. Pockets of mixtures at $\phi > 1$ eventually pass through $\phi = 1$, a high NO_x-producing region, and would generate higher NO_x than represented by the NO_x generation curves used in these analysis. Therefore, for high levels of unmixedness, the lowering of NO_x formed for a flame near $\phi = 1$ may be an artifact of the model.

2.2.1 Modeling

The flame was modeled using a literature reaction set, GRI-MECH 2.11, and its accompanying thermochemistry.[5] This reaction set consists of 49 species and 277 reactions and has been validated over a wide range of pressure and equivalence ratios. A PSR code, developed by Glarborg *et al.*,[6] and a network code, developed at UTRC, were

[1] Bhargava, A., Colket, M.B., Sowa, W., Castleton, K., and Maloney, D., "An Experimental and Modeling Study of Humid Air Premixed Flames," AMSE Paper No. 99-GT-8, 1999.

[2] Fric (1992), Mongia *et al*. (1996), and Rutar *et al*. (1997) have studied the effect of unmixedness on NO_x emissions.

[3] Mongia, R.K., Tomita, Eiji, Hsu, F.K., Talbot, L., Dibble, R.W., *Twenty-Sixth Symposium (International) on Combustion*, The Combustion Institute, Pittsburgh, p. 2749, 1996.

[4] Rutar, T., Martin, S.M., Nicol, D.G., Malte, P.C., Pratt, D.T., ASME Gas Turbine and Aeroengine Congress, Orlando, FL, 1997.

[5] Bowman, C.T., Hanson, R.K., Davidson, D.F., Gardiner, W.C., Jr., Lissianski, V., Smith, G.P., Golden, D.M., Frenklach, M., and Goldenberg, M., 1994, (http://www.me.berkeley.edu/gri_mech).

[6] Glarborg, P., Kee, R.J., Grcar, J.F., Miller, J.A., "PSR: A Fortran Compiler for Modeling Well-Stirred Reactors," *Sandia National Laboratories Report*, SAND86-8209, Livermore, CA, February 1986.

used to simulate combustion. Three different PSR arrangements are shown in Figure 2-23. Computations were made with the following:

- One PSR having a residence time of 5 ms (a)
- A series of PSRs consisting of a PSR having a residence time of 2 ms, followed by 25 small PSRs (each with a residence time of 0.12 ms) (b)
- A network of PSRs with recirculation to account for inhomogeneities in the combustor (c).

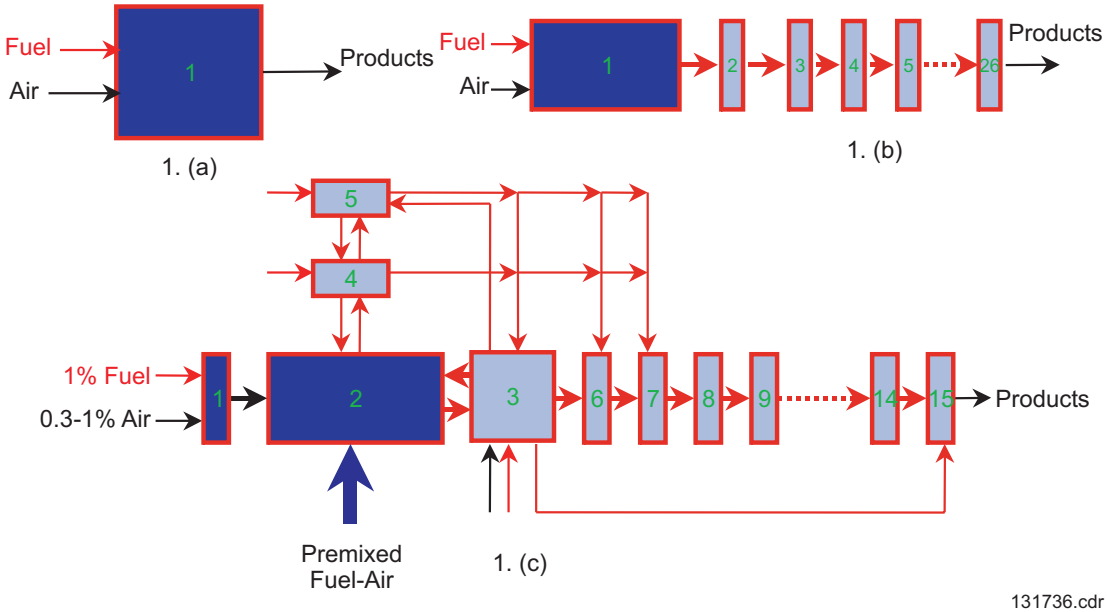

Figure 2-23. A Schematic of the Single PSR, a PSR Followed By 25 Smaller PSR, and a PSR Reactor Network Used to Model the Flame

The results from the three different models were compared with each other and with literature. The network closely simulates results from a single PSR (2 ms) followed by a single plug flow reactor (PFR) of 25 × 12 = 3 ms.

The network was designed to simulate the mixing and flow characteristics of experiments, as closely as possible.[1] A total of 15 reactors were used to represent the combustor. A small amount of fuel and air mixture was introduced in the first reactor. This represented the central pilot which provided the initial spark to light the flame and provide stability under lean conditions. The products of reactor 1 along with most of the fuel (75 to 79 percent) and air (80 to 90 percent) were introduced in reactor 2. Twenty percent of the fuel along with 10 percent of air enters the system through reactor 3. The combination of reactors 2 and 3 represent the inhomogeneity that may be present in the combustor. Reactors 2 and 3 represent the flame zone. Providing recycle between reactors 2 and 4, reactor 5 simulated recirculation. The rest of the reactors (6 to 15) represent the post-flame zone. Residence time varied with flow rates as air was fixed while the fuel flow rate was changed in order to achieve the required equivalence ratio. Residence time in each reactor was a function of the flow rate through the reactor and reactor volume. The residence time in all the reactors combined was between 4.5 and 6 ms.

Modeling of unmixedness or incomplete mixing was performed by assuming a Gaussian distribution of ϕ in the network PSR or a single PSR. Unmixedness number, U, was defined as

$$U = \frac{\sigma^2}{\bar{f}(1-\bar{f})}$$

[1] Bhargava, A., Colket, M.B., Sowa, W., Castleton, K., and Maloney, D., "An Experimental and Modeling Study of Humid Air Premixed Flames," AMSE Paper No. 99-GT-8, 1999.

Where σ is the standard deviation about the mean fuel air ratio (molar) and $\bar{f}$ is the mean fuel air ratio. The unmixedness number was changed numerically by varying σ. Figure 2-24 shows the possible distribution of ϕ at different σ. Higher σ would mean larger distribution of equivalence ratio present in the mixture, and therefore, higher unmixedness numbers.

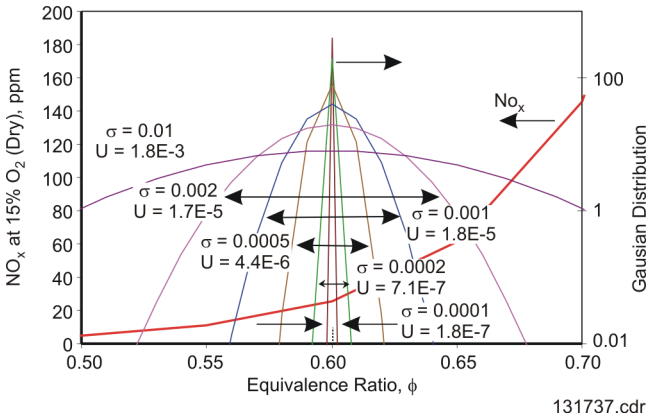

Figure 2-24. Predicted NO_x Emissions as a Function of ϕ and a Gaussian Distribution About ϕ = 0.6 at Different Standard Deviation (σ)

2.2.2 Results

Initially, calculations were performed using the three different reactor networks at zero level of unmixedness to compare the results among themselves and with the literature. Results from one PSR calculation and recirculation network compare well and are shown in Figure 2-25. These results, along with the series PSR model, compare well with the literature too. Figure 2-26 and Figure 2-27 show the comparison between the NO_x emissions for the recirculation network at different moisture levels for a flame at 13.6 atm, $T_{air+fuel}$= 730K and a T_{adb} of 1829K. For comparison purposes, results for a 1-atm flame ($T_{air+fuel}$ = 700K, and T_{adb} = 1800K) from Mongia *et al*. is also shown.[1] As seen in Figure 2-27, moisture does not only reduces NO_x formation, but the increase in NO_x emissions due to a higher level of unmixedness is also mitigated, as indicated by the slope of the NO_x generation line for different moisture contents in Figure 2-27. The same results are also observed in Figure 2-28, where NO_x emissions at 0 percent and 15 percent moisture content (in the air feed) are plotted at different sigma (σ, which represents different unmixedness levels). The broadness of the two bands, which are enclosed by NO_x generation at perfect mixing and at a σ of 0.1, indicates the variation of NO_x with varying unmixedness degrees. As seen in Figure 2-28, the band at 15 percent moisture content is thinner than that of the dry flame (even on a logarithmic scale) and clearly demonstrates that moisture in the flame mitigates the effect of unmixedness on NO_x emissions.

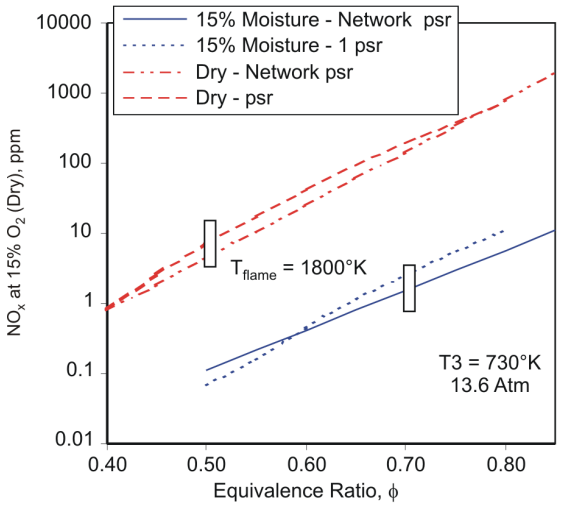

Figure 2-25. Comparison of the NO_x Formation With a Single PSR and Network PSR Under Dry and Humid Conditions

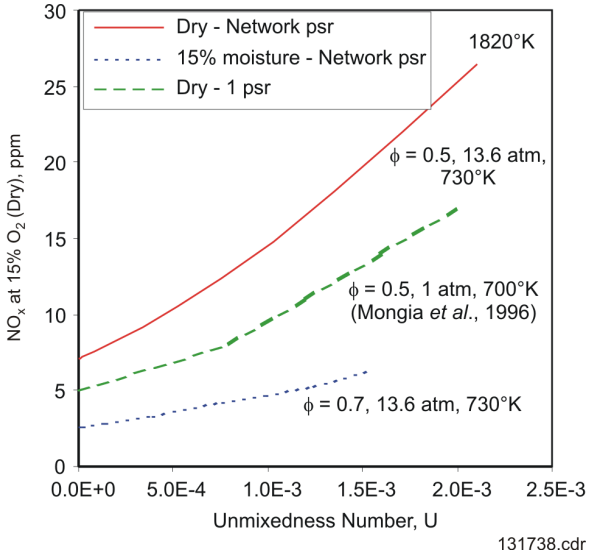

Figure 2-26. Comparison of the NO_x Formation at Different Levels of Unmixedness for Dry and Humid Flames at 1 Atm and 13.6 Atm and at a T_{adb} of 1820K

[1] Mongia, R.K., Tomita, Eiji, Hsu, F.K., Talbot, L., Dibble, R.W., *26th Symposium (International) on Combustion*, The Combustion Institute, Pittsburgh, p. 2749, 1996.

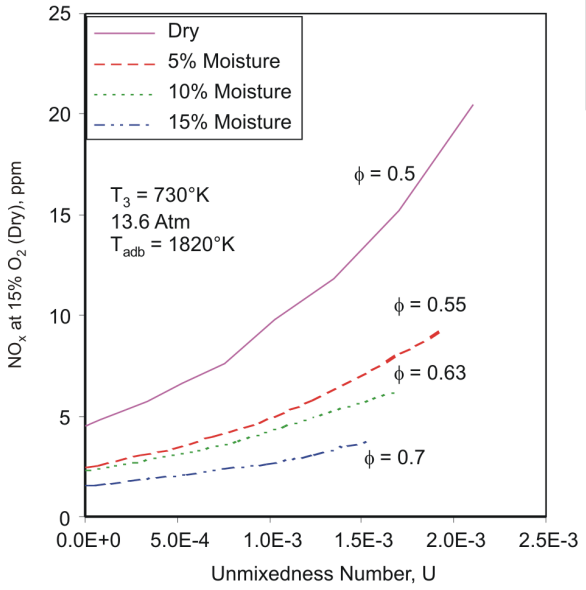

Figure 2-27. Comparison of the NO_x Formation in the Network PSR at Different Unmixedness Number (U) for Flames at 13.6 Atm, T_3 = 730K, T_{adb} of 1820K, and Different Moisture Conditions

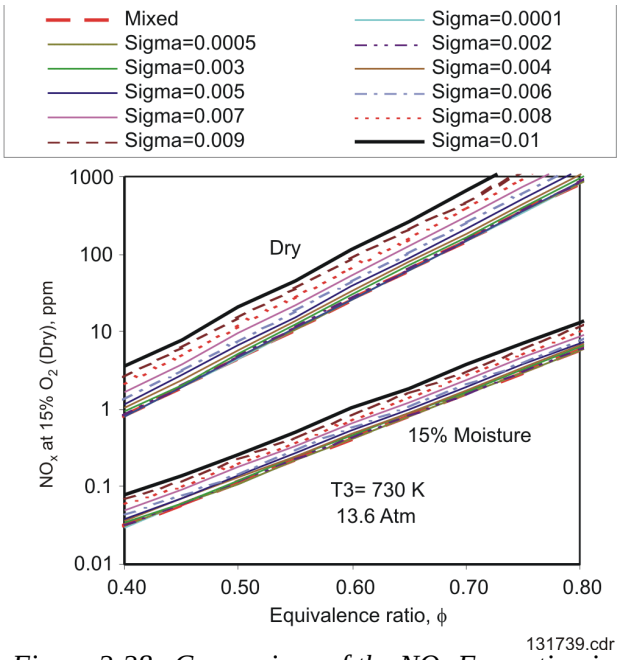

Figure 2-28. Comparison of the NO_x Formation in the Network PSR at Different Levels of Unmixedness for Flames at 13.6 Atm, T_3 = 730K, and Different Moisture Contents

2.3 PRESSURE EFFECT ON NO_X AND CO EMISSIONS IN INDUSTRIAL GAS TURBINES

In order to determine the effect of pressure on emissions and stability limit, an experimental and modeling study has been performed jointly by UTRC and the NETL. Experiments have been performed at lean conditions in the 100 to 400 psi range with two different nozzles. Measured NO_x and CO concentrations have been modeled with a PSR network using detailed chemistry. Agreement between the data and model predictions over a wide range of conditions indicate the consistency and reliability of the measured data and validity of the modeling approach.

Experiments were conducted at the NETL facility in Morgantown, West Virginia. A simple refractory combustor liner with a fuel/air premixing nozzle was used to map stability margins, emission levels of NO_x and CO, and combustion efficiency. Each experimental nozzle had a centerbody and wall pilot for flame stabilization. Data was collected at four different pressures of 100 psi, 200 psi, 300 psi, and 400 psi, and at different diffusion pilot and moisture levels. The premixing nozzle hardware could be easily lit and operated over a broad range of flame temperatures with minimal combustion generated noise. Two different nozzles designed at UTRC were used to determine pressure and nozzle effects.

Computations were made for comparison with the experiments. The GRI-MECH 2.11 kinetics and thermodynamic database was used for modeling the flame chemistry. A PSR network code, developed internally at UTRC, was used to create a network of PSRs to simulate the flame and combustor. A total of 10 to 15 reactors were used in the network. Residence time varied with the flow rates (air was fixed while fuel flow rate was varied to obtain the required equivalence ratio of ϕ).

Agreement between the measured and modeled NO_x (5 to 10 percent) was obtained, but the agreement between CO measurements (model predictions are higher by 30 to 50 percent) was not as good as for NO_x. The experimental data and the modeling predictions indicate that the NO_x emission functionality with pressure is dependent on both equivalence ratio and absolute pressure. The CO levels tend to go down with an increase in pressure as $P^{-0.5}$, at different equivalence ratios, which is consistent with an equilibrium analysis.

Achieving low NO_x emissions while maintaining acoustic stability over all power levels is essential to the viability and durability of any gas turbine.Continued reductions in governmental emissions regulations have been driving lean premixed combustion systems toward their lean stability limits. Yet turbines have to operate under a wide range of pressure in order to attain the desired operating characteristics. Several studies have been carried out in the last few years to ascertain the effect of pressure on lean premixed combustion in gas turbines.

- Correa (1992) performed a review on NO_x formation under gas turbine conditions.The results from his study indicate a diminishing influence of pressure on NO_x in lean premixed combustion. If expressed as (NO_x/NO_x at 1 atm) = p^m, then *m* approaches zero at low equivalence ratios and is larger than zero for rich flames.
- Leonard and Stegmaier concluded that NO_x emissions in well-premixed flames are independent of pressure.[1] They indicate that with well-designed lean premixed systems, it is possible to operate a combustor from 1 atm to 30 atm without any significant change in NO_x emissions. The authors do state that at higher equivalence ratio, NO_x emissions do show slight pressure dependence that increases with increasing ϕ.
- Mongia *et al*. studied the effect of unmixedness on NO_x emissions at different pressures.[2] Their simulation at an equivalence ratio of 0.5 indicated that at low unmixedness levels, NO_x emissions are independent of pressure; but as the unmixedness level is increased, pressure dependence increases. Their conclusions were in agreement with the observations made by Leonard and Stegmaier.
- Steele *et al*. (1996) performed experiments with a high-pressure jet-stirred reactor in the pressure range of 1 to 7.1 atm. They found a slightly negative dependence of pressure on NO_x emissions (NO_x equivalent to $P^{-0.20}$). They also investigated the effect of residence time on NO_x emissions at different pressures.
- Rutar *et al*. investigated the effect of pressure and unmixedness on NO_x emissions.[3] Their model predicted very little pressure dependence (for pressure between 10 to 14 atm) for a wide range of equivalence ratio and unmixedness levels.

In an effort to control emissions over the entire operating range, lean premixed combustion systems are frequently designed to maintain constant flame temperature as the engine changes power levels. In all cases, stability of the lean premixed combustion system relies upon the ability of the premixing fuel injector to maintain stable combustion while it is subjected to changes in nozzle equivalence ratio, inlet air temperature, and inlet air pressure. Furthermore, advanced high-efficiency engines are anticipated to operate at significantly higher pressures than conventional engines. The sensitivity of the premixer to these pressure changes forms the basis of this study. This paper examines the emission characteristics of two fuel/air mixing swirler designs (aerodynamic and bluff body flame stabilization designs). These configurations are based on earlier TENs.[4] Besides studying the effect of pressure, the influence of premixing, scale-up, and moisture content on CO and NO_x levels has also been studied. NO_x and CO emissions were then modeled using PSR network. As shown in a previous paper, the model was able to capture features of NO_x and CO generation from combinations of the main flame, a premixed central pilot, a diffuser flame pilot, and different humidity levels.

[1] Leonard G. and Stegmaier, J.,"Development of an Aeroderivative Gas Turbine Dry Low NO_x Emissions Combustion System," ASME Paper No. 93-GT-288, 1994.

[2] Mongia, R.K., Tomita, Eiji, Hsu, F.K., Talbot, L., Dibble, R.W., *Twenty-Sixth Symposium (International) on Combustion*, The Combustion Institute, Pittsburgh, p. 2749, 1996.

[3] Rutar, T., Martin, S.M., Nicol, D.G., Malte, P. C., Pratt, D.T., ASME Gas Turbine and Aeroengine Congress, Orlando, FL, 1997.

[4] Snyder, T., Rosfjord, T., McVey, J., Hu, A., and Schlein, B., "Emission and Performance of a Lean-Premixed Gas Fuel Injection System for Aeroderivative Gas Turbine Engines," ASME Paper No. 94-GT-234, 1994.

2.3.1 Experiments

Figure 2-29 details an earlier aerodynamic nozzle design whose centerbody was modified for the present series of tests (Figure 2-30) through the addition of a bluff plate and diffusion pilot in lieu of the central premixing tube.Although the addition of a centerbody diffusion pilot will negatively impact NO_x performance, it was shown to be invaluable in mitigating acoustic instabilities over the power range relative to its predecessor's premixed version.[1] Because the design relies upon a tangential entry of air for enhanced mixing, it will be referred to as a TEN.

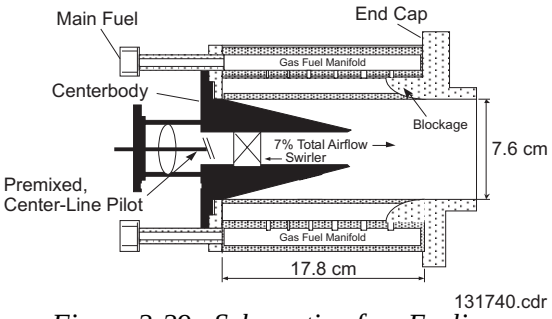

Figure 2-29. Schematic of an Earlier Aerodynamic Nozzle

The second nozzle (Figure 2-31) tested as part of the pressure scaling exercise differed from the TEN in that it featured an axial mixer, as opposed to a tangential entry or radial swirler design.[2] For this reason, it will be referred to as the axial nozzle. Fuel is issued at right angles into the incoming flow through fuel spokes arranged radially around the centerbody. Centerbody tip piloting and cooling schemes were identical to its tangential-body counterpart. Both nozzles were designed with an identical swirl and effective flow area (ACd)[3] of 45 degrees and 12.9 cm^2, respectively. Consult Figure 2-31 for a sketch of the axial swirler.

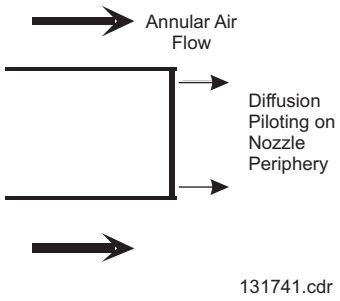

Figure 2-30. Modified Centerbody for the Tangential Entry Nozzle

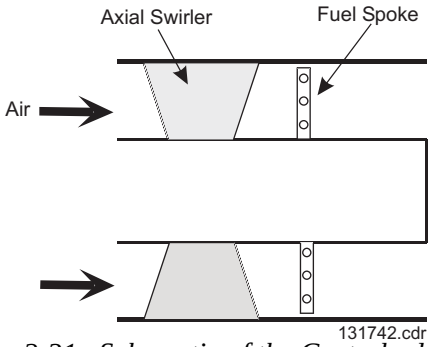

Figure 2-31. Schematic of the Centerbody End Detail for the Axial Nozzles

All experiments were conducted in the Low Emissions Combustor Test and Research (LECTR) facility located at the NETL (Figure 2-32). Details of the experimental procedure have been described in an earlier publication.[4]

2.3.2 Modeling

Experimental data covered a wide range of equivalence ratios and pressure and were performed with two different nozzles. The experimental results for the axial nozzle are indicated in Figure 2-33. The data for the TEN is similar and will be discussed along with the axial nozzle in the next section. Observations made from the experiments include the following:

[1] Kendrick, D.W., Anderson, T.J., Sowa, W.A., and Snyder, T.S., "Acoustic Sensitivities of Lean-Premixed Fuel Injectors in A Single Nozzle Rig," AMSE Paper No. 98-GT-382.

[2] Snyder, T., Rosfjord, T., McVey, J., Hu, A., and Schlein, B., "Emission and Performance of a Lean-Premixed Gas Fuel Injection System for Aeroderivative Gas Turbine Engines," ASME Paper No. 94-GT-234, 1994.

[3] ACd is an empirical determination of the product of flow area and discharge coefficient.

[4] Bhargava, A., Colket, M.B., Sowa, W., Castleton, K., and Maloney, D., "An Experimental and Modeling Study of Humid Air Premixed Flames," AMSE Paper No. 99-GT-8, 1999.

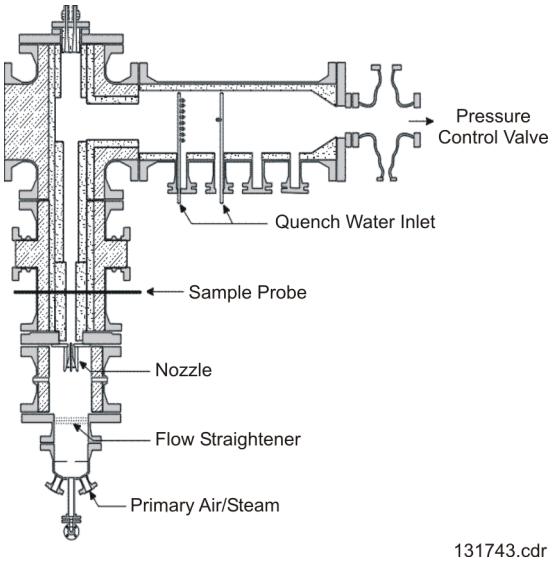

Figure 2-32. A Schematic of the Experimental Setup

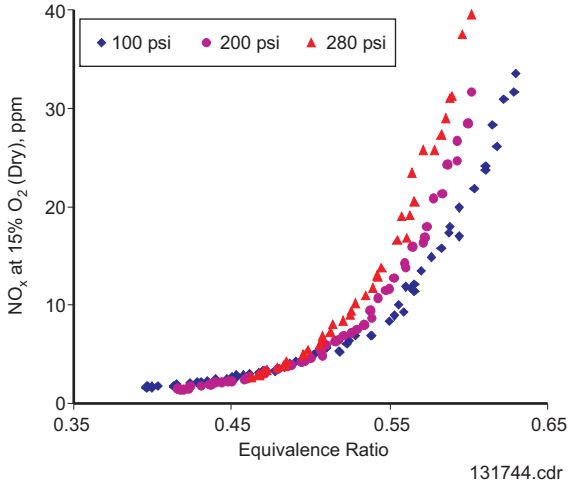

Figure 2-33. NO_x Emissions at Different Psi Levels

- NO_x emissions appear to be nearly pressure independent at low-equivalence ratio ($\phi < 0.5$). However, plots of log(NO_x) and log(P) yield low, but measurable pressure dependence (Figure 2-34).
- Pressure dependence (NO_x equivalent to P^n) on NO_x emissions increase with an increase in ϕ (as shown in Figure 2-34) labeled experimental, for both nozzles. For the axial nozzle, it levels at around 0.55. For the TEN, it seems to be steadying at n = 0.5 for an equivalence ratio around 0.5, but it starts rising again above $\phi = 0.55$.
- CO emissions go down with increases in pressure. While this trend was clearly visible for the axial nozzle, results for the TEN show a less clear trend or dependence of CO emissions on pressure.
- The two nozzles indicate different pressure characteristics. This might be due to different mixing characteristics exhibited by the two nozzles.
- The axial nozzle shows small pressure effect until reaching an equivalence ratio of 0.52, but shows higher NO_x than the TEN.
- The TEN shows a pressure dependence at lower equivalence ratios (near 0.45), but indicates similar emissions numbers at 200 psi and 300 psi.

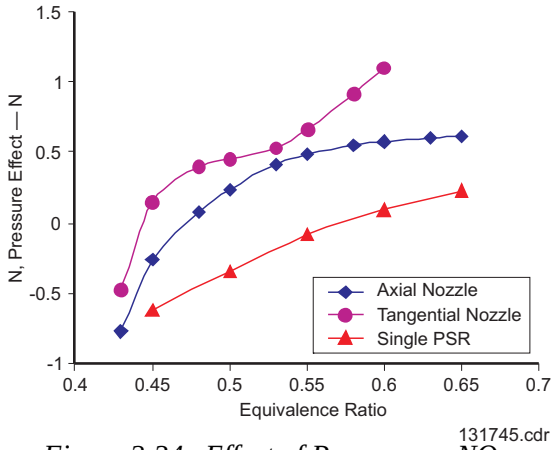

Figure 2-34. Effect of Pressure on NO_x Emissions as a Function of Equivalence Ratio

The experiments were modeled using a literature reaction set, GRI-MECH 2.11, and its accompanying thermochemistry.[1] The GRI-MECH 2.11 reaction set consists of 49 species and 277 reactions and has been validated over a wide range of pressure and equivalence ratios. A PSR network code developed at UTRC was used to simulate the combustor. The basis for the network PSR code is the Chemkin PSR model.[2]

[1] Bowman, C.T., Hanson, R.K., Davidson, D.F., Gardiner, W.C., Jr., Lissianski, V., Smith, G.P., Golden, D.M., Frenklach, M., and Goldenberg, M., 1994 (http://www.me.berkeley.edu/gri_mech).

[2] Glarborg, P., Kee, R.J., Grcar, J.F., Miller, J.A., "PSR: A Fortran Compiler for Modeling Well-Stirred Reactors," *Sandia National Laboratories Report*, SAND86-8209, Livermore, CA, February 1986.

In an earlier paper, a 15-reactor network design was used to model the effect of moisture and pilot level on NO_x emissions.[1] At first the same reactor configuration was used in an attempt to model the effect of pressure on NO_x emissions. This reactor configuration failed to capture the pressure effect seen experimentally. Therefore, it was decided to restart the modeling exercise, or design a reactor network, from the beginning. The first step was to model the process using a single PSR.Comparison between the model predictions from a single PSR calculation at different pressures and the experimental data for the TEN is shown in Figure 2-35. As seen in Figure 2-35, a single PSR fails to predict the pressure effect on NO_x formation as seen in the experiment. The single PSR model predicts a negative pressure dependence at equivalence ratios less than 0.55, while at higher equivalence ratios, it shows only a slight positive dependence.

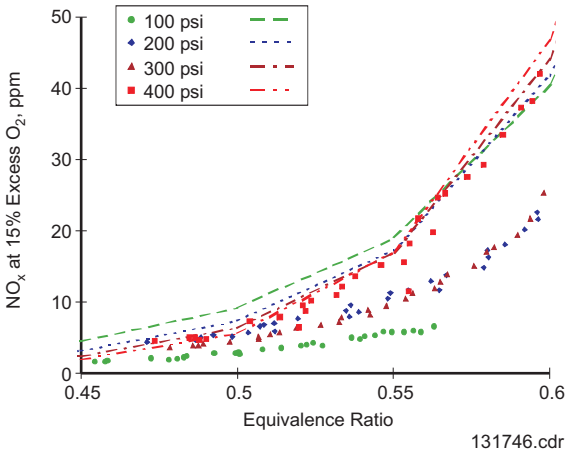

Figure 2-35. NO_x Predictions at Different Pressures Using a Single PSR

The next step was to design a reactor network that would predict NO_x emissions comparable to the experimental data at one pressure as the equivalence ratio is varied. Figure 2-36 and Figure 2-37 depict the two reactor networks that were designed to predict emissions that match well with experiments at 200 psi. The same network was then used, without changing the distribution of the fuel/air flow, to predict emissions at the other pressures. The two networks were unable to predict variations in emissions with pressure. No single reactor network was able to predict pressure dependence (no reactor single network with the same flow distribution at the different pressures). The next logical step was to keep the network design the same, but vary the flow distribution among the reactors at different pressures. This would simulate a situation wherein changes in pressure would lead to changes in mixing and flow characteristics in the combustor. This approach was more successful than earlier network designs and resulted in model predictions at the different pressures in line with experiments.

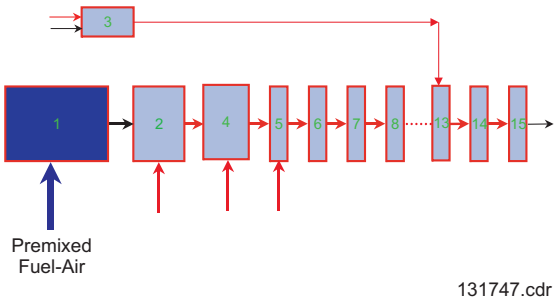

Figure 2-36. Schematic of the PSR Reactor Network Used To Model the Flow Distribution Varied With Pressure

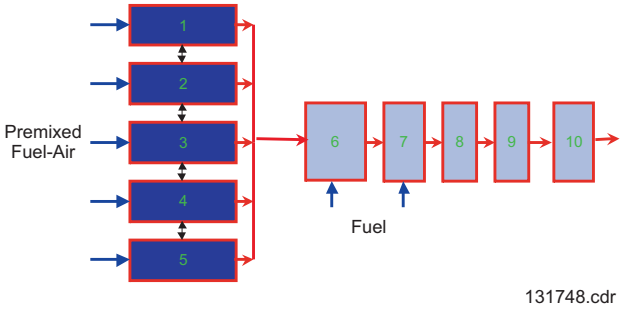

Figure 2-37. Schematic of the PSR Reactor Network Used To Predict NO_x Emissions at Different Pressures

A modified version of the network shown in Figure 2-36 was then used to model the experimental data. The modification made was that the flow distribution was varied with pressure. The residence time in all the reactors combined was between 5.5 and 6 ms. The network structure remained the same for all conditions, except the amount of fuel flowing in reactors 1, 2, 4, and 5. A different flow distribution was used to simulate the changes in flow characteristics and mixing that may arise due to variation in pressure. The differences in the distribution of fuel and air flows in the different reactors at different pressures are summarized in Table 2-1. As seen in Table 2-1**,** the flow distribution used in the two nozzles to predict NO_x emissions at the same pressure is slightly different.This indicates that the flow distribution in the two nozzles is slightly different. This exercise led to the development of the network shown in Figure 2-37.

[1] Bhargava, A., Colket, M. B., Sowa, W., Castleton, K., and Maloney, D., "An Experimental and Modeling Study of Humid Air Premixed Flames," AMSE Paper No. 99-GT-8, 1999.

Table 2-1. Distribution of Fuel and Air in the Network for the Two Nozzles Shown in Figure 2-36

	Reactor Number				
Pressure	***1***	***2***	***3***	***4***	***5***
Axial – 100 psi	0.75	0.1	0.005	0.145	
	0.997	0	0.003	0	
Axial – 200 psi	0.85	0.1	0.005	0.045	
	0.997	0	0.003	0	
Axial – 300 psi	0.95	0.045	0.005	0	
	0.997	0	0.003	0	
Tangential – 100 psi	0.695	0.1	0.005	0.1	0.1
	0.99	0	0.003	0	0
Tangential – 200 psi	0.795	0.1	0.005	0.1	0
	0.997	0	0.003	0	0
Tangential – 300 psi	0.895	0	0.005	0	0
	0.997	0	0.003	0	0
Tangential – 400 psi	0.995	0	0.005	0	0
	0.997	0	0.003	0	0

The network shown in Figure 2-37 was modified and used to predict NO_x emissions at the different pressures. Previous modeling exercises indicated that there might be some changes in mixedness levels and flow distribution with pressure changes. To incorporate these effects in the model, fuel flow in reactors 1 to 5 was varied. These variations are indicated in Table 2-2. All of the air was distributed equally in reactors 1 to 5. For the axial nozzle, 90 percent of the fuel is introduced through reactors 1 to 5, while 10 percent of the fuel enters through reactor 6. For the TEN, 80 percent of the fuel is introduced through reactors 1 to 5, while the remaining 20 percent of the fuel enters through reactors 6 and 7. The new PSR network had 10 reactors. The residence time in all the reactors combined was still between 5.5 and 6 ms.

Table 2-2. Distribution of Fuel in Reactors 1 to 5 in the Network Shown in Figure 2-37

	Reactor Number				
Pressure	***1***	***2***	***3***	***4***	***5***
Axial – 100 psi	0.18	0.18	0.18	0.18	0.18
Axial – 200 psi	0.16	0.17	0.18	0.19	0.20
Axial – 300 psi	0.14	0.16	0.18	0.20	0.22
Tangential – 100 psi	0.16	0.16	0.16	0.16	0.16
Tangential – 200 psi	0.13	0.13	1.18	0.16	0.22
Tangential – 300 psi	0.13	0.13	0.15	0.16	0.23
Tangential – 400 psi	0.13	0.13	0.15	0.15	0.24

2.3.3 Results

Numerous experiments were performed to ascertain the effect of pressure, moisture content, and pilot levels on the amount of NO_x and CO formed at different equivalence ratios. The effect of pilot level (0, 1, 3, and 5 percent fuel) and moisture level (0, 5, 10, and 15 percent water in the air by mass) on NO_x and CO emissions have been

reported earlier.[1] All experiments indicate that dependence of NO_x emissions on pressure is a function of equivalence ratio. As shown in Figure 2-34**,** dependence of NO_x on pressure can be expressed as $NO_x \sim P^n$, where *n* varies from -0.18 to 1.6 for the TEN, and from -0.77 to 0.61 for the axial nozzle, as the equivalence ratio increases from 0.43 to 0.65. The NO_x variation with pressure is much more significant for the TEN than for the axial nozzle.

Different reactor configurations were used to model pressure effect on NO_x emissions. The first reactor configuration to be used was the one designed for modeling moisture and pilot level effects on NO_x emissions.[2] The modeling results indicated that NO_x emissions show little pressure dependence in the 0.4 to 0.55 equivalence ratio range. Above 0.55, NO_x emissions increase as the pressure is increased. The pressure dependence increases as equivalence ratio increases. As compared to experimental data, modeling results indicate the right trend ($NO_x = P^n$; *n* increasing with equivalence ratio), but the point at which NO_x emissions begin to show pressure dependence is not well predicted. The same behavior in NO_x emissions was obtained when the calculation was performed with a single PSR. In fact, according to Figure 2-35, a single PSR has a negative pressure dependence at low-equivalence ratios (0.45 and lower) and a subsequent change to positive dependence at higher equivalence ratios. The trends seen in the experiment and subsequent modeling indicate that there might be regions of locally higher equivalence ratio in the rig (unmixedness and flow characteristics related to pressure) that exhibit stronger pressure dependence than seen at a lower overall equivalence ratio. Therefore, to model pressure effects, pressure dependent flow characteristics and unmixedness need to be treated.

Two different reactor networks were designed specifically to model pressure effect on NO_x emissions. These reactor networks are shown in Figure 2-36 and Figure 2-37. Both reactor networks were designed to model NO_x emissions at 100 psi and, with fine tuning of the network, a good match with the experiments was obtained. The same network was then used to model NO_x emissions at the different pressures. Without flow modifications, both networks failed to capture pressure effects, especially the advent of the point at which NO_x emissions diverge with pressure, again indicating that pressure is affecting NOx formation rate. Both the networks were then modified in order to model changes in mixedness that may arise with pressure changes.

The final reactor design used to model is shown in Figure 2-37. Changes in fuel flow distribution were necessary to explain the variation in NO_x emissions with pressure. The inability to model the pressure effects without changing the flow distribution, such as modeling NO_x emissions at the different pressures with the same network configuration, can be attributed to several factors:

- There is a change in mixedness level with pressure.
- Variation in pressure leads to changes in flow distribution.
- The kinetic mechanism that is used to model the process fails to address changes in reaction kinetics that may be introduced by pressure changes.
- Limitations to the use of PSR models in describing performance of a lean premixed combustor; pressure may lead to changes in flame geometry, size, and characteristics that may be difficult to model with the PSR network.
- Uncertainties in the experimental data, especially at lower equivalence ratios.

[1] Bhargava, A., Colket, M. B., Sowa, W., Castleton, K., and Maloney, D., "An Experimental and Modeling Study of Humid Air Premixed Flames," AMSE Paper No. 99-GT-8, 1999.

[2] *Ibid*.

As seen in Figure 2-38 and Figure 2-39, the modified network is able to predict the shape and magnitude of NO_x emissions at the different pressure conditions for an equivalence ratio between 0.45 and 0.65. The distribution of the fuel among the various reactors was varied with pressure and is shown in Table 2-2. In order to model pressure effects, the fuel distribution in reactors 1 to 5 (i.e., the flame zone) was continuously changed, while the overall equivalence ratio remained the same. Specifically, as the pressure is increased, the network PSR model becomes more unmixed. As seen in Table 2-2, at 100 psi, the system has been modeled with minimum unmixedness (with a narrow distribution of equivalence ratio among reactors 1 to 5). At 400 psi, a higher degree of unmixedness was used in order to predict experimental NO_x (equivalence ratio varied by more than 50 percent of the overall ϕ). This indicates that unmixedness levels increased with an increase in pressure. Favorable comparison between experimental data and model predictions was made using the above mentioned fuel flow distribution criterion for both nozzles at pressures ranging from 100 to 400 psi.

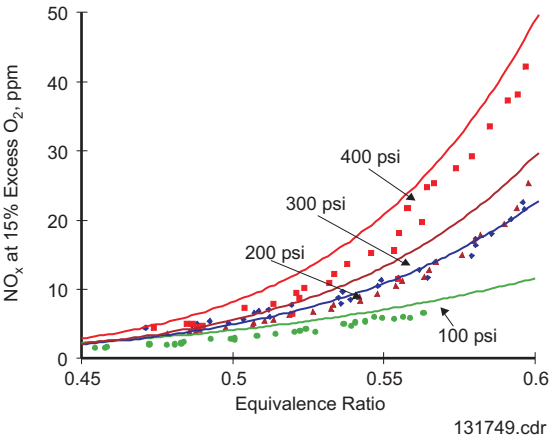

Figure 2-38. NO_x Predictions for a Tangential Entry Nozzle

Some subtle differences were observed for the two nozzles. The emissions for 100 psi were much lower for the TEN compared to the axial nozzle. While the trend with pressure increase was the same for the two nozzles, the magnitude of increase in NO_x emissions was smaller for the TEN than for the axial nozzle. As indicated earlier, both nozzles were modeled with the same network design with some minor flow variations. Experiments were also performed in order to ascertain the effect of scale-up on NO_x emissions. These effects have been discussed and modeled using a PSR network design similar to the one used for pressure effects.[1]

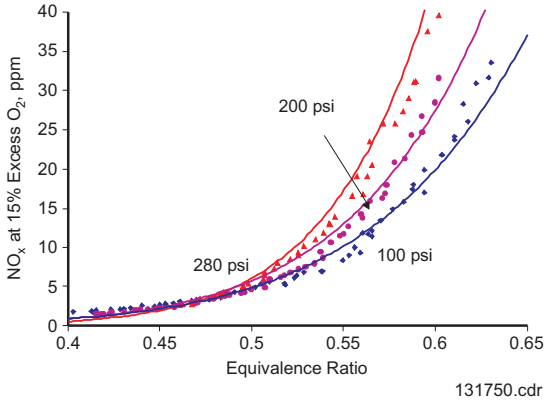

Figure 2-39. NO_x Model Predictions for an Axial Nozzle Using the Modified Version of the PSR Network Shown in Figure 2-37

A study to investigate the effect of pressure on the three routes of NO_x formation, the *Zeldovich* NO_x pathway, the *Fenimore* NO_x pathway, and the *N_2O* pathway, was performed. The NO_x formation reactions were divided into these three different, but coupled, groups in the following manner:

- *Zeldovich* or *Thermal* NO_x mechanism,[2] as extended by Bowman and Seery[3] — The NO_x is initiated by the reaction of N_2 with the O atom. This well-established, three-step reaction sequence is the dominant NO_x-forming route at temperatures above 2950°F. *Zeldovich*, or *Thermal* NO_x mechanism, was suppressed by making the $N_2 + O \leftrightarrow N + NO$ reaction proceed in the reverse direction only.
- *N_2O* mechanism, consisting of reactions involving N_2O that form NO — The NO_x formed through this mechanism can be effectively suppressed by making the N_2O (+M) $\rightarrow N_2 + O$ (+M) proceed in the forward direction only.

[1] Kendrick, D. W., Bhargava, A., Colket, M. B., Sowa, W. A., Maloney, D. J., and Casleton. K. H., "NO_x Scaling Characteristics for Industrial Gas Turbine Fuel Injectors," Proceedings of ASME Turbo Expo, Paper No. 2000-GT-98, 2000.

[2] Zeldovich, J., "The Oxidation of Nitrogen Combustion and Explosions," *Acta Physicochimica*, URSS, 21, 577, 1946.

[3] Bowman, C. T., and Seery, D. J., *Emissions from Continuous Combustion Systems*, (W. Cornelius and W.G. Agnew, eds.), p. 123, 1972.

- *Fenimore* NO_x mechanism — All NO_x forming reactions, beside the *Zeldovich* and N_2O pathways, are included in this route. The main steps influencing this reaction sequence are $N_2 + CH = HCN + N$, $N_2 + CH_2 = HCN + NH$, and other reactions involving N_2 and hydrocarbon radicals. This extensive sequence was suppressed by inhibiting the forward rates for reactions between hydrocarbon fragments and molecular nitrogen.

To study the contribution of each pathway, the other two channels were suppressed. Therefore, in order to analyze the importance of the *Zeldovich* mechanism, NO_x formation through the *Fenimore* and N_2O mechanisms was removed. Similar computations were performed to evaluate the importance of the *Fenimore* and N_2O mechanisms. Initially, this analysis was performed with a single PSR. This calculation indicated little difference in pressure dependence on the three routes; NO_x formation through the three routes remained the same as the pressure was changed from 100 psi to 400 psi. Analysis with the modified reactor network was then performed and it showed that the effect of pressure on the three pathways was different. As seen in Figure 2-40**,** this analysis indicates that pressure effect is most significant; in fact, more significant than the effect on overall NO_x formation of the *Zeldovich* mechanism followed by the *Fenimore* and the *N2O* mechanisms, in that order. Even though the total amount of NO_x generated by the N_2O mechanism was much more than with the *Fenimore* pathway, the change in NO_x production rate with pressure was caused more by the *Fenimore* mechanism than by the N_2O mechanism.

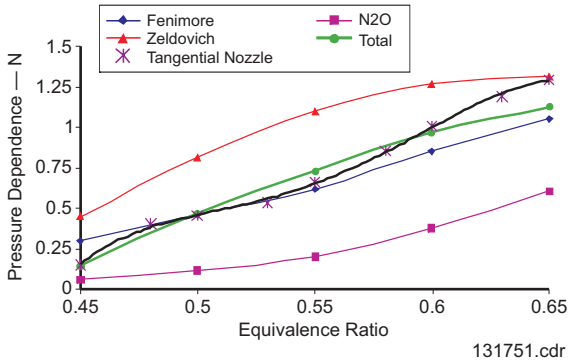

Figure 2-40. Effect of Pressure on the Different NO_x Formation Pathways

While NO_x predictions are good, predictions for CO are off by as much as 50 percent. This trend, shown in Figure 2-41 and Figure 2-42 for the two nozzles, was observed in all simulations. An increase in CO concentration as the pressure is decreased was clearly evident in the axial nozzle, though this trend was not very apparent in the TEN. Based on overall equilibrium, $CO + \frac{1}{2} O_2 \rightarrow CO_2$, the pressure dependence of CO should follow $X_{CO} \propto P^{\frac{1}{2}} X_{CO2} X_{O2}^{-\frac{1}{2}}$. With the modified reactor network it was possible to predict reduction in CO with increase in pressure. The CO predictions were close to the equilibrium levels and highly sensitive to the mixture (air and fuel) temperature. A small (equivalent 50°F) discrepancy in the measured air/fuel temperature can account for the difference

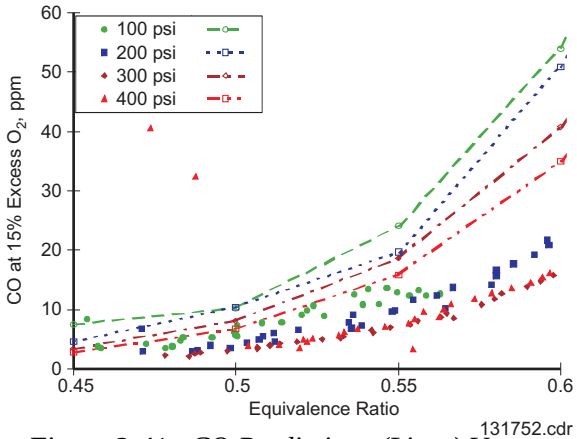

Figure 2-41. CO Predictions (Lines) Versus Experimental Data (Symbols) for the Tangential Entry Nozzle

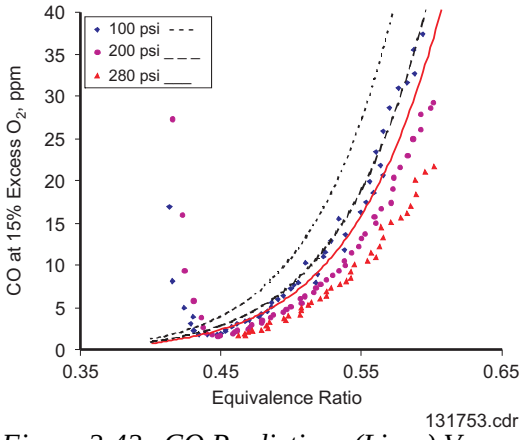

Figure 2-42. CO Predictions (Lines) Versus Experimental Data (Symbols) for the Axial Nozzle

in the measured and computed CO. Alternatively, the sample probe's impact on the CO may explain the lower experimental values. A study of the probe effect on CO measurements has been presented by Nguyen *et al*.[1] They measured CO in an atmospheric pressure flame using line-of-sight tunable diode laser absorption and extractive probe sampling and compared it with CO prediction using a numerical model. They found that the measurements made with extractive sampling technique were as much as ten times less than the laser-based experiments for fuel lean flames; whereas, for fuel-rich flames, the agreement between the two techniques was good.

2.3.4 Conclusions

Data was collected over a wide range of equivalence ratios and pressures for the two different nozzles. The TEN, at lower pressures, has lower NO_x emissions than the axial nozzle; but at higher pressures, lower NO_x was measured in the axial nozzle. Other trends in the measured data have been used to evaluate the effect of various parameters, like pressure, equivalence ratio, and nozzle design, on NO_x and CO emissions. While NO_x emissions go up with pressure in both nozzles, CO emissions go down with pressure (this effect is more apparent in the axial nozzle than in the TEN). The data has also been modeled using a PSR network and a literature reaction set. Agreement between the data and modeling suggests that the approach used for modeling the combustor is useful. The PSR reactor model that was used to model the emissions and the modifications that needed to be made to the PSR network to model NO_x emissions at the different pressures suggest there may be a change in mixedness level with pressure. There may also be changes in flow distribution with pressure. The kinetic mechanism that is used to model the process is inadequate, as it fails to address changes in reaction kinetics that may be introduced by pressure changes. Pressure may also bring about a change in the flame geometry, size, and characteristics that are difficult to model using the present approach.

2.4 AN EXPERIMENTAL AND MODELING STUDY OF HUMID AIR PREMIXED FLAMES

An experimental and modeling study has been performed jointly by UTRC and the NETL to determine the effect of humidity in the combustion air on emissions and stability limits of gas turbine premixed flames.This study focuses on developing gas turbine combustor design criteria for the HAT cycle. The experiments were conducted at several moisture levels (0, 5, 10, and 15 percent by mass in the air) at a total pressure of 200 psi, different pilot levels (0, 1, 3, and 5 percent total fuel), and several equivalence ratios (0.4 to 0.8, depending on the moisture levels). The moisture levels were achieved by injecting steam into dry air well upstream of the fuel/air premixing nozzle. Computations were made for comparison to the experiments using GRI-MECH 2.11 kinetics and thermodynamic database for modeling the flame chemistry. A PSR network code was used to create a network of PSRs to simulate the flame. Excellent agreement between the measured and modeled NO_x (5 to 10 percent) was obtained. Trends of added moisture reducing NO_x and the effects of equivalence ratios and piloting level were well predicted. The CO predictions were higher by about 30 to 50 percent. The CO discrepancies are attributed to in-probe oxidation. The agreement between the data and model predictions over a wide range of conditions indicate the consistency and reliability of the measured data and usefulness of the modeling approach. An analysis of NO_x formation revealed that at constant equilibrium temperature, T_{eq}, the presence of steam leads to lower O-atom concentration that reduces *Zeldovich* and N_2O NO_x, while higher OH-atom concentration reduces *Fenimore* NO_x.

The Advanced Turbine System (ATS) Program sponsored by the DOE has among its objectives the development of gas turbine-based power systems that will reduce the cost of generating electricity, while increasing gas turbine efficiency and lowering emissions.

[1] Nguyen, Q.V., Edgar, B.L., Dibble, R.W., and Gulati, A., "Experimental and Numerical Comparison of Extractive and In Situ Laser Measurements of Non-Equilibrium Carbon Monoxide in Lean-Premixed Gas Combustion," *Combustion and Flame*, 100:395-406, 1995.

One engine cycle under study is the advanced-cycle HAT.[1] The definition and preliminary engineering of a HAT cycle that is based on aeroderivative engine technology was undertaken by UTC, Fluor Daniel, Inc., Texaco, and EPRI in 1991.[2] This cycle, shown simplistically in Figure 2-43, uses low temperature gas turbine exhaust heat, as well as heat from within the cycle (intercooler and aftercooler) to supply heated water to a saturator. Here, the compressor discharge is humidified, then the water vapor laden air passes through a recuperator and combustor, and then to the turbine. Both the increased mass flow of the humid air and higher specific enthalpy of the mixture provide additional power, but require no additional compression work from the turbine, resulting in efficiency and power output gains.

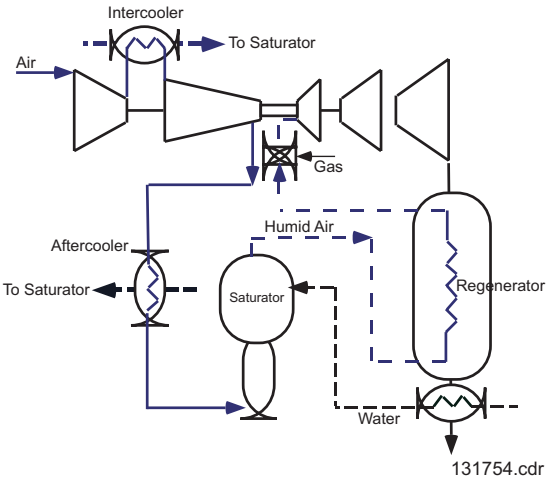

Figure 2-43. A Schematic of the HAT Cycle

Several preliminary design studies have been performed on the HAT cycle.[3] HAT cycles were identified that had over 60 percent efficiency and emissions estimates that met the DOE goals. These emissions, however, were based on estimates of NO_x formation in the presence of water vapor. A series of experimental and modeling studies, described in the following sections, have been performed to characterize the effect of humidity on the emissions and combustion stability of HAT cycle configurations.

Several studies have been undertaken to understand the influence of moisture in air on NO_x and CO emissions. Dryer,[4] Miyauchi *et al.*,[5] Touchton,[6] Blevins and Roby,[7] and Meyer and Grienche[8] have all investigated the influence of moisture on emissions under different operating conditions. Most of these studies have dealt with diffusion flames. With diffusion flames, it was concluded that almost all of the NO_x reduction took place due to a reduction in the flame temperature. In a diffusion flame, where the overall equivalence ratio may be as low as 0.4 to 0.5, the high temperature stoichiometric regions are the primary source of NO_x. Moisture reduces the peak temperatures, which brings about a drastic reduction in NO_x emissions. Not much work has been carried out for premixed systems, required to meet low emissions regulation. Moisture addition into the air reduces NO_x emissions even in premixed systems. Initial investigation of premixed systems revealed several different pathways, which may account for the drastic reduction in NO_x emissions when moisture is increased. Some of the possible routes include:

- Reduction in equilibrium temperature (T_{eq})
- Reduction of peak temperature of pilot diffusion flames
- Equivalence ratio change in humid air flames for constant T_{eq} (as the moisture level increases, the equivalence ratio must increase resulting in a lower O-atom concentration)
- Dilution effect (in humid air flames for constant T_{eq}, as the moisture level increases, the O-atom and N_2 mole fraction ratios decrease.)

[1] Rao, A.D., "Process for Producing Power," U.S. Patent 4,829,763, May 1989.

[2] TurboPower & Marine, "Humid Air Turbine Cycle Public Report," 1993.

[3] Robson, F.L., "Advanced Turbine Systems Study-System Scoping and Feasibility Study," DOE Contract DE-AC21-92MC29247, UTRC, March 1993.

[4] Dryer, F.L., "Water Addition to Practical Combustion Systems-Concepts and Applications," *Sixteenth Symposium (International) on Combustion*, The Combustion Institute, Pittsburgh, PA, 1976.

[5] Miyauchi, Y., Mori, Y., Yamaguchi, T., "Effect of Steam Addition on NO Formation," *Eighteenth Symposium (International) on Combustion*, The Combustion Institute, Pittsburgh, PA, 1981.

[6] Touchton, G.L., "Influence of Gas Turbine Combustor Design and Operating Parameters on Effectiveness of NO_x Suppression by Injected Steam or Water," ASME paper No. 84-JPGC-GT-3, 1985.

[7] Blevins, L.G., and Roby, R.J., "An Experimental Study of NO_x reduction in Laminar Diffusion Flames by Addition of High Levels of Steam," ASME Paper No. 95-GT-327, 1995.

[8] Meyer, Jean-Louis, and Grienche, G., "An Experimental Study of Steam Injection in an Aeroderivative Gas Turbine', ASME Paper No. 97-GT-506, 1997.

- O-atom suppression (the presence of moisture promotes the reaction $O + H_2O \rightarrow OH + OH$, leading to O-atom suppression and reducing NO_x through the *Zeldovich* and N_2O pathways)
- Heat release rate reduction lowering peak temperatures and super-equilibrium O-atom.

2.4.1 Experiments

Experiments were conducted in the LECTR facility at the NETL. The LECTR facility is a refractory lined pressure vessel containing test modules configured to meet specific test requirements. The facility was designed for pressurized operations up to 450 psig with access to a preheated (1000°F maximum) air supply capable of delivering up to 3.2 pps of air.

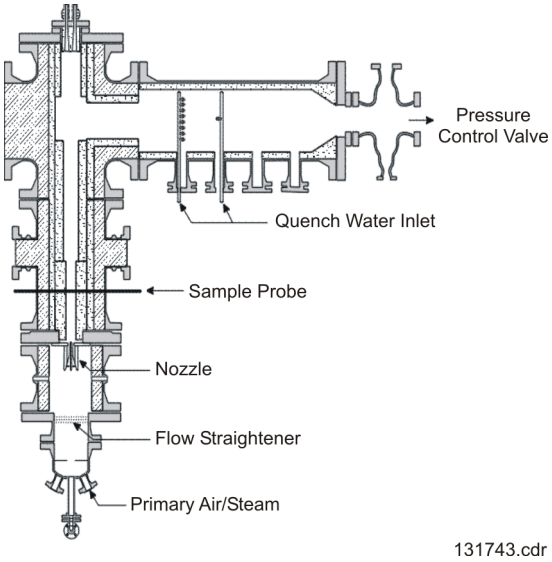

Figure 2-44. A Schematic of the Experimental Setup

In the present test configuration (see Figure 2-44), superheated steam was added to the preheated combustion air and then injected into an inlet plenum. The flow was straightened through a series of perforated metal plates and passed through the test nozzle, where it was mixed with the primary fuel supply. Two diffusion flame pilot fuel streams were also employed. A sidewall pilot fuel flow was injected through the wall of the combustor approximately ½ in. above the tip of the nozzle. In addition, centerbody pilot fuel was injected along the centerline of the nozzle. Combustion products passed upward across an area-averaged sample probe that spanned the combustor diameter. The flow continued upward into a plenum; it turned 90 degrees before entering a water quench zone where the gas temperature was reduced prior to passing through a pressure control valve and out an exhaust stack.

Experiments were conducted to evaluate emissions performance as a function of firing conditions for a 2 $in.^2$ effective flow area scaled version of the tangential entry fuel nozzle. Larger scale versions of the nozzle have been reported in the literature.[1] The 2 $in.^2$ effective area nozzle tests were conducted at 200 psi with an airflow flow rate of 2.2 pps and a combustor insert diameter of 4.25 in.

Test parameters examined included percentage of total fuel flow as sidewall pilot (0, 1, or 5 percent), percentage of total fuel flow as centerbody pilot (0, 1, 3, or 5 percent), percentage of steam relative to combustion air (0, 5, 10, 15, or 20 percent) and air/steam mixture temperature (varied from 935° to 725°F depending on steam loading and air preheat). All percentages were taken as mass percent. All fuel, air, and steam flows were measured using precision orifice runs with flow control valves tied to an automated control system. Excellent mass balance closure (typically within 1 to 2 percent) was observed when comparing input flow measurements with measured combustion product compositions.

Experiments were performed by establishing the required air and steam flows for a given test condition. The sidewall, centerbody, and main fuel flows were then set based on a prescribed equivalence ratio. The nozzle was held at the above condition for a period of 10 to 15 minutes to establish a steady baseline. The three fuel streams were then simultaneously ramped to lower flows (leaner conditions), keeping their relative ratios constant while the air and steam flows remained fixed. Fuel ramp rates were established based on the gas sample system response time and typically involved reducing fuel flow approximately 30 percent during a 1-hr ramp. The starting equivalence ratios for these tests were selected based on previous experience with the test nozzle to give a starting CO emission level of 50 ppm or greater. As the fuel was ramped to leaner conditions, CO emissions passed through a minimum and rose rapidly as the lean blow-off limit was approached. Fuel ramps were discontinued when CO lev-

[1] Kendrick, D.W., Anderson, T.J., Sowa, W.A., and Snyder, T.S., "Acoustic Sensitivities of Lean-Premixed Fuel Injectors in A Single Nozzle Rig," AMSE Paper No. 98-GT-382, 1998.

els exceeded 200 ppm. As steam loading in the combustion air was increased, the starting equivalence ratio was increased as well, to stay on the rich side of the CO minimum.

Gas samples were obtained using water-cooled rake probes designed to extract representative gas samples across the area of the combustor. The sample probe was located approximately 15 in. above the nozzle tip. Extracted gas samples were transported through heated transfer lines to a pressure letdown station, followed by a chiller to remove water. The dried sample gas was then passed through an analyzer train configured to measure O_2, CO_2, CO, total NO_x, and UHC.

2.4.2 Modeling

Experimental data covered a wide range of equivalence ratios and humidity levels. The fuel concentration in the pilots was also varied from 0 to 5 percent fuel to determine the optimum level of side pilot required to keep NO_x emissions low, but provide enough stability to the lean flame. Observations made from the experiments included the following:

- For dry flames at constant T_{eq}
  - — NO_x emissions increase with increasing fuel in the pilot, while CO emissions show no dependence on pilot level.
- For humid air experiments
  - — NO_x and CO levels decrease with an increase in the humidity levels
  - — Similar effect of pilot levels as in dry flames.

The experiments were modeled using a literature reaction set, GRI-MECH 2.11, and its accompanying thermochemistry.[1] The GRI-MECH 2.11 reaction set consists of 49 species and 277 reactions and has been validated over a wide range of pressure and equivalence ratios. A PSR network code developed at UTRC was used to simulate the combustor. The basis for the network PSR code is the Chemkin PSR model.[2] The network used to model the experiment is shown in Figure 2-45. The network was designed to simulate the mixing and flow characteristics of the experiment as closely as possible. A total of 15 reactors was used to represent the combustor. That number was arbitrarily chosen to simulate the process in a reasonable manner and without a high-computational burden. The combined volume of the 15 reactors gave a residence time equal to the experimental residence time in the equipment. A small amount of fuel and air mixture was introduced in the first reactor; this represented the central pilot. The products of reactor 1, along with most of the fuel (75 to 79 percent) and air (80 to 90 percent), were introduced in reactor 2. Twenty percent of the fuel, along with 10 percent of air, enters the system through reactor 3. The combination of reactors 2 and 3 represents the inhomogeneity that may be present due to the less than perfect mixing. Reactors 2 and 3 represent the flame zone. The side pilot was simulated by flowing 0 to 5 percent of the fuel through reactors 4 and 5. Providing recycle between reactors 2 and 4 simulated recirculation. The rest of the reactors (6 to 15) represent the post-flame zone. NO_x is primarily formed in reactors 2 and 3, while the rest of the reactors, 4 to 15, are for mixing of the side and central pilots with the flame and for CO burnout. In this manner, the network was designed to match experimental NO_x and CO. Residence time varied with flow rates, as air was fixed while the fuel flow rate was changed to achieve the required equivalence ratio. Residence time in

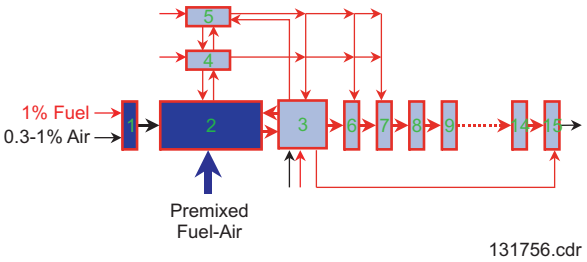

Figure 2-45. A Schematic of the PSR Reactor Network Used To Model the Flame

[1] Bowman, C.T., Hanson, R.K., Davidson, D.F., Gardiner, W.C., Jr., Lissianski, V., Smith, G.P., Golden, D.M., Frenklach, M., and Goldenberg, M., 1994 (http://www.me.berkeley.edu/gri_mech).

[2] Glarborg, P., Kee, R.J., Grcar, J.F., Miller, J.A., "PSR: A Fortran Compiler for Modeling Well-Stirred Reactors," *Sandia National Laboratories Report*, SAND86-8209, Livermore, CA, February 1986.

each reactor was a function of the flow rate through the reactor and reactor volume. The residence time in all the reactors combined was between 4.5 and 6 ms. The flame zone (reactor 2 and 3) accounted for most of the residence time (nearly 60 percent). The network structure remained the same for all conditions but minor alterations for fuel/air distribution had to be done from one case to another to stabilize the network and to simulate the flow characteristics. For example, with very fuel-lean conditions or for cases with 10 to 15 percent moisture, fuel in the first reactor had to be increased to stabilize the network. With different fuel flows across the pilot, fuel/air distribution in reactors 2 and 3 had to be slightly modified.

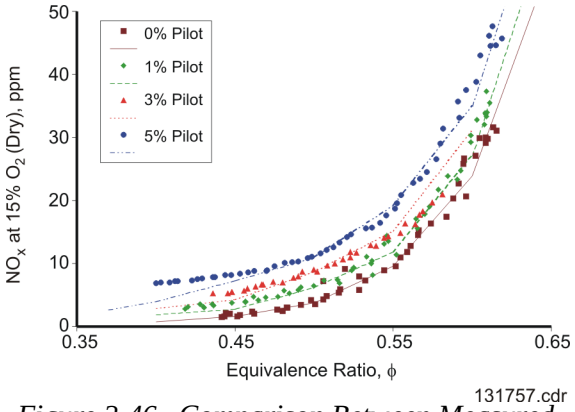

Figure 2-46. Comparison Between Measured and Computed NO_x at 200 Psi at Different Pilot Levels

Solutions were compared with experiments on the basis of combustor exit temperature, which is equal to T_{eq} and based on local equivalence ratio. The combustor exit temperature is different, generally, from the local temperature in the PSR, as the local temperature can be kinetically limited.

2.4.3 Results and Discussion

Numerous experiments were performed to ascertain the effect of moisture, equivalence ratio, and inlet temperature on the amount of NO_x and CO formed. The effect of pilot level (0, 1, 3, and 5 percent fuel) and moisture level (0, 5, 10, and 15 percent water in the air by mass) on NO_x and CO emissions can be seen in Figure 2-46 to Figure 2-49.

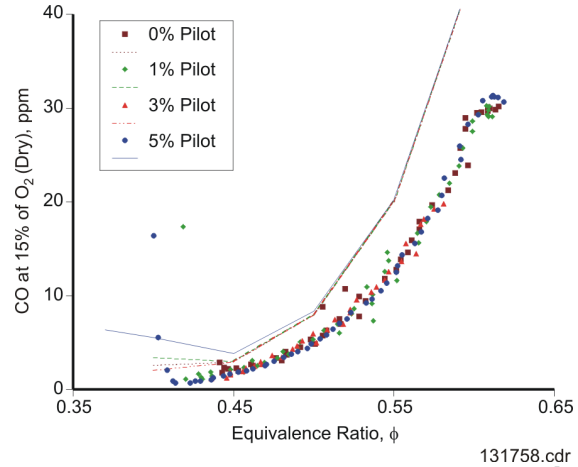

Figure 2-47. Comparison Between Measured and Computed CO at 200 Psi at Different Pilot Levels

As seen in Figure 2-46, higher side pilot levels lead to higher NO_x. The effect is more pronounced at very lean conditions. This result agrees well with the findings of Leonard and Stegmaier,[1] and Maghon *et al*.[2] Further analysis of the NO_x formed at different pilot levels in this study indicated that with a 1 percent increase in the fuel injected through the side pilot, NO_x emissions go up by 1.5 ppm (±0.2 ppm). This increase is less than the increase observed by Maghon *et al*. CO emissions remain more or less unaffected by the pilot level, as observed in Figure 2-47. The effect of moisture level in the air is seen in Figure 2-48 and Figure 2-49. NO_x and CO emissions show a significant drop with increasing amounts of moisture in the air stream. Much of the reduction shown in these figures can be attributed to a reduction in flame temperatures at constant ϕ with increasing moisture. As will be shown later, even at constant flame temperature, NO_x and CO is reduced with increasing moisture levels.

Simulations examined the influence of pilot and humidity level consistent with the experiments. Figure 2-46 and Figure 2-47 show the comparison between the experiments and modeling as piloting level varies. NO_x predictions are very good, but the predictions for CO are off by as much as 50 percent. This trend was observed in all simulations. The CO predictions were close to the equilibrium levels and are highly sensitive to the mixture (air and fuel) temperature. A small (equivalent to 50°F) discrepancy in the measured air/fuel temperature can account for the difference in the measured and computed CO. Alternatively, the sample probe's impact on the equilibrating CO

[1] Leonard, G., and Stegmaier, J., "Development of an Aeroderivative Gas Turbine Dry Low Emissions Combustion Systems," ASME Paper No. 93-GT-288, 1994.

[2] Maghon, H., Berenbrink, P., Termuehlen, H., Gartner, G., "Progress in NO_x and CO Emission Reduction of Gas Turbines," ASME Paper No. 90-JPGC/GT-4, 1990.

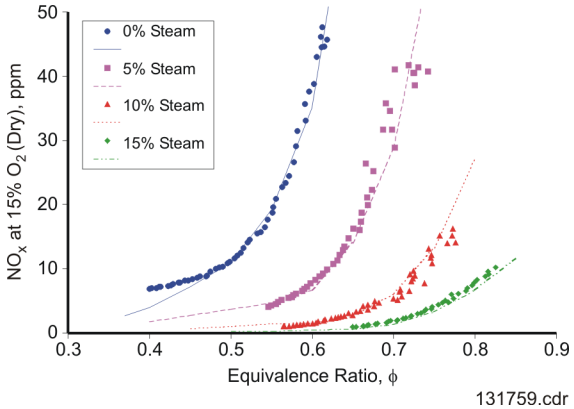

Figure 2-48. Comparison Between Measured and Computed NO_x for a 5 Percent Side Pilot Flame at 200 Psi for Different Steam Loading

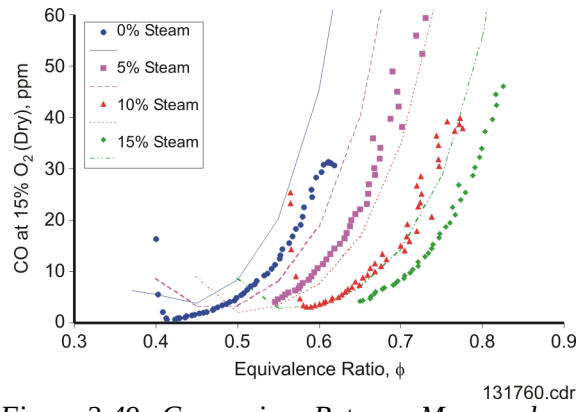

Figure 2-49. Comparison Between Measured and Computed CO for a 5 Percent Side Pilot Flame at 200 Psi for Different Steam Loading

that is still undergoing reaction may explain the lower experimental values. Small levels of additional CO destruction in the probe could also explain the discrepancy. A study of the probe effect on CO measurements has been presented by Nguyen *et al.*[1] They. measured CO in an atmospheric pressure flame using line-of-sight tunable diode laser absorption and extractive probe sampling and compared it with CO prediction using a numerical model.They found that the measurements made with extractive sampling technique were as much as 10 times less than the laser-based experiments for fuel-lean flames, whereas for fuel-rich flames, the agreement between the two techniques was good.

The same network design developed for the dry air cases was extended to humid air cases. Shown in Figure 2-48 and Figure 2-49 is the comparison for NO_x and CO mole fraction measured in the flame and simulated by the network. Higher humidity brings about a drastic reduction in the formation of NO_x. As the amount of moisture increases, the lean blowout limit moves to higher equivalence ratios consistent with the shift seen in Figure 2-48 and Figure 2-49. For a dry air flame at T_{air} = 860°F and at P = 200 psi, the boundary between equilibrium CO and the onset of lean blowout dynamics occurs at an equivalence ratio of 0.41. This boundary shifts as more moisture is introduced. It goes up to 0.55 for 5 percent moisture and to 0.65 for 15 percent moisture in the air stream. The network PSR is able to capture the behavior of the NO_x concentrations to within 5 to 10 percent of the measurements, further corroborating the modeling approach. CO predictions are higher (20 to 40 percent) than the measurements. This effect was similar to the one seen in the piloting data.

As seen in Fig. 7, flame stability limits move to higher equivalence ratios as moisture content increases. Moisture in the air reduces flame temperatures. Flames with different humidity levels have different temperatures for the same equivalence ratio. For example, a 0.54 equivalence ratio flame with no steam has the same T_{eq} as a flame with 15 percent steam in the air: An equivalence ratio of 0.75. Another method, therefore, of comparing flames is to compare NO_x and CO emissions formed in flames at different moisture levels as a function of T_{eq}. The computations of T_{eq} were carried out using equilibrium code called STANJAN, developed by Reynolds[2] and modified by Kee and Lutz.[3] The computation included 49 species. The GRI-MECH 2.11 thermodynamic database was used for these computations. The temperatures in Figure 2-50 and Figure 2-51 (and also Figure 2-52 to Figure 2-55) are the T_{eq} for the entire fuel/air mixture in the combustor. Actual flame temperatures in the experiment are distributed and somewhat lower due to heat losses to the burner and surrounding air in the chamber. Figure 2-50 and Figure 2-51

[1] Nguyen, Q.V., Edgar, B.L., Dibble, R.W., and Gulati, A., "Experimental and Numerical Comparison of Extractive and In Situ Laser Measurements of Non-Equilibrium Carbon Monoxide in Lean-Premixed Gas Combustion," *Combustion and Flame*, 100:395-406, 1995.

[2] Reynolds, W.C., "STANJAN, Interactive Computer Programs for Chemical Equilibrium Analysis," Stanford University, January 1981.

[3] Kee, R.J., and Lutz, A., private communication.

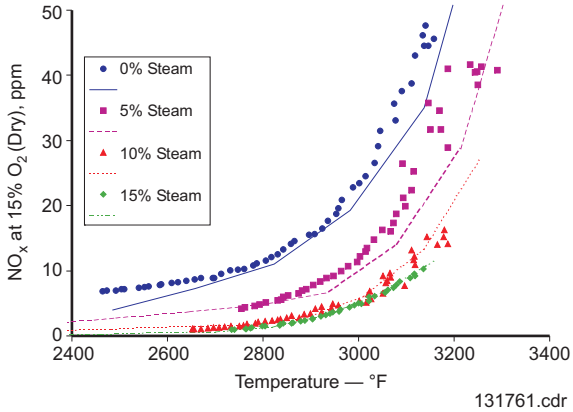

Figure 2-50. Comparison Between Measured and Computed NO_x for a 5 Percent Side Pilot Flame at 200 Psi for Different Steam Loading

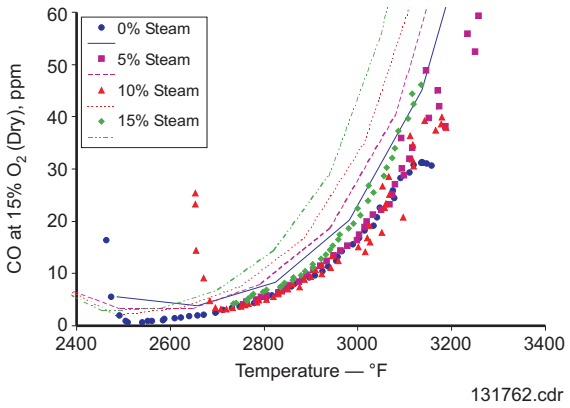

Figure 2-51. Comparison Between Measured and Computed CO for a 5 Percent Side Pilot Flame at 200 Psi for Different Steam Loading

indicate the dependence of NO_x and CO on T_{eq}. As seen in Figure 2-50, calculations and measurements indicate that a dry air flame at $\phi = 0.54$ would have a T_{eq} of 2950°F and NO_x emissions of around 15 ppm. At the same time, a flame with humid air (15 percent steam content) at $\phi = 0.75$ has the same T_{eq} of 2950°F, but its NO_x emissions are only 3 ppm. This means that besides reducing NO formation in flames by reducing the flame temperature (Toughton[1] and Blevins and Roby[2]), humidity also reduces NO by some other mechanism. This reduction can be due to the change in the radical pool because of varying amounts of moisture and different equivalence ratios at the same temperature, or due to any of the other factors mentioned in the introduction. The flame at 0.54 equivalence ratio (dry air) is richer in O-atom than a humid air flame (15 percent steam) at 0.75 equivalence ratio, even though both flames are at the same T_{eq}. One of the other possibilities that can account for the drastic reduction in NO_x is the temperature attained in each of the PSRs in the network. As mentioned in the introduction, moisture in the feed stream can slow heat transfer rates and therefore, a different moisture content can lead to a different maximum temperature (residence time in the different PSRs is fixed) attained in PSR 2 and PSR 3 of the network, which account for most of the NO_x formed. An analysis of the temperatures attained in the different PSRs in the network for flames with different moisture content, but at the same T_{eq}, indicated that moisture content does not alter the temperature attained in each of the reactors. Therefore, a reduction in NO_x concentration with increased moisture content is not due to lowering of peak temperatures in the reactors. CO emission levels at one T_{eq} do not vary with humidity, as seen in Figure 2-51.

To determine the roles of various mechanisms on the production of NO_x, several modifications were made to the reaction set. NO_x formation reactions were divided into three different, but coupled, groups:

- *Zeldovich* or *Thermal* NO_x mechanism,[3] as extended by Bowman and Seery[4] — The NO_x is initiated by the reaction of N_2 with the O atom. This well-established, three-step reaction sequence is the dominant NO_x-forming route at temperatures above 2950°F. *Zeldovich*, or *Thermal* NO_x mechanism, was suppressed by making the $N_2 + O \leftrightarrow N + NO$ reaction proceed in the reverse direction only.
- *N_2O* mechanism, consisting of reactions involving N_2O that form NO — The NO_x formed through this mechanism can be effectively suppressed by making the N_2O (+M) $\rightarrow N_2 + O$ (+M) proceed in the forward direction only.

[1] Touchton, G.L., "Influence of Gas Turbine Combustor Design and Operating Parameters on Effectiveness of NO_x Suppression by Injected Steam or Water," ASME Paper No. 84-JPGC-GT-3, 1985.

[2] Blevins, L.G., and Roby, R.J., "An Experimental Study of NO_x reduction in Laminar Diffusion Flames by Addition of High Levels of Steam," ASME Paper No 95-GT-327, 1995.

[3] Zeldovich, J., "The Oxidation of Nitrogen Combustion and Explosions," *Acta Physicochimica*, URSS, 21, 577, 1946.

[4] Bowman, C.T., and Seery, D.J., *Emissions from Continuous Combustion Systems*, (W. Cornelius and W.G. Agnew, eds.), p. 123, 1972.

- *Fenimore* NO_x mechanism — All NO_x forming reactions, beside the *Zeldovich* and N_2O pathways, are included in this route. The main steps influencing this reaction sequence are $N_2 + CH = HCN + N$, $N_2 + CH_2 = HCN + NH$, and other reactions involving N_2 and hydrocarbon radicals. This extensive sequence was suppressed by inhibiting the forward rates for reactions between hydrocarbon fragments and molecular nitrogen.

The NO_x formation rates of each of these reaction sequences can be enhanced through super-equilibrium levels of O-atoms and other radical species in the flame front.

To study the contribution of each pathway, the other two channels were suppressed. Therefore, in order to analyze the importance of the *Zeldovich* mechanism, NO_x formation through the *Fenimore* and N_2O mechanisms was removed. Similar computations were performed to evaluate the importance of the *Fenimore* and N_2O mechanisms. The analysis was carried out for 0 and 5 percent pilot levels at 0 and 15 percent moisture loading. Figure 2-52 and Figure 2-53 show the contributions of the different mechanisms for the four cases. Also shown in the figures is the NO_x computed with a single PSR. The differences between these calculations and those of the network analysis indicates the effect of mixing in the combustion chamber and circulation on NO_x formation and finite reaction times required to approach T_{eq}. The NO_x prediction for the one PSR case is higher than the network PSR, primarily due to residence time distribution. In the network, reactors 2 and 3 are the reactors primarily responsible for making NO_x and CO. In order to simulate the experiments with the network, reactor volume, which determines the residence time in the reactor, was used as one of the adjustable parameters. Once established for one case, the volumes were not changed for any of the other cases. Therefore, by keeping the residence time low, NO_x generation may be inhibited. On the other hand, in the case of the one PSR, residence time was not a variable and was similar to the whole network combined.

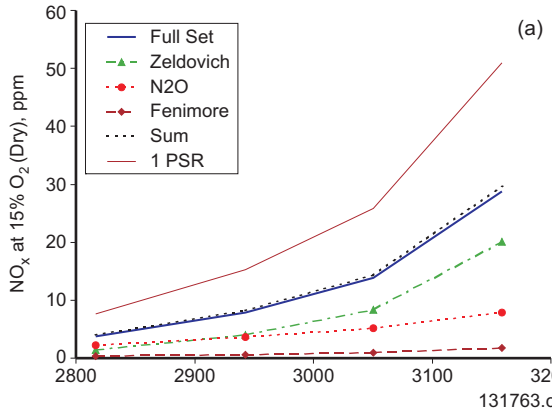

Figure 2-52. Influence of Different Pathways on NO_x Formation for a Flame With a 0 Percent Side Pilot and 0 Percent Steam

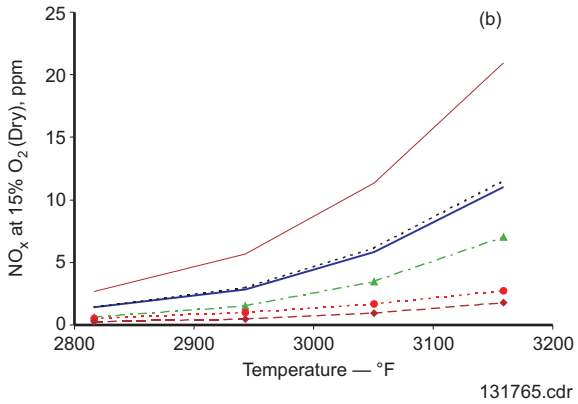

Figure 2-53. Influence of Different Pathways on NO_x Formation for a Flame With a 0 Percent Side Pilot and 15 Percent Steam

Zeldovich NO_x dominated the other NO_x formation channels in the temperature range studied, except for the 0 percent side pilot flame for dry air. For this case, seen in Figure 2-52, the N_2O pathway dominates the *Zeldovich* pathway in the lean operating range (2800° to 2900°F). This is the range in which most of the industrial gas turbines operate.

Figure 2-52 and Figure 2-53 show the behavior of NO_x formed at two moisture levels, 0 and 15 percent, for flames with 0 percent fuel coming in from the side pilot. As seen in these figures, at temperatures around 2950°F, NO_x formed by the N_2O pathway is comparable to the *Zeldovich* or *Thermal* NO_x, but at temperatures around 3050°F, *Zeldovich* NO_x starts increasing much more rapidly and becomes the dominant NO_x formation channel. Comparing the NO_x formed in the flames with and without moisture, it can be seen that at the same temperature, NO_x formed in the cases with 15 percent moisture is much less than the NO_x formed in dry air flames. At temperatures around 2800°F, the decrease is close to a factor of eight, while at higher temperatures it is around a factor of

three. These calculations indicate that NO_x formation decreases in flames with added moisture, as compared to dry flames, even when the T_{eq} for the two flames is the same. This suggests that all the reduction in NO_x cannot be attributed to thermal effects (as defined by T_{eq}).

The decrease in the *Zeldovich* and *N_2O* NO_x can be attributed to the reduction in O-atom concentration. As mentioned earlier in the paper, at the same equivalence ratio, the high humidity flames are of lower temperatures than dry flames. Therefore, to evaluate the different flames at the same temperature, high-humidity flames had to be at a higher equivalence ratio than dry flames. Scarcity of O_2 and hence, lower O-atom concentration in the higher equivalence ratio humid flames, would lead to lower NO_x formation by the *Zeldovich* and *N_2O* mechanism. Humidity promotes O + H_2O reaction, and suppresses O-atom concentration. A reduction in the *Fenimore* NO_x can be attributed to the change in the OH radical concentration in the flame. Higher OH concentration in humid air flames promotes oxidation of the hydrocarbon radicals, which would reduce Fenimore NO.[1] Similar behavior was seen in the 5 percent side pilot flame (Figure 2-54 and Figure 2-55). Due to the side pilot, NO_x levels were higher than the flame with no side pilot. The increase in NO_x for the flame, with 5 percent fuel coming in from the side pilot, was more predominant at the lower temperatures and was mostly due to higher *Fenimore* NO at the lean conditions (especially for the dry flame).

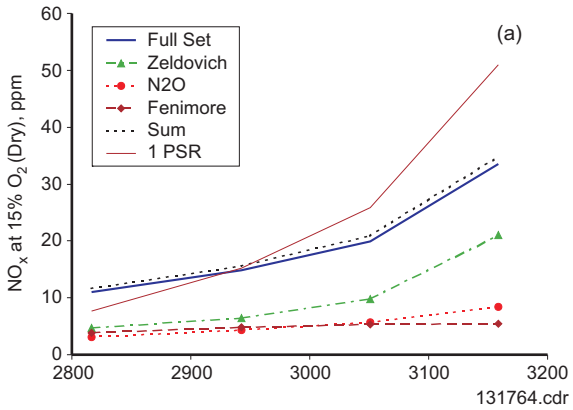

Figure 2-54. Influence of Different Pathways on NO_x Formation for a Flame With a 5 Percent Side Pilot and 0 Percent Steam

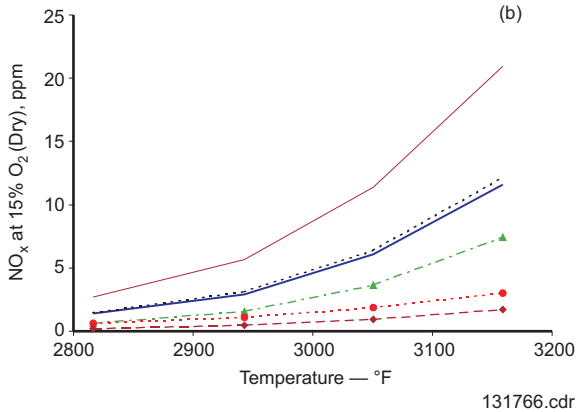

Figure 2-55. Influence of Different Pathways on NO_x Formation for a Flame With a 5 Percent Side Pilot and 15 Percent Steam

The factors mentioned in the introduction were also considered. There is definitely some reduction in NO_x due to lowering of temperature. Reduction of the peak temperature of the side pilot can also reduce NO_x formation, though the analysis with 0 percent side pilot indicates that this may not be the dominant factor. Suppression and delay of heat transfer rates due to added moisture would slow down the combustion process and lower super-equilibrium O-atom concentration and temperatures in reactors 2 and 3. These two reactors account for most NO_x formation and a lower temperature in these reactors (even though T_{eq} for the whole flame could be the same as the case with dry air) would lead to lower overall NO_x. Lower super-equilibrium O-atom concentrations would also lead to lower NO_x (reduction in *Zeldovich* and *N_2O* NO_x).

The percentage of NO reduction from the three mechanisms was similar for dry run and for humid air run. This indicates that even with moisture addition, which has the effect of lowering T_{eq}, the thermal NO channel remained the most dominant NO formation channel for most of the conditions examined in this study.

2.4.4 Conclusions

Data was collected over a wide range of equivalence ratios, levels of moisture in the air stream, and pilot levels. The trends in the measured data have been used to evaluate the effect of various parameters on NO_x and CO

[1] Miyauchi, Y., Mori, Y., Yamaguchi, T., "Effect of Steam Addition on NO Formation," *Eighteenth Symposium (International) on Combustion*, The Combustion Institute, Pittsburgh, PA, 1981.

emissions. The data has also been modeled using a PSR network and a literature reaction set. Good matches between the data and modeling suggests that the approach used for modeling the combustor is useful. Addition of moisture to the air stream brings about a significant reduction in NO_x emissions. This reduction in NO_x is primarily due to a decrease in the T_{eq}, but reduction in NO_x with increasing moisture is also observed for flames in which T_{eq} is held constant. Analysis of the reaction set and computations for the three different NO_x formation pathways indicate the importance of O-atom concentration on NO_x formation. Moisture loading of 15 percent in the air reduces NO_x emissions by as much as a factor of three to eight (depending on the T_{eq}) at the same T_{eq} as a dry flame. This reduction is attributed to the decrease in O-atom concentration. Even with 15 percent moisture content, most of the NO_x formation takes place through the *Zeldovich* pathway.

2.5 NO_X SCALING CHARACTERISTICS FOR INDUSTRIAL GAS TURBINE FUEL INJECTORS

An experimental and numerical investigation into the effects of nozzle scale was undertaken at the NETL under the auspices of UTRC. Experiments were conducted at operating pressures from 100 psia to 400 psia, and at primary zone equivalence ratios from 0.4 to 0.75. Results reported herein summarize tests at 100 psia and with 0 and 4 percent piloting levels (expressed as mass fractions of total fuel). Computations for comparison with the experimental data were made using the GRI-MECH 2.11 kinetics and thermodynamics database for flame chemistry modeling. A PSR was used to create a network to simulate the flame. From these investigations, concentrations of NO_x and CO, expressed in parts per million, were seen to increase and remain virtually unchanged, respectively, during comparison of a quarter to a full square bluff-body nozzle. Simple heat transfer modeling and CO emissions were shown to prove that any variations in thermal characteristics within the combustors were solely responsible for the observed NO_x variations. Using the PSR network modeling, the NO_x trends were explained by variations in macroscopic mixing scales that increase with nozzle size and create progressively less uniform mixing and therefore, higher NO_x levels with increasing scale.

Industrial gas turbine engine testing on smaller scale laboratory rigs offer economies of scale in both developmental costs and turn-around time for trial validation. Reduced-size systems afford the researcher the ability to implement critical diagnostics to analyze flowfield features that, under most circumstances, are impractical to implement in the full-scale engine. Enormous incentives, therefore, are in place for accurately conducting scaled tests to aid combustion hardware development. The challenge, however, is to take into account the geometric and fluid dynamic differences for extrapolation to full scale without sacrificing valid performance.[1] It often happens, for instance, that when low-NO_x burners are installed into geometrically different or sized furnaces, unacceptable NO_x emissions result due to alterations in any one of the following: fluid dynamics, strain rates, combustion zone heat transfer, unmixedness, and flow distribution.[2] Each effect may have subtle influences on the NO_x-generating mechanisms, so efforts must be made to account for such variations. It becomes crucial, therefore, that accurate scaling laws/theories exist to justify such reduced scale testing. Current scale-up methods, such as geometric similarity and velocity matching, have proven unreliable in predicting performance over any appreciable size range.[3]

[1] Dahm, W., Driscoll, J., Hsieh, T., "Scaling Characteristics of Aerodynamics and Low-NO_x Properties of Industrial Natural Gas Burners: The Scaling 400 Study," Final Report, GRI, 1998; Sayre, A., Lallemant, N., Dugue J., and Weber, R., *Twenty-Fourth Symposium (International) on Combustion*, The Combustion Institute, Pittsburgh, PA, pp. 235-242, 1994; Al-Fawaz, A., Dearden, L., Hedley, J., Missaghi, M., Pourkashanian, Williams, A. and Tap, L., "NO_x Formation in Geometrically Scaled Gas Fired Industrial Burners," *Twenty-Fifth Symposium (International) on Combustion*, The Combustion Institute, Pittsburgh, PA, pp. 1027-1034, 1994; and Rokke, N., Hustad, J., Sonju, O., Williams, F., "Scaling of Nitric Oxide Emissions from Buoyancy-Dominated Hydrocarbon Turbulent-Jet Diffusion Flames," *Twenty-Fourth Symposium (International) on Combustion*, The Combustion Institute, Pittsburgh, PA, pp. 385-393, 1992.

[2] Sayre, A., Lallemant, N., Dugue J., and Weber, R., *Twenty-Fourth Symposium (International) on Combustion*, The Combustion Institute, Pittsburgh, PA, pp. 235-242, 1994; Fric, T., "Effects of Fuel-Air Unmixedness on NO_x Emissions," AIAA Paper 92-3345, 1992; and Rokke, N., Hustad, J., Sonju, O., Williams, F., "Scaling of Nitric Oxide Emissions from Buoyancy-Dominated Hydrocarbon Turbulent-Jet Diffusion Flames," *Twenty-Fourth Symposium (International) on Combustion*, The Combustion Institute, Pittsburgh, PA, pp. 385-393, 1992.

[3] Dahm, W., Driscoll, J., Hsieh, T., "Scaling Characteristics of Aerodynamics and Low-NO_x Properties of Industrial Natural Gas Burners: The Scaling 400 Study," Final Report, GRI, 1998.

Theoretical combustion scaling has seen significant efforts.[1] All such work treats variations in fluid flow, chemical kinetics, and heat transfer in the near burner field.[2] Simple scaling laws based on Reynolds and Froude number correlations have been formulated,[3] but have seen limited success in the industrial burner arena.[4]

This work examines the NO_x emissions characteristics of two geometrically similar bluff-body nozzles:[5] a quarter-scale and full-scale design. Both were designed with close attention to matching dump ratios, convection velocities, and time scales. Independent variables investigated for the larger program, of which nozzle scale exercises constituted a significant portion, include primary zone flame temperatures (2500º to 3200ºF), operating pressure (100 to 400 psia), centerline and sidewall piloting levels (1 to 3 percent), and inlet air humidity levels (0 to 20 percent). Results presented here include only the effects of flame temperature and piloting levels.

The experimental data show distinct variations in NO_x levels with scale, shown through simple heat transfer, CO emissions, and kinetic modeling to be attributable to variations in mixing variations.

2.5.1 Experimental Setup

Fuel Nozzle Design

Figure 2-56 details an earlier aerodynamic nozzle design whose centerbody was modified for the present series of tests (Figure 2-57) through the addition of a bluff plate and diffusion pilot. Although the addition of a centerbody diffusion pilot will negatively impact NO_x performance, it was shown to be invaluable in mitigating acoustic instabilities over the power range, relative to its predecessor's premixed version.[6] Because the design relies upon a bluff body for flame stability, it will be referred to as a bluff-body nozzle. For the present tests, two nozzle scales (or ACd) were examined, based on the constant velocity scaling approach.[7] Each configuration exhibited identical interior air velocities and gaseous fuel penetration characteristics, thereby reducing departures from perfect similarity. In order to preserve dump ratios (area based) and combustor velocities (residence times), the burner diameter was also altered with each nozzle through the insertion of a ceramic sleeve. Table 2-3 summarizes each nozzle/combustor configuration.

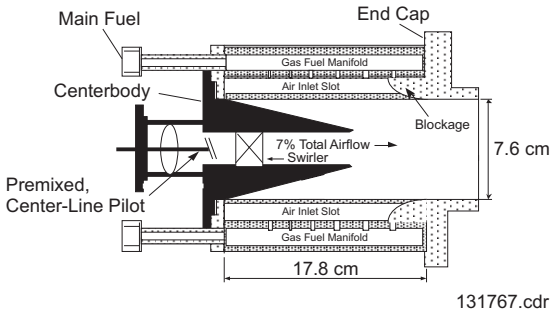

Figure 2-56. Schematic of an Earlier Aerodynamic Nozzle

[1] Rhine, J., and Tucker, R., "Modeling of Gas Fired Furnaces and Boilers," *British Gas*, McGraw-Hill, London, U.K., 1991; Gupta, A., and Lilley, D., "Predictive Techniques," *Flowfield Modeling and Diagnostics*, Chapter 3, Abacus Press, Kent, U.K., 1985; Beer, J. and Chigier, N., "Modeling of Combustion Systems," *Combustion Aerodynamics*, Chapter 7, Wiley Press, New York, 1965; and Spalding, D., "The Art of Partial Modeling," *Ninth Symposium (International) on Combustion*, The Combustion Institute, Pittsburgh, pp. 833-843, 1962.

[2] Dahm, W., Driscoll, J., Hsieh, T., "Scaling Characteristics of Aerodynamics and Low-NO_x Properties of Industrial Natural Gas Burners: The Scaling 400 Study," Final Report, GRI, 1998.

[3] Rokke, N., Hustad, J., Sonju, O., Williams, F., "Scaling of Nitric Oxide Emissions from Buoyancy-Dominated Hydrocarbon Turbulent-Jet Diffusion Flames," *Twenty-Fourth Symposium (International) on Combustion*, The Combustion Institute, Pittsburgh, PA, pp. 385-393, 1992; and Peters, N., and Donnerhack, S., "Structure and Similarity of NO_x Production in Turbulent Diffusion Flames," *Eighteenth Symposium (International) on Combustion*, The Combustion Institute, Pittsburgh, pp. 33-42, 1981.

[4] Al-Fawaz, A., Dearden, L., Hedley, J., Missaghi, M., Pourkashanian, Williams, A. and Tap, L., "NO_x Formation in Geometrically Scaled Gas Fired Industrial Burners," *Twenty-Fifth Symposium (International) on Combustion*, The Combustion Institute, Pittsburgh, PA, pp. 1027-1034, 1994.

[5] Kendrick, D.W., Anderson, T.J., Sowa, W.A., and Snyder, T.S., "Acoustic Sensitivities of Lean-Premixed Fuel Injectors in A Single Nozzle Rig," *Journal of Engineering for Gas Turbines and Power*, 121, pp. 429-436, July 1999.

[6] *Ibid*.

[7] Dahm, W., Driscoll, J., Hsieh, T., "Scaling Characteristics of Aerodynamics and Low-NO_x Properties of Industrial Natural Gas Burners: The Scaling 400 Study," Final Report, GRI, 1998.

Table 2-3. Nozzle/Combustor Configurations

Nozzle Scale	*ACd (in.^{2})*	*Liner Diameter (in.)*	*Liner Length (in.)*
Quarter Scale	1	3	16
Full Scale	4	6	16

Combustion Test Facility

All experiments were conducted in the LECTR facility located at the NETL (Figure 2-58). The combustion rig mimics other single nozzle rigs detailed elsewhere in that it allowed independent, but automated, control of the air and gas fuel flows and inlet temperature and pressure supplied to the premixing fuel nozzle.[1] A prescribed fuel and airflow ramp could be programmed slow enough for the system to reach thermal equilibrium for accurate emissions measurements. The facility was designed for operating pressures up to 400 psia (P_3) and inlet/preheat temperatures (T_3) up to 980ºF. A refractory lined pressure vessel was employed to simulate an ideal adiabatic combustion chamber, thereby alleviating the need for secondary or liner cooling airflow. Natural gas was used for all tests in this study. Airflow was metered using ASME standard orifices and heated using a nonvitiated indirect gas-fired heater. A perforated plate, located upstream of the fuel nozzle, provided a uniform feed of air to the nozzle to simulate the air supply volume of an engine.

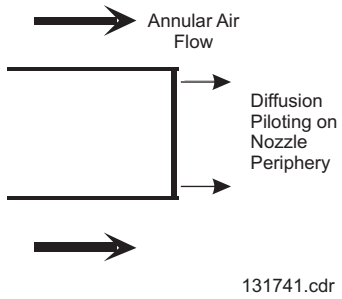

Figure 2-57. Schematic of the Centerbody End Detail

In addition to the nozzle's diffusion pilot, a second sidewall pilot was added 0.75 in. downstream of the dump plane (nozzle exit plane) to assist in lightoff and to examine the system's performance at small levels of piloting. After burning in the liner, combustion products passed upwards across an area average gas-sample probe that spanned the combustor's diameter. The flow continued upwards into a plenum, where it turned at right angles into a water quench zone to reduce exhaust velocities prior to passing into the exhaust stack. The water cooled gas-sample probe was designed to extract a representative sample across the combustor's exit plane some 16 in. downstream of the dump plane. Gas samples were acquired on a continuous basis and transported to appropriate analyzers through heated sample lines. Typical emissions species were analyzed: NO_x, CO, CO_2, O_2, and unburned hydrocarbons (UHC). Mass balance closures, made by comparing the emissions based fuel/air ratios to the metered flow, typically agreed within 5 percent.

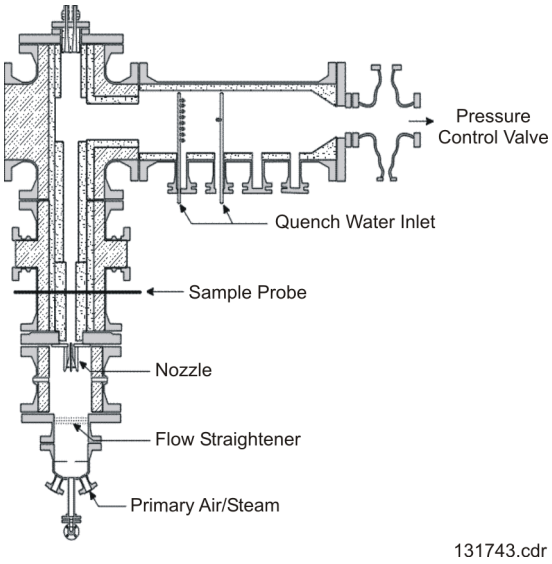

Figure 2-58. Schematic of the Combustion Test Facility

A typical test plan entailed slowly ramping the air and fuel flow rates with appropriate piloting levels (to mitigate any transitory combustor dynamics) to the base operating point. The range of equivalence ratios examined was defined by the CO emissions on the lean side (where kinetic CO production dominates) and NO_x emissions on the rich side. Fuel ramps were discontinued when CO levels approached 200 to 300 ppm, or when NO_x levels approached around 100 ppm. Correspondence between operating conditions and emissions measurements was obtained by ramping the gas flow rates slow enough, commensurate with the gas sample's system response time, and time shift-

[1] Kendrick, D.W., Anderson, T.J., Sowa, W.A., and Snyder, T.S., "Acoustic Sensitivities of Lean-Premixed Fuel Injectors in A Single Nozzle Rig," *Journal of Engineering for Gas Turbines and Power*, 121, pp. 429-436, July 1999; and Snyder, T., Rosfjord, T., McVey, J., Hu, A., and Schlein, B., "Emission and Performance of a Lean-Premixed Gas Fuel Injection System for Aeroderivative Gas Turbine Engines," ASME Paper No. 94-GT-234, 1994.

ing the data (pressures, temperatures, etc.) relative to the emissions measurements. This typically involved ramping up the fuel flow rate approximately 30 percent per hour.

To assess the nozzles over a wide operating range, the operating conditions detailed in Table 2-4 were examined.

Table 2-4. Operating Conditions[1]

Operating Pressure (P_3)	100 psia
Inlet Temperature (T_3)	860ºF
Equivalence Ratio (ϕ)	0.4 to 0.77
Sidewall Pilots (Percent Sidewall)	0 to 3%
Diffusion Centerline Pilots (Percent Centerbody)	0 to 1%
Nozzle Pressure Drop (Percent P_3)	3%

[1] Piloting levels are mass percentages of the total fuel flow rate.

2.5.2 Emissions Modeling

The experiments were modeled using a literature reaction set, GRI-MECH 2.11, and its accompanying thermochemistry.[1] The GRI-MECH 2.11 reaction consists of 49 species and 277 reactions and has been validated over a wide range of pressure and equivalence ratios. A PSR network code developed at UTRC was used to simulate the combustor. The foundation of the network PSR code is the Chemkin PSR model.[2] The aim of the network was to simulate the essential flow-field features (mixing, in particular) that are strong factors in emissions generation. A total of 10 reactors were used to represent the present combustor. This number was arbitrarily chosen to accurately simulate the combustor without being computationally intensive. The combined residence time within all 10 reactors totaled the experimental residence times (time from the dump plane to the emission sampling probes).

2.5.3 Results

NO_x Comparisons Between Quarter-Scale and Full-Scale Nozzles

Figure 2-59 and Figure 2-60 reveal the NO_x emissions for both the quarter-scale and full-scale nozzles under conditions of no piloting and piloting (1 percent centerbody and 3 percent sidewall, respectively). All data has been corrected to 15 percent excess air and is plotted versus the adiabatic flame temperature calculated for the particular operating point.[3] Clearly shown is the strong nonlinear dependence of NO_x values with combustion zone flame, as described by others,[4] which is due to the exponential temperature dependence on the primary NO_x-generating

[1] Bowman, C.T., Hanson, R.K., Davidson, D.F., Gardiner, W.C., Jr., Lissianski, V., Smith, G.P., Golden, D.M., Frenklach, M., and Goldenberg, M., 1994, (http://www.me.berkeley.edu/gri_mech).

[2] Glarborg, P., Kee, R.J., Grcar, J.F., Miller, J.A., "PSR: A Fortran Compiler for Modeling Well-Stirred Reactors," *Sandia National Laboratories Report*, SAND86-8209, Livermore, CA, February 1986.

[3] Reynolds, W.C., "STANJAN, Interactive Computer Programs for Chemical Equilibrium Analysis," Stanford University, January 1981.

[4] Dahm, W., Driscoll, J., Hsieh, T., "Scaling Characteristics of Aerodynamics and Low-NO_x Properties of Industrial Natural Gas Burners: The Scaling 400 Study," Final Report, GRI, 1998; Strand, T., "Dry Low NO_x Combustion Systems Development and Operating Experience," ASME Paper No. 96-GT-274, 1996, presented at the International Gas Turbine and Aeroengine Congress and Exhibition, June 10-13, Birmingham, U.K.; Leonard, G. and Stegmaier, J., "Development of an Aeroderivative Gas Turbine Dry Low Emissions Combustion System," ASME *Journal of Engineering for Gas Turbines and Power*, Vol. 116, pp. 542-546, 1994; and Lefebvre, A., *Gas Turbine Combustion*, Taylor and Francis Publishing, 1983.

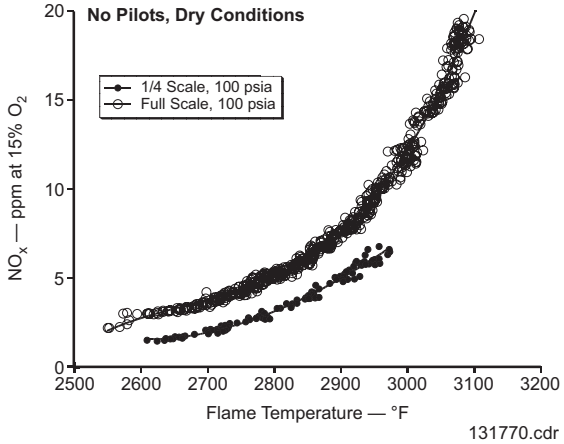

Figure 2-59. NO_x Versus Flame Temperature Under Nonpiloting Conditions

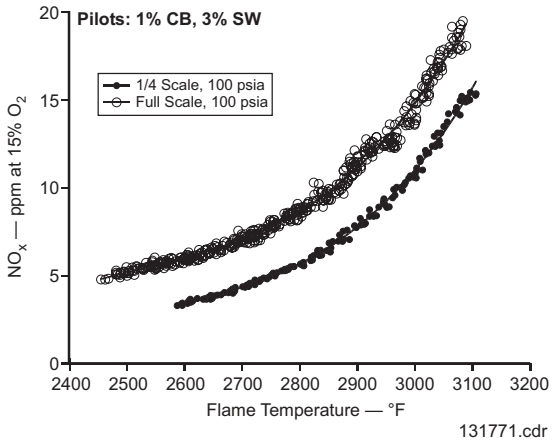

Figure 2-60. NO_x Versus Flame Temperature Under Piloting Conditions

mechanism for these conditions.[1] The interesting observation, however, is that under both piloting and nonpiloting conditions, the NO_x levels show a clear upward shift with nozzle scale: Approximately 3 ppm for each case. This variance appears fairly constant over the excursion in flame temperature. The data does suggest that through appropriate/artificial flame temperature increases/decreases, both data sets could be forced to collapse. That is, if each quarter-scale nozzle's combustion zone temperature was artificially increased by 120ºF (nonpiloting) and 140ºF (piloting)[2] by some mechanism, such as heat transfer, the NO_x levels for both scales and piloting conditions would coincide. This issue will be explored in Section 2.5.4. Despite the small shift in the data, the repeatability and lack of data scatter ensure that the trends are indeed real.

The adverse influence of the diffusion piloting is clearly evident when comparing equivalent scales, resulting in an approximate 3 to 5 ppm increase for the full-scale design and a 2 to 4 ppm increase for the quarter-scale nozzle. It can also be seen that the NO_x separation seems linked to the pilots, since the piloting data is further apart relative to their nonpiloting counterparts. The question to answer is the mechanism(s) for the observed shifts.

As previously mentioned, both configurations were designed on the constant velocity scaling approach, whereby nozzle velocities and interior fuel penetration characteristics that are linked to NO_x levels are held constant.[3] Furthermore, combustor diameters were correspondingly altered and nozzle pressure drops were held constant to ensure combustor velocities (and convection time scales), although less critical to NO_x production, were preserved under both conditions. Other parameters essential to NO_x generation, combustor pressure, inlet air and fuel temperature, and geometric similarity, were held constant between both scales and data sets and therefore, do not explain the observed trends. What remains, therefore, are more subtle factors linked to NO_x emissions: Changes in flow distribution, such as unmixedness,[4] which may be linked to geometric scales/thermal alterations in the combustor near field[5] that may alter the heat exchange to the flame zone and therefore, flame temperature,

[1] Peters, N., and Donnerhack, S., "Structure and Similarity of NO_x Production in Turbulent Diffusion Flames," *Eighteenth Symposium (International) on Combustion*, The Combustion Institute, Pittsburgh, pp. 33-42, 1981.

[2] Precisely the flame temperature spacing.

[3] Rutar, T., Martin, S.M., Nicol, D.G., Malte, P.C., Pratt, D.T., "Effects of Incomplete Premixing on NO_x Formation at Temperature and Pressure Conditions of LP Combustion Turbines," ASME Paper No. 97-GT-335, 1997; Fric, T., "Effects of Fuel-Air Unmixedness on NO_x Emissions," AIAA Paper No. 92-3345, 1992; and Lefebvre, A., *Gas Turbine Combustion*, Taylor and Francis Publishing, 1983.

[4] Rutar, T., Martin, S.M., Nicol, D.G., Malte, P.C., Pratt, D.T., "Effects of Incomplete Premixing on NO_x Formation at Temperature and Pressure Conditions of LP Combustion Turbines," ASME Paper No. 97-GT-335, 1997; Mongia, R.K., Tomita, Eiji, Hsu, F.K., Talbot, L., Dibble, R.W., *Twenty-Sixth Symposium (International) on Combustion*, The Combustion Institute, Pittsburgh, PA, p. 2749, 1996; and Fric, T., "Effects of Fuel-Air Unmixedness on NO_x Emissions," AIAA Paper No. 92-3345, 1992.

[5] Sayre, A., Lallemant, N., Dugue J., and Weber, R., *Twenty-Fourth Symposium (International) on Combustion*, The Combustion Institute, Pittsburgh, PA, pp. 235-242, 1994.

and NO_x levels.[1] Although the combustion intensity (heat release per unit volume) remains constant between the two scales, the surface-to-volume ratio is different. Including the end effects, one has:

$$\left.\frac{S}{V}\right|_{1/4S} = \frac{\pi D_{1/4} L + \frac{1}{2}\pi D_{1/4}^{\ 2}}{\frac{1}{4}\pi D_{1/4}^{\ 2} L} = 1.46$$

$$\left.\frac{S}{V}\right|_{FS} = \frac{\pi D_{FS} L + \frac{1}{2}\pi D_{FS}^{\ 2}}{\frac{1}{4}\pi D_{FS}^{\ 2} L} = 0.79$$

The full-scale nozzle has less surface area encasing the combustion volume, or the potential for hotter walls that could elevate surrounding gas temperatures.[2]

2.5.4 Combustor Thermal Analysis

Evidence of a departure from perfect thermal similarity within the combustor can be obtained through detailed temperature measurements within the flame itself, the surrounding recirculation zone, and adjacent surfaces (such as combustor walls and nozzle). Through these measurements, the relative magnitudes of the governing energy exchange mechanisms can be deduced.[3] The difficulty of nonobtrusively instrumenting the hostile flow-field within the combustor makes the equation impractical. Furthermore, attaching thermocouples through a ceramic shell was also deemed impractical. Finally, the absence of optical access for thermal pyrometry measurements made any surface measurements impossible. As a result, thermocouples were instrumented in the only practical location: On the nozzle itself. Two locations were chosen: in the middle of the bluff end plate or nozzle tip (T_{tip}) and 0.5 in. upstream of the dump plane on the surface of the nozzle's centerbody. As both measurement locations yielded similar results and since the tip location had the largest solid angle viewing the combustion zone, only its measurements will be displayed (Figure 2-61).

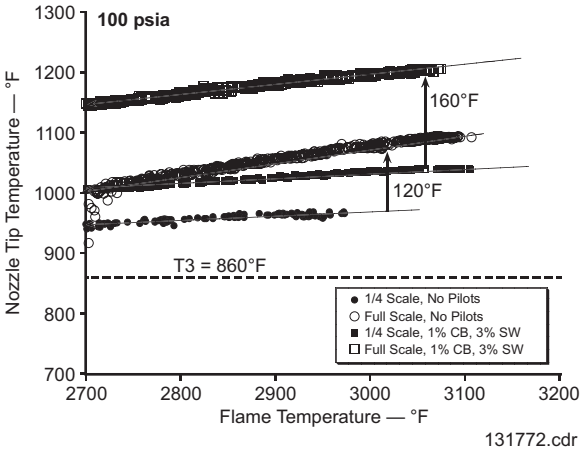

Figure 2-61. Nozzle Tip Temperature Versus Flame Temperature

[1] Turns, R., and Myhr, F., *Combustion and Flame*, 87, pp. 319, 1991; and Gore, J., and Faeth, G., *Twenty-First Symposium (International) on Combustion*, The Combustion Institute, pp. 1521, 1986.

[2] Dahm, W., Driscoll, J., Hsieh, T., "Scaling Characteristics of Aerodynamics and Low-NO_x Properties of Industrial Natural Gas Burners: The Scaling 400 Study," Final Report, GRI, 1998.

[3] Kreith, F., and Bohn, M., *Principles of Heat Transfer*, Harper and Row, Cambridge, U.K., 1986.

Figure 2-61 details the nozzle tip temperatures over the flame temperatures excursions for both data sets (piloting and nonpiloting) and for both nozzle scales. The dotted line indicates the inlet air temperature, T_3. The gradual increase in temperature with flame temperature (stoichiometry) was expected. The interesting feature is the more rapid increase in temperature for both full-scale designs and the greater disparity between the two piloting curves (160ºF) relative to their nonpiloting counterparts (120ºF). The jump, however, from both quarter-scale nozzles to their respective full-scale designs is striking and suggests that near field thermal characteristics (near the dump plane) are different between scale. Whether this difference exists due to alterations in the thermal exchange from the flame to the gases comprising the outer recirculation zone/combustor walls, or merely from shifts in the location of the combustion zone due to the prevailing aerodynamics, remains to be determined.[1]

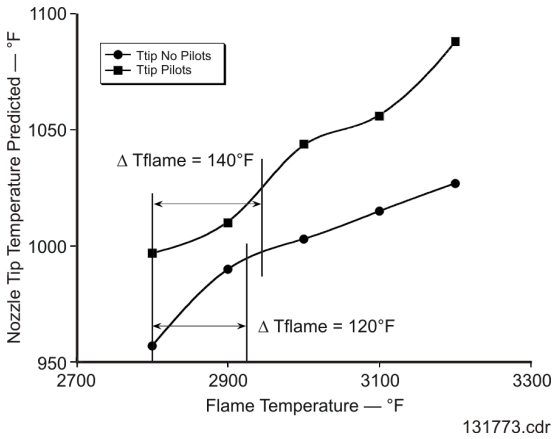

Figure 2-62. T_{tip} Predictions from Combustion Flame Temperature Increases

To explore this point, a simple thermal analysis incorporating the chief energy exchange mechanism was undertaken to assess how much the primary zone flame temperature would have to increase to explain the jumps in T_{tip} with the full-scale design relative to its quarter-scale counterpart. The results are shown in Figure 2-62. The code was referenced at a flame temperature of 2800ºF and adjusted to yield an initial tip temperature of around 950ºF (nonpiloting) and 1000ºF (piloting), respectively. The two curves clearly show that for a 120ºF (nonpiloting) and 140ºF (piloting) increase in flame temperature (Tflame) (necessary Tflame increase to make the quarter-scale data coincident with the respective full-scale data), this would constitute only a mere 30º to 40ºF increase in tip temperature. This is clearly inconsistent with Figure 2-61.

A further confirmation that an extreme thermal imbalance does not exist between both nozzle scales is seen when one examines the CO emissions. Figure 2-63 details the CO emissions for the nonpiloting case only (the piloting data leads to an identical conclusion). The full-scale values appear modestly higher (equivalent to 1 ppm) overall than their quarter-scale counterparts. More importantly, the *knee* of the CO curve, which divides kinetic CO production from equilibrium produce CO, lies at a near identical flame temperature location for both nozzles.[2] If the primary zone flame temperature was truly higher than expected for the full-scale design, when compared to the quarter-scale nozzle, the CO curve would have shifted to the left, as shown by the solid line. The equilibrium CO, which lies to the right of the minimum, would have increased, since equilibrium levels scale with temperature.[3] The kinetically-produced CO, conversely, would have decreased, since reaction rates would have increased (exponential temperature dependence), allowing more time for CO oxidations to CO_2.[4]

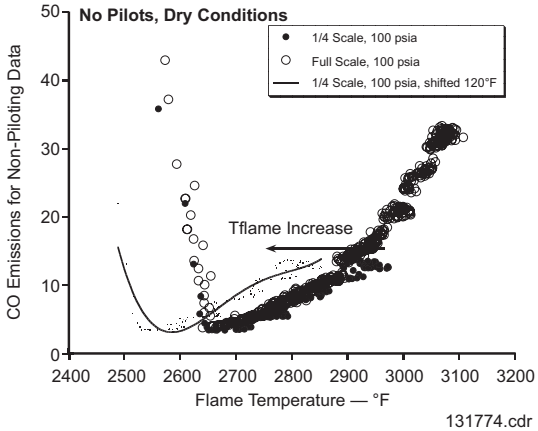

Figure 2-63. CO Emissions for Nonpiloting Data and Expected Trends Under the Flame Temperature Increases

[1] Kendrick, D.W., Anderson, T.J., Sowa, W.A., and Snyder, T.S., "Acoustic Sensitivities of Lean-Premixed Fuel Injectors in A Single Nozzle Rig," *Journal of Engineering for Gas Turbines and Power*, 121, pp. 429-436, July 1999.

[2] Lefebvre, A., *Gas Turbine Combustion*, Taylor and Francis Publishing, 1983.

[3] Bhargava, A., Colket, M.B., Sowa, W., Castleton, K., and Maloney, D., "An Experimental and Modeling Study of Humid Air Premixed Flames," AMSE Paper No. 99-GT-8, 1999.

[4] The equilibrium CO levels were taken at a flame temperature 120ºF higher than that calculated for the particular flame temperature indicated in the abscissa, and reflects the added temperature necessary for making both the full- and quarter-scale model's NO_x levels coincident

The above discussion does not preclude the influences of thermal variations within the main NO_x-generating zone, only that its effects cannot be largely responsible for the observed trends in T_{tip}. It is concluded that the large jumps in T_{tip} are due to axial shifts in the combustion zone location as seen elsewhere.[1] The final section will show that the most likely explanation for the trends concerns increasing mixing scales with nozzle size, which creates fuel-rich pockets and augments NO_x levels.[2]

PSR Combustor Modeling

As mentioned in an earlier paper, a 15-reactor network design was used to model the effects of moisture and pilot level on NO_x emissions.[3] At first, the same reactor configuration was used to model the effect of scale on NO_x emissions. This reactor configuration failed to capture the geometric effect seen experimentally in Figure 2-59 and Figure 2-60. Therefore, it was decided to start a modeling exercise, or to design a reactor network from the beginning. The reactor design was focused into modeling the anticipated flow-field features responsible for the experimental trends: Variations in the flow distribution arising from a change in nozzle scale, which would simulate changes in the flow characteristics and mixing. This approach proved very successful relative to earlier concepts and resulted in model predictions in line with the experimental data.[4]

The resulting network used to simulate the experiments is shown in Figure 2-64. Table 2-5 summarizes the distributions of fuel and air fractions in reactor volumes for each nozzle scale. For completeness, a hypothetical half-scale nozzle was also modeled. As previously mentioned, the network was designed to simulate the mixing and flow characteristics of the experiment, as closely as possible, using an arbitrary number of reactors (15) to effectively simulate the essential physics of the problem. Most of the fuel, 69.5 to 77.5 percent of the total, and 99.7 percent of the air, was introduced in reactor 1. This represented the flame zone and accounted for more than a quarter of the total residence time. The remainder of the fuel was introduced in reactors 2, 4, and 5. A rich zone was created in reactor 3 with ½ percent fuel and 0.3 percent air. The combination of reactors 2 through 5 represent the inhomogeneity that could exist due to variations in flow distributions with nozzle scale. As such, the fuel distributions are accordingly altered with each geometry. The rest of the reactors (6 to 15) represent the post-flame zone. The residence time in all the reactors combined was between 4.5 and 6 ms, closely matching their experimental values.

Table 2-5. Initial PSR Network Fuel and Air Distributions

Reactor	***1***	***2***	***3***	***4***	***5***
Quarter Scale (fuel)	0.695	0.1	0.005	0.1	0.1
Quarter Scale (air)	0.997	0.0	0.003	0.0	0.0
Half Scale (fuel)	0.745	0.1	0.005	0.1	0.05
Half Scale (air)	0.997	0.0	0.003	0.0	0.0
Full Scale (fuel)	0.775	0.1	0.005	0.1	0.02
Full Scale (air)	0.997	0.0	0.003	0.0	0.0

[1] Kendrick, D.W., Anderson, T.J., Sowa, W.A., and Snyder, T.S., "Acoustic Sensitivities of Lean-Premixed Fuel Injectors in A Single Nozzle Rig," *Journal of Engineering for Gas Turbines and Power*, 121, pp. 429-436, July 1999.

[2] Rutar, T., Martin, S.M., Nicol, D.G., Malte, P.C., Pratt, D.T., "Effects of Incomplete Premixing on NO_x Formation at Temperature and Pressure Conditions of LP Combustion Turbines," ASME Paper No. 97-GT-335, 1997; and Dahm, W., Driscoll, J., Hsieh, T., "Scaling Characteristics of Aerodynamics and Low-NO_x Properties of Industrial Natural Gas Burners: The Scaling 400 Study," Final Report, GRI, 1998.

[3] Bhargava, A., Colket, M.B., Sowa, W., Castleton, K., and Maloney, D., "An Experimental and Modeling Study of Humid Air Premixed Flames," AMSE Paper No. 99-GT-8, 1999.

[4] Bhargava, A., Kendrick, D.W., Colket, M.B., Sowa, W.A., Casleton, K., and Maloney, D., "Pressure Effect on NO_x and CO Emissions in Industrial Gas Turbines," Proceedings of ASME Turbo Expo, Paper No. 2000-GT-97, 2000.

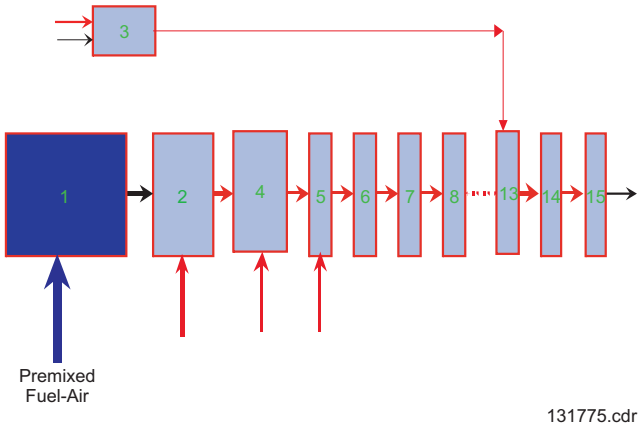

Figure 2-64. Initial PSR Network for Combustor Modeling

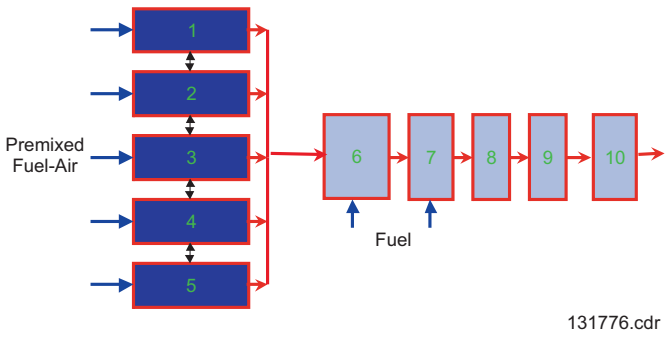

Figure 2-65. Final PSR Network To Assess Mixing Nonuniformity

The results of the above network, although not shown, effectively tracked the scale-up effects found experimentally. One uncertainty with the current PSR network, however, is its inability to deconvolute the separate effects comprising an alteration in the flow distribution; it fails to discern whether true unmixedness variations are responsible for the experimental trends, as shown by others, or whether an axial redistribution caused by some other mechanism is responsible.[1] The PSR network, which effectively resolves this issue, appears in Figure 2-65 together with the specific fuel distributions in Table 2-6. Here, the initial reactor (1) is broken into five separate reactors, themselves having a distribution in equivalence ratio that would mimic a radial nonuniformity in the equivalence ratio caused, for instance, through inadequate mixing. Air was equally divided among the five reactors, while the fuel was set to progressively less uniform profiles with increasing nozzle scale. Despite this, 80 percent of the total fuel was always added into reactors 1 to 5, while a constant 10 percent was added in reactors 6 and 7 for each case. Total residence times were preserved from before. The numeric results are plotted with their experimental counterparts in Figure 2-66. Excellent agreement with the data is observed. The model was also adjusted to incorporate the effects of the pilot through insertion of a single reactor feeding reactors 1 through 5. Again, the results compare well to the experimental data (Figure 2-67). It is postulated, therefore, that the NO_x trends are indeed likely the result of poorer mixing with increasing nozzle scale. Larger scales appear less effective in smoothing spatial nonuniformities so critical in reducing NO_x levels.

Table 2-6. Final PSR Modeling Fuel Distributions

Reactor	***1***	***2***	***3***	***4***	***5***
Quarter Scale	0.16	0.160	0.16	0.160	0.16
Half Scale	0.13	0.145	0.16	0.175	0.19
Full Scale	0.12	0.140	0.16	0.180	0.20

[1] Fric, T., "Effects of Fuel-Air Unmixedness on NO_x Emissions," AIAA Paper 92-3345, 1992.

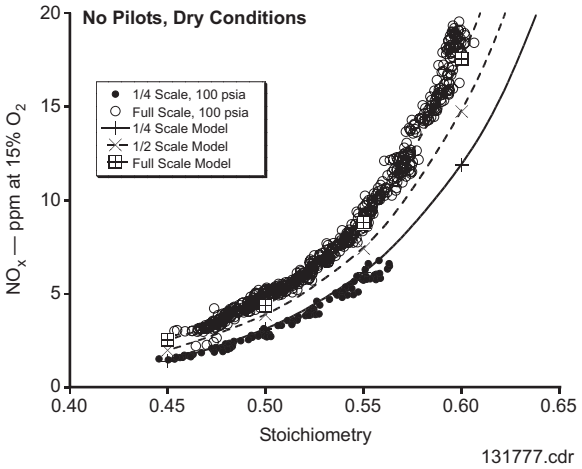

Figure 2-66. Final PSR Network Modeling Comparison With Nonpiloting Experimental Data

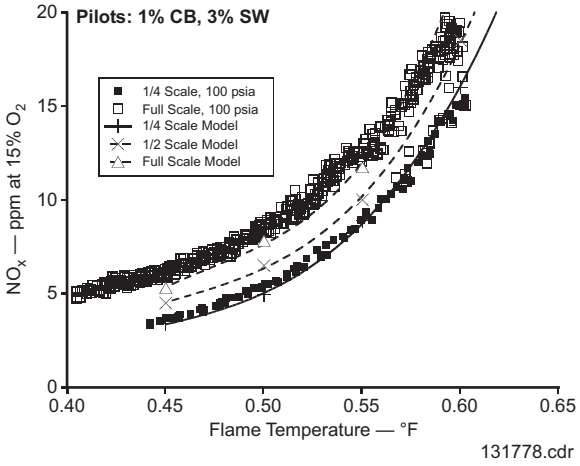

Figure 2-67. Final PSR Network Modeling Comparison With Piloting Experimental Data

After establishing an accurate network that depicted the experimental data, a study was performed to investigate the separate effects of each of the three NO_x generation mechanisms on nozzle scale: *Zeldovich* or *Thermal* NO_x, the *$N_2$0* mechanism, and the *Fenimore* (*Prompt*) mechanism. NO_x formation reactions were divided into these three different, but coupled, groups in the following manner:

- *Zeldovich* or *Thermal* NO_x mechanism,[1] as extended by Bowman and Seery[2] — The NO_x is initiated by the reaction of N_2 with the O atom. This well-established, three-step reaction sequence is the dominant NO_x-forming route at temperatures above 2950°F. *Zeldovich*, or *Thermal* NO_x mechanism, was suppressed by making the $N_2 + O \leftrightarrow N + NO$ reaction proceed in the reverse direction only.
- *N_2O* mechanism, consisting of reactions involving N_2O that form NO — The NO_x formed through this mechanism can be effectively suppressed by making the N_2O (+M) $\rightarrow N_2 + O$ (+M) proceed in the forward direction only.
- *Fenimore* NO_x mechanism — All NO_x forming reactions, beside the *Zeldovich* and *N_2O* pathways, are included in this route. The main steps influencing this reaction sequence are $N_2 + CH = HCN + N$, $N_2 + CH_2 = HCN + NH$, and other reactions involving N_2 and hydrocarbon radicals. This extensive sequence was suppressed by inhibiting the forward rates for reactions between hydrocarbon fragments and molecular nitrogen.

To study the contribution of each pathway, the other two channels were suppressed. Therefore, in order to analyze the importance of the *Zeldovich* mechanism, NO_x formation through the *Fenimore* and *N_2O* mechanisms was removed. Similar computations were performed to evaluate the importance of the *Fenimore* and *N_2O* mechanisms.

The results are presented in Figure 2-68. What is plotted on the y-axis, *n*, is the exponent of the combustor's area in a plot of $(\text{area})^n$ versus NO_x, similar to a plot of NO_x versus P^n.[3] The plot reveals that scale has the most influence on the *Thermal* mechanism, followed by the *Fenimore*, and finally by the *Prompt* mechanism (in that order). The combined effects of all three mechanisms are also shown and appear lower than the individual effect of the *Thermal* mechanism.

[1] Zeldovich, J., "The Oxidation of Nitrogen Combustion and Explosions," *Acta Physicochimica*, URSS, 21, 577, 1946.

[2] Bowman, C.T., and Seery, D.J., *Emissions from Continuous Combustion Systems*, (W. Cornelius and W.G. Agnew, eds.), p. 123, 1972.

[3] Bhargava, A., Colket, M.B., Sowa, W., Castleton, K., and Maloney, D., "An Experimental and Modeling Study of Humid Air Premixed Flames," AMSE Paper No. 99-GT-8, 1999.

2.5.5 CONCLUSIONS

Experimental data obtained from two geometrically similar but differently sized nozzles has shown that generated NO_x levels increased with scale, increasing at a greater rate when diffusion piloting was engaged. Simple thermal modeling and examination of CO emissions which, for the most part, are equilibrium controlled, suggest that thermal alternations in the combustor near field that may influence NO_x generation through highly temperature dependent kinetic mechanisms, are not sufficient to explain the experimental trends.[1] Through correctly modeling the flow distributions, PSR network modeling has shown that the dominant cause for the NO_x scale up effects is increasingly poorer mixing with larger nozzles. This can be attributed to the increasingly larger mixing scales that result from larger physical sizes, which inhibit spatial smoothing in the equivalence ratio within the combustion zone. Scale effects appear to have the greatest influence on the *Thermal* or *Zeldovich* mechanism, followed by the *Fenimore*, and finally, by the *N_20* mechanism.

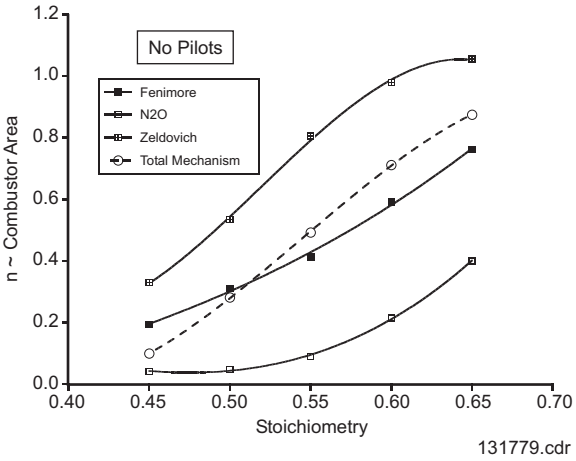

Figure 2-68. Effects of the Three Mechanisms

2.6 CYCLE DEFINITION: ANALYSES OF HAT CYCLE SYSTEMS

2.6.1 Summary

Analyses were carried out to identify the performance potential of aeroderivative gas turbines used in a HAT cycle. Emphasis was placed on an intercooled version of an industrialized PW4000, a nominal 100,000-lb thrust turbofan engine. In its basic configuration as a twin-spool engine, the FT4000 intercooler (I/C) has an output of 148 MW and an efficiency of 47.5 percent (LHV). The baseline HAT cycle identified in this analysis operates at the design point of the FT4000 I/C at a combustor exit temperature of 2715°F and an overall pressure ratio of approximately 60. In the FT4000 I/C, the operating temperature is limited not by turbine cooling considerations, but by NOx production. At these conditions, the efficiency of the HAT cycle is estimated to be 58.7 percent (LHV); a value quite close to the 60 percent (LHV) goal set by the DOE for the ATS combined cycle project.

Parametric analyses indicated that operation at combustor exit temperatures in excess of the 2715°F limit would result in HAT cycles with efficiencies equal to or above the 60 percent goal. At these temperatures, the concern was whether NO_x production would be an issue. A series of tests were carried out by personnel from P&W, UTRC, and the NETL to identify the role of humidity and unmixedness on NO_x generated in a gas turbine. The results of these tests, detailed in prior sections of this report, indicate that at the moisture levels used in the HAT cycle, NO_x production is within the 9 ppm goal of the ATS goal, even at temperatures above 3000°F.

Alternative configurations of the FT4000 I/C HAT cycle were analyzed: One operating at 3100°F with an efficiency of 61.2 percent, and the other reheat version operating at 2715°F, with reheat to 2500°F and an efficiency of 60.3 percent. To complete the analyses, two versions of the FT8, a nominal 38 percent efficient 25 MW unit now in commercial operation, were investigated. The first version was the simple cycle, which in a simplified HAT configuration without an I/C would have an estimated output of 44.3 MW at an efficiency of 47 percent (LHV). The second FT8 version was a proposed FT8 I/C, which would have an efficiency of 38.9 percent and an output of 57.8 MW at design point operation. In HAT configuration, the estimated output was 83.7 MW at an efficiency of 53.3 percent.

2.6.2 Introduction

Over the next several decades, the U.S. utility industry will need to replace existing plants nearing the end of their useful life, as well as add new generating capacity. The potential additions for the U.S. could approach 300

[1] *Ibid.*

GW by 2020. These new additions and replacement units must meet increasingly stringent emission requirements, conserve fuel, and reduce production of CO_2 and other *Greenhouse* gases, all the while producing electricity at a cost savings that justifies their development.

Developments in the last decade in gas turbine technology have provided a basis for simple-cycle power systems having high efficiencies (equivalent to 40 percent), lower capital cost, more rapid installation, and lower emissions. The projected availability of competitively priced natural gas has made possible the consideration of these gas turbine-based plants as high load factor plants. In fact, combined-cycle systems based on large, heavy *frame* machines have become the power system of choice for base-load utility use. Smaller machines, typically aeroderivative turbines, are being widely used by independent power producers and private operators for industrial cogeneration.

UTC has been in the forefront of providing the utility market with aeroderivative turbines. Since its first installation of an aeroderivative turbine for industrial use in 1960, over 1200 units have been marketed, providing over 22,000 MW in peaking and combined cycle use. Currently, UTC has adapted the JT8D, the most widely used aircraft engine (over 14,000 in airline operation) to industrial service, introducing the FT8 in 1989. Since then, nearly 150 of these nominal 25 MW machines operating at a pressure ratio of 18 and at firing temperatures of over 2200°F are installed or on order.

The application of aircraft turbine technology to large-scale utility use can be accomplished in two ways:

1. The introduction of the advanced aerodynamics and turbine cooling techniques to large heavy frame machines
2. The development of advanced power cycles taking direct advantage of the high-pressure ratios and high-turbine temperatures.

The first method has been practiced by most aircraft turbine manufactures, including UTC, who supplied material and cooling technology to Siemans, now Siemans-Westinghouse, for use in their V-series of heavy frame machines.

A recent example of infusing advanced technology is through the ATS Program, which is sponsored by the NETL/DOE. This program has, among its objectives, the development of utility scale gas turbine-based power systems, which will demonstrate:

- 60 percent or greater cycle efficiency (natural gas LHV)
- Emissions of NO_x, CO, and hydrocarbons of less than 10 ppm
- Cost of electricity comparable to, or less than, current state-of-the-art power systems.

To date, the emphasis of this portion of the ATS Program has been on improving the materials and cooling technologies for large industrial *frame-type* gas turbines. These turbines are used in conventional combined-cycle configurations with the exhaust of the gas turbine supplying heat to raise steam for a steam turbine bottoming cycle. Several ATS configurations use some of the steam to cool the gas turbine.

Another approach to the DOE goals is based on the use of aircraft engine technology in an aeroderivative gas turbine engine. In addition to the benefits resulting form the advanced materials and cooling technologies available in aircraft engines, this type of engine is more easily adapted to highly efficient advanced-cycle configurations, such as the HAT cycle, patented by Fluor Daniel, Inc.[1]

[1] Rao, A.D., *Process for Producing Power*, U.S. Patent No. 482763, May 16, 1989.

The definition and preliminary engineering of a HAT power cycle based on advanced aeroderivative engine technology was undertaken in 1991 by a team with members from UTC, Fluor Daniel, Texaco, and EPRI using private funding.[1] This cycle, shown simplistically in Figure 2-69, uses gas turbine exhaust heat, as well as heat from within the cycle (intercooler and aftercooler) to supply heated water to a saturator. Here, the compressor discharge is humidified and then the water vapor-laden air passes through a recuperator and then to the turbine. Both the increased mass flow of the humid air and the higher specific work function of the mixture provide additional power, but require no additional compression work from the turbine, resulting in both efficiency and power output gains.

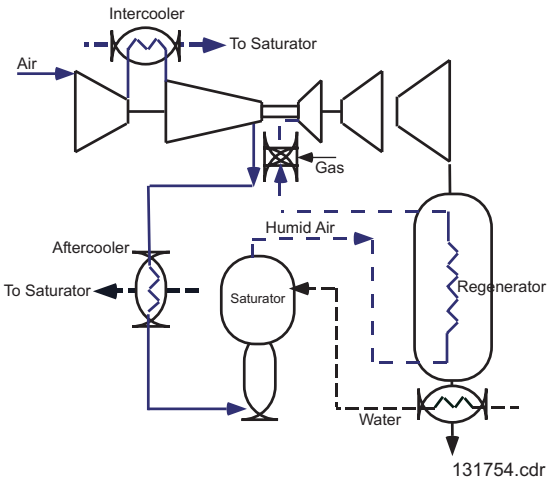

Figure 2-69. Simplified HAT Cycle Schematic

In both efforts, HAT cycles were identified that had over 60 percent efficiency and emissions estimates that met DOE goals. These emission estimates, however, were based on preliminary theories of NO_x formation in the presence of water vapor. A series of experimental and modeling studies, described in the other sections of this report, have been required to characterize the effect of humidity on the emissions and combustion stability of HAT cycle configurations.

2.6.3 HAT Cycle Basics

The HAT cycle is one of several alternative cycles that are available to increase the power output and efficiency of gas turbines. The majority of these involve the addition of various heat exchangers, such as I/Cs and recuperators for air and boilers for steam generation, to the basic gas turbine cycle and require some modification to the flowpath to allow air to be taken from and returned to the gas turbine. The major exception, and the most widely used cycle for power generation, the combined cycle, requires no changes to the basic gas turbine. The HAT cycle, Figure 2-69, can use all of the foregoing equipment in some form. Prior to discussing the HAT cycle options, the alternatives will be briefly described, starting with the combined cycle.

Combined Cycle

In the combined cycle (Figure 2-70), the exhaust heat from the gas turbine is recovered in a heat recovery steam generator (HRSG), where high-pressure steam is produced for expansion in a Rankine cycle steam turbine. Overall system efficiencies greater than 55 percent (LHV) have been demonstrated with commercially-available equipment, and efficiencies over 60 percent have been projected for combined cycles based on the gas turbines being developed as part of the ATS Program. In the most efficient of the combined cycles, the steam-bottoming cycle adds approximately 50 percent to the power output (the equivalent of 0.5 MW steam/1 MW gas turbine), increases the system efficiency by as much as 50 percent (e.g., 35 percent gas turbine versus 55 percent combined cycle), and adds 100 percent or more to the cost of a simple-cycle gas turbine ($275/kW gas turbine versus $550+/kW combined cycle). Emissions from the gas turbine in terms of parts per million exhaust are unchanged, although the emissions per unit of output are reduced by approximately one-third.

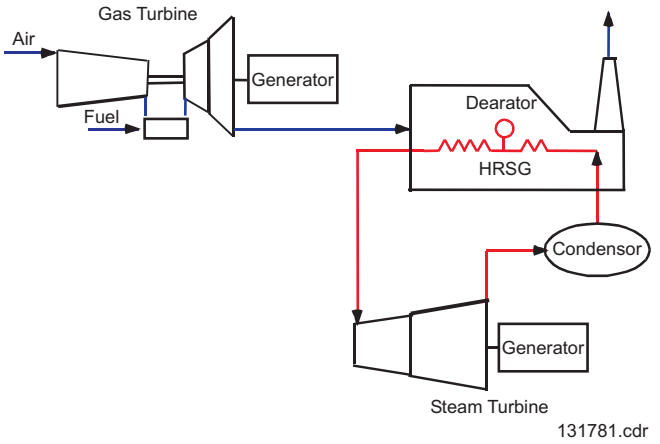

Figure 2-70. Combined Cycle

[1] TurboPower & Marine, "Humid Air Turbine Cycle Public Report," April 1993.

Intercooled Cycle

The I/C turbine (Figure 2-71) requires air to be removed from the gas turbine compressor, cooled either by water or air in an external heat exchanger, and returned to the gas turbine for further compression. By reducing the power needed to compress air to the desired pressure level, intercooling can increase gas turbine power output by a factor of two or more. The more complicated compressor sections and the I/C add cost, but the net result is generally lower cost per kW. Efficiency can decrease somewhat due to increased pressure drop. Emissions may be reduced because of the lower compressor discharge temperature and, possibly, the lower firing temperature needed to obtain the desired power.

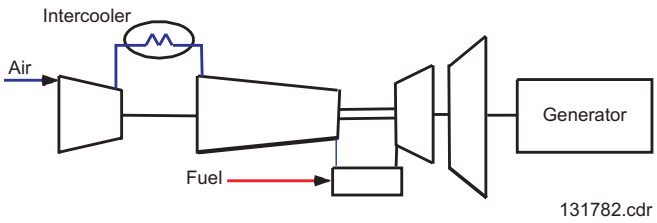

Figure 2-71. Intercooled Gas Turbine

Recuperated Cycle

The recuperated turbine (Figure 2-72) also requires air to be removed from the diffuser of the gas turbine compressor and then returned at essentially the same place. The size of a recuperator is very dependent on its effectiveness, a nonlinear function. Recuperator effectiveness tends towards 80 percent and higher, generally requiring significant heat transfer area/footprint. Power is somewhat reduced due to increased pressure drop and turbine backpressure, but efficiency increases by 25 percent or more, depending on effectiveness. The recuperator typically adds 10 percent to 15 percent to the cost of the gas turbine. Emissions on a parts per million basis would be essentially unchanged, but reduced on a unit output basis.

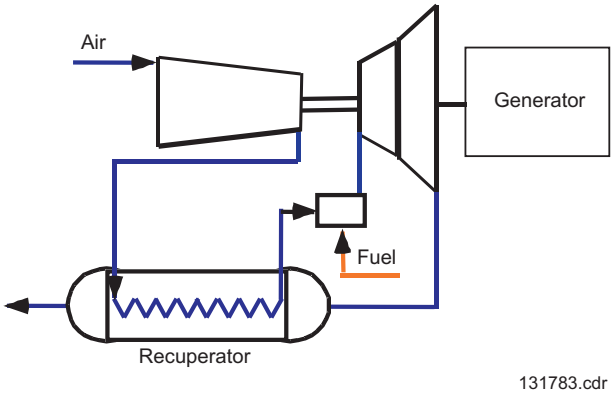

Figure 2-72. Recuperated Gas Turbine

The HAT cycle uses each of the above components to achieve both specific power and efficiencies greater than any of the cycles described above. A more detailed HAT cycle schematic is shown in Figure 2-73.

HAT Cycle

The HAT cycle system operation is as follows: Filtered air is first compressed in the low-pressure compressor and then enters an I/C where the majority of the compression energy is recovered for air saturation by the air saturator circulating water and makeup water. The cooled compressed air is further compressed in the high-pressure compressor, cooled in an aftercooler with air saturator circulating water and then sent to the air saturator. In the saturator, the air is humidified in a multistage counter-current heat exchanger as it passes through a packed bed filled with heated water. It exits the saturator at essentially 100 percent humidity. The humidified air (up to approximately 25 percent by mass water vapor) then passes through a recuperator, where it is heated against the gas turbine exhaust before going to the combustor. The low-grade heat for the saturator is

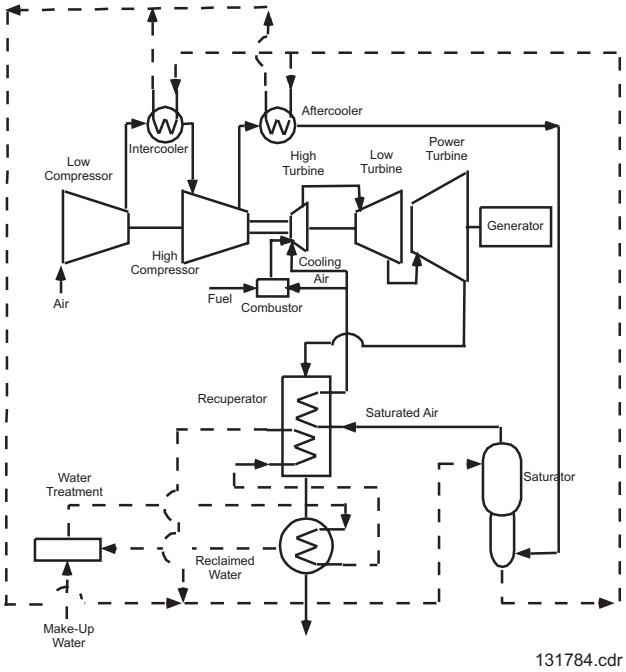

Figure 2-73. Detailed HAT Cycle Schematic

supplied by the I/C, the aftercooler, and an HRSG located in the back end of the gas turbine exhaust. Natural gas is preheated with hot water before being sent to the combustor. The hot gas expands through the high-pressure turbine, driving the high-pressure compressor on the same shaft. The gas leaving the high-pressure turbine is further expanded in the low-pressure turbine, which drives the low-pressure compressor, and in a power turbine connected on a separate shaft to the electric generator. The power of the gas turbine is increased by the additional mass flow and the efficiency is increased by both the recuperation of exhaust heat and the use of the remaining low-temperature exhaust heat to heat the water for the saturator.

With the exception of the advanced gas turbine, all other equipment is either commercially available or, in the case of the recuperator, consists of elements that are commercial available. The recuperator would resemble the HRSG portion of a combined cycle, as the duties are similar. The HAT operating conditions are well within the demonstrated operating conditions of HRSGs. The first two rows of tubes would be 1.25 percent chrome steel, with the remaining tube banks made of carbon steel. The advanced gas turbine is described below.

The efforts of the current program are based on the previously referenced background work on the HAT cycle done by Fluor, P&W, and the UTRC.[1] Considerable other analytic HAT cycle effort has been done,[2] or is being conducted.[3] The only operational HAT cycle is described in Argen *et al*[4]. This nominal 600 kW HAT-cycle installation is for demonstration and analysis purposes.

2.6.4 Baseline HAT Cycle

A baseline HAT cycle has been identified to serve as a starting point for performance estimates and also for use in carrying out parametric analyses. This baseline HAT cycle uses the PW FT4000 I/C, an intercooled aeroderivative (ICAD) based on the PW4000 aircraft engine. The characteristics of this engine are given in Table 2-7. The HAT cycle configuration has been shown previously in Figure 2-73.

Table 2-7. FT4000 Intercooler Characteristics

Inlet Flow (lb/sec)	610.3
Overall Pressure Ratio	56.4
Fuel Flow (lb/sec)	14.26
Combustor Exit Temperature (°F)	2715
Gas Turbine Exhaust Temperature (°F)	710
Gas Turbine Exhaust Flow (lb/sec)	623.4
Gross Power (MW)	147.5
Gross Efficiency (Percent LHV)	47.5

[1] Rao, A.D., Process for Producing Power, U.S. Patent No. 482763, May 16, 1989; Turbo Power & Marine, "Humid Air Turbine Cycle Public Report, April 1993; Robson, F.L., "Phase 1: Advanced Turbine Systems Study - System Scoping and Feasibility Study," DOE Contract DE-AC21-92MC29247, UTRC, March 1993; and Rao, A.D., and Joiner, J.R., "A Technical and Economic Evaluation of the Humid Air Turbine Cycle," *Seventh Annual International Pittsburgh Coal Conference*, September 1990.

[2] Day, W.H. and Rao, A.D., "FT4000 HAT with Natural Gas Fuel, ASME Cogen-Turbo," Vol. 7, 1992.

[3] TurboPower & Marine Systems, "Phase 1: Study of Advanced Aero-Derivative Gas Turbine Power Systems," *Collaborative Advanced Gas Turbine Project*, December 1993; Rosen, P.M., "Evaporative Gas Turbines - A Thermodynamic Evaluation of Their Potential," Report. No. ISRN LUTMDN/TMVK-7010-SE, Department of Heat and Power Engineering, Lund Institute of Technology, 1993; Gallo, W., Bidini, G., Bettagli, N., and Facchini, B., "The Evaporator Process Simulation and the HAT Cycle Performance," ASME Paper 95-CTP-59, ASME Turbo Power Congress, 1995; and Carcasci, C., Cosi, L., Fiaschi, D., and Manfrida, G., "Semi-Closed HAT (SC-HAT) Power Cycle," 2000-GT-154, ASME Turbo Expo 2000, May 2000.

[4] Argen, N.D., Westermark, M.O., Bartlett, M.A., and Lindquist, T., "First Experiments on an Evaporative Gas Turbine Pilot Plant: Water Circuit Chemistry and Humidification Evaluation," 2000-GT-0168, ASME Turbo Expo 2000, May 2000.

In addition to the baseline engine, a simple cycle FT4000 version was also considered. To assess the impact of HAT cycle operation on current commercial products, the nominal 25 MW FT8 was selected for consideration as a HAT cycle. A possible intercooled version of this engine was also analyzed. All of these variations will be discussed in later sections.

The major characteristics of the baseline HAT cycle version of the FT4000 I/C described by Table 2-7 are shown in Table 2-8.

Table 2-8. Baseline HAT FT4000 Intercooler

Inlet Flow (lb/sec)	610.3
Overall Pressure Ratio	56.4
Fuel Flow (lb/sec)	19.4
Combustor Exit Temperature (°F)	2715
Saturator Output (lb/sec)	115
Mass Fraction (percent)	20.3
Gas Turbine Exhaust Temperature (°F)	776
Gas Turbine Exhaust Flow (lb/sec)	743.8
Gross Power (MW)	248.4
Gross Efficiency (Percent LHV)	58.7

The FT4000 I/C HAT shows a nearly 25 percent increase in efficiency and a nearly 70 percent increase in power in comparison to the base FT4000 I/C. The efficiency of 58.7 percent (LHV) is very near the DOE goal of 60 percent for the ATS combined cycle, without all of the additional rotating equipment represented by the steam bottoming cycle.

Parametric Analysis

The effects of pressure ratio and combustor exit temperature were assessed in a parametric analysis. The results are shown in Figure 2-74.

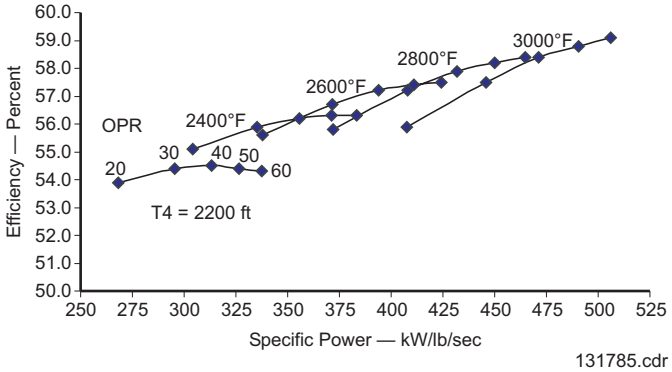

Figure 2-74. Parametric Performance Analysis of FT4000 I/C HAT Cycle

The results displayed in Figure 2-74 are of interest in defining trends in performance. The results should not be viewed as absolutes as the values used, while internally consistent, are based on assumptions aimed at reducing the variables used in the calculations. For example, while adjustments are made in cooling flows as the temperatures increase, at each temperature level the cooling flows are assumed to be the same, independent of pressure ratio. Also, auxiliary system losses are held constant, independent of temperature and pressure ratio. Design point calculations have all the detail needed to assure accurate representation of performance.

Other parametric analyses were made for the HAT cycle. These are shown in Figure 2-75 to Figure 2-78. For comparative purposes, both the FT4000 I/C and the FT4000 simple cycle versions (described in a later section) are shown on the same chart.

In Figure 2-75, the efficiency of the HAT cycle is shown as a function of moisture addition. As the moisture fraction increases, the cycle efficiency increases. This is due to the reduction in stack temperature, as the *low end* stack heat is used to preheat the water for the humidifier, and to an increase in recuperation, as the more humidified water is heated by the *high end* stack heat. The amount of humidification is limited by the heat available for use in the humidifier. In the simple cycle, only the compressor discharge heat and the stack heat is available. In the intercooled cycle, additional heat from the intercooler is available.

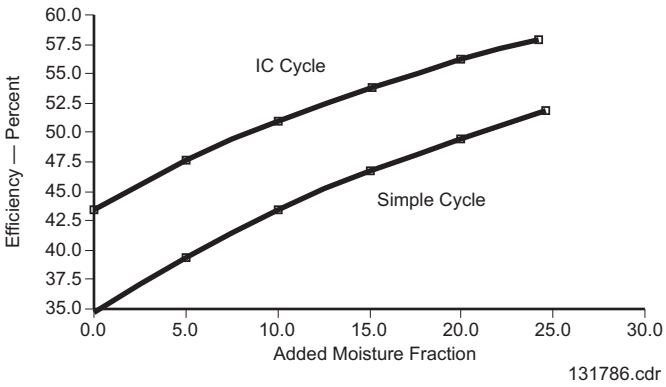

Figure 2-75. Efficiency as a Function of Moisture Addition

The specific power is a direct function of moisture addition. The added mass flow and higher specific heat of the water vapor results in significant power production.

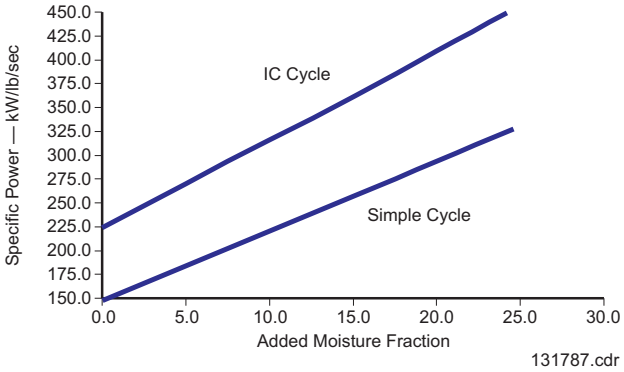

Figure 2-76. Specific Power as a Function of Moisture Added

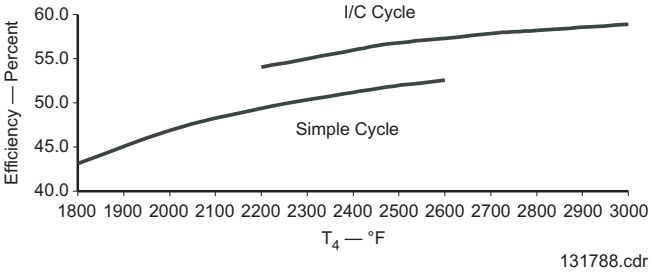

Figure 2-77. Efficiency as a Function of Combustor Exit Temperature

The dependence of cycle efficiency on turbine temperature (Figure 2-77) is similar for the HAT and normal gas turbine configurations. At temperatures of 3000°F, the HAT can have an efficiency over 60 percent.

As in the case of specific power, the actual power of the FT4000 is directly related to moisture fraction. The HAT version can have more than double the output of the non-HAT version.

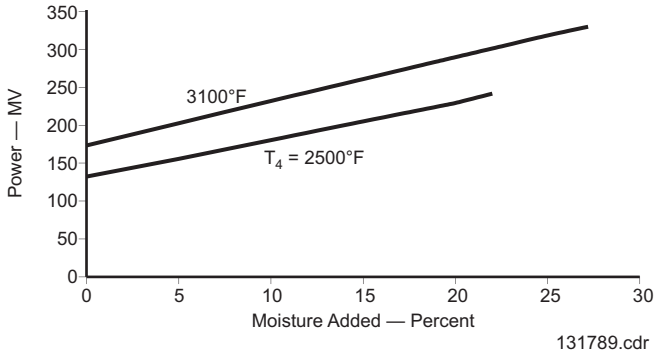

Figure 2-78. Output Power Versus Moisture Addition

Design Considerations

The HAT cycle requires some design modifications to typical gas turbine configurations. The compressor discharge air must be taken off-board the centerline design and sent to the coolers and humidifier. A method of returning the heated humidified air must be provided. Changes in the gaspath design may also be required if sufficient moisture addition is desired since the swallowing capacity of the turbine may be exceeded. The cooling of the first stage(s) of the turbine may also be changed from standard practice.

Air Handling

Most frame and aeroderivative gas turbines have in-line combustors; the combustors are located parallel to the centerline of the engine with the compressor discharge exiting a diffuser directly to the front end of the combustor. The combustor design proposed for the FT4000 I/C would use convectively cooled canted combustors, as shown in Figure 2-79.

The compressor discharge air is directed countercurrently along the walls of the combustor, cooling them and being preheated. A volute is located at the top of the combustor taking the air off-board to the coolers and humidifier. The humidified and recuperated air is returned to the *front end* of the combustor. This approach allows several benefits while retaining the same bearing span as the non-HAT version.

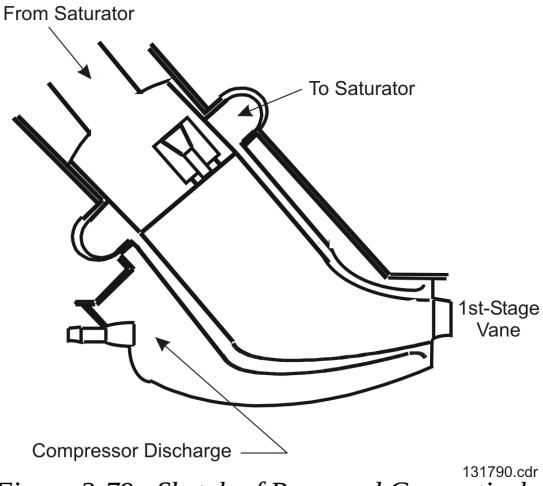

Figure 2-79. Sketch of Proposed Convectively Cooled Canted Combustor

Gaspath Changes

The swallowing capacity of a given gaspath is limited by the area of the 1st-stage vanes. Generally, this area can be adjusted by reclassifying the vanes, or inserting vanes with greater stagger, thereby opening the turbine. Typically, an additional 10 to 13 percent flow rate can be accommodated. Figure 2-80 shows the output at these conditions. Depending on the exact cycle conditions, as much as 25 percent mass fraction of water (lb water/lb inlet air) can be added in the humidifier, far exceeding the swallowing capability of the turbine. Thus, most HAT designs will require a new turbine section. While incurring additional design and development costs, the turbine is significantly less expensive than the compressor, which can be used intact.

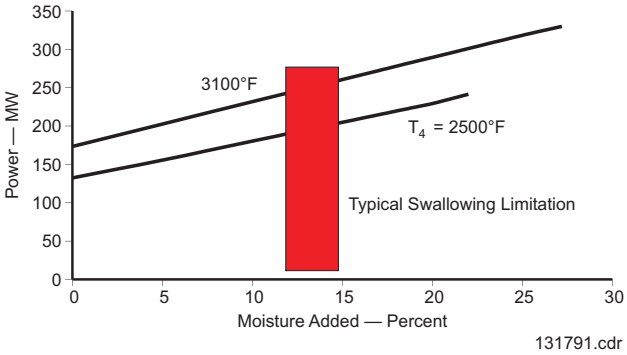

Figure 2-80. Limitation Set By Gas Turbine Area

Cooling Changes

The cooling in aeroderivative engines is similar to that in the aircraft version in that compressor air is withdrawn from various points and sent to the turbine for cooling and buffering. In the HAT cycle, the compressor discharge air is humidified giving it a greater cooling capability because of the increased specific heat of the air water mixture. In the configurations analyzed, the humidified air was used to cool the first stage vanes and blades. The cooling flow was set at the same level as would be used were the blades air cooled; this is because, while the cooling capability is greater, the intrastage temperature drop is smaller, due to the higher work function, and the subsequent stage sees a higher stagnation temperature. Efforts outside of the current program exist to develop cooling relationships for the HAT cycle.

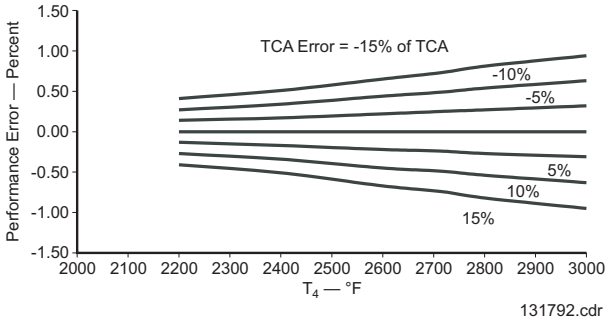

Figure 2-81. Effect of Errors in Turbine Cooling Flow on Performance

A brief parametric study was conducted to assess the effect of errors in cooling on HAT performance. The results are shown in Figure 2-81. Here it is seen that in the worst-case event, such as a 15 percent over/under esti-

mate of cooling flow at maximum temperature, an error of less than 1 percent in performance would occur. This is 1 percent, not 1 percentage point. This means that at the 60 percent efficiency level, an error of ±15 percent in cooling would result in a difference of only 0.6 percentage points in performance.

2.6.5 Alternative Configurations

A number of alternative HAT cycle configurations were considered:

1. 3100°F FT4000 I/C
2. Reheat FT4000 I/C
3. Simple cycle FT4000
4. Both simple and intercooled versions of the FT8.

High Temperature FT4000 I/C HAT

Operation at FT4000 I/C design point resulted in a HAT cycle with 58.7 percent efficiency, just over 1 percentage point shy of the DOE ATS goal of 60 percent. Increasing the turbine temperature could raise the efficiency to 60 percent or beyond. In the initial ATS study done by UTRC, several material and cooling changes were suggested that would result in a FT4000 I/C capable of meeting utility operational goals with a combustor exit temperature of 3100°F.[1] This value is significantly higher than the 2715°F of the baseline HAT. The 2715°F value, however, was not limited by design considerations, but by NO_x production in the non-HAT version. Tests carried out as part of this program indicate that DOE NO_x goals for the ATS can be met by a HAT version operating at temperatures over 3000°F (Figure 2-82). Even at a reduced moisture fraction (15 percent versus the more than 25 percent for the 3100°F version), NO_x emissions are predicted to be under 9 ppm. The performance of the 3100°F HAT is given in Table 2-9.

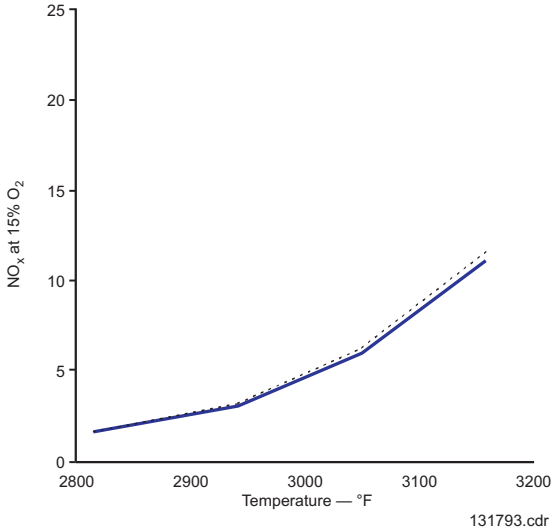

Figure 2-82. Predicted NO_x Emission for 15 Percent Moisture Fraction

Table 2-9. Performance of the 3100°F HAT

Cycle Alternative	*3100°F*	*Reheat*
System Performance		
Total Net Power (MW)	329.3	287.9
Gross Gas Turbine Power (MW)	333.1	293.7
Cycle Efficiency (Gross LHV)	61.2	60.3

Reheat HAT Cycle

A second alternative high performance HAT cycle involves the use of reheat before the low-pressure turbine (see Figure 2-73 for a schematic). In this version, the main combustor outlet temperature is 2715°F and the reheat combustor exit is 2500°F. The performance of this version is also given in Table 2-9. The use of the reheater requires considerably more cooling air, somewhat reducing the performance of this cycle.

Simple Cycle FT4000

Typically, the development of an engine such as the FT4000 I/C would be predicated on a successful simple cycle version. The simple cycle engine could be used in a HAT cycle, as shown in the Figure 2-83 schematic. Because there is no I/C, the OPR is reduced and there is less heat available in the compressor discharge. Thus, the mass fraction of moisture added is less and the efficiency is reduced. Also, the humidifier discharge temperature is higher, mitigating the recuperator effectiveness. The performance of the simple cycle HAT is shown in Table 2-10. The parametric analysis for this variation is shown in Figure 2-84.

[1] Robson, F.L., "Phase 1: Advanced Turbine Systems Study - System Scoping and Feasibility Study," DOE Contract DE-AC21-92MC29247," UTRC, March 1993.

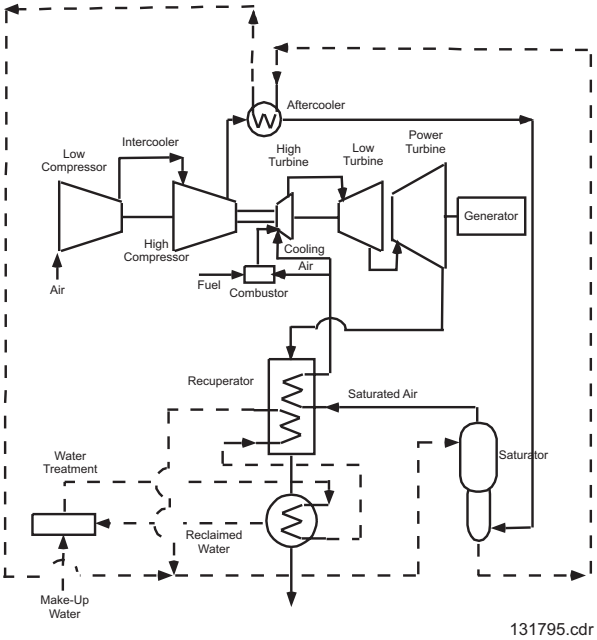

Figure 2-83. Simple Cycle HAT

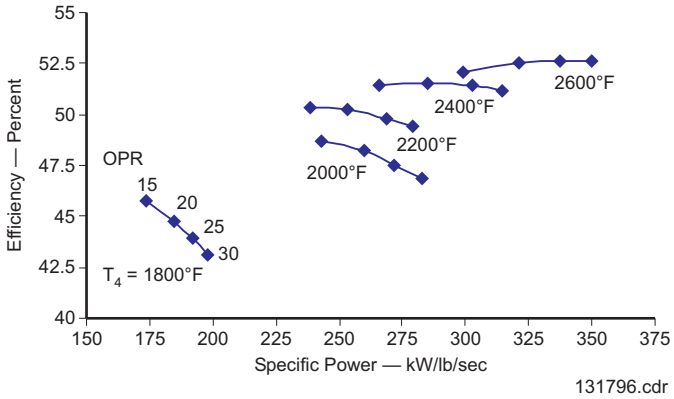

Figure 2-84. FT4000 Simple Cycle HAT Parametric Performance

Table 2-10. Performance of the Simple Cycle HAT

Cycle Alternative	*3100°F*	*Reheat*
Gas Turbine Performance		
Gas Turbine HPT Temperature (°F)	3100	2715
Gas Turbine Reheat (°F)	N/A	1887
Gas Turbine LPT (Power Turbine) Temperature (°F)	2335	2500
Gas Turbine Exhaust Temperature (°F)	952	1020
Gas Turbine Stack Temperature (°F)	250	280
Turbine Cooling (Percent Inlet)	31.5	41.8
Gas Fuel Flow Rate (lb/sec)	24.7	22.4
Saturator Flow Rate (lb/sec)	153.3	126.7
Saturator Outlet Temperature (°F)	394	385
Water from Saturator (Percent)	27.0	23.6

FT8-Based HAT Cycles

The FT8 is currently offered by P&W to the utility market. Nearly 150 of these 25-MW machines are installed or on order for use as peaking units or in combined-cycle operation. A design study for an intercooled version was carried out several years ago and for the current program, HAT cycles based on both versions have been considered. The performance of the FT8 engine and the HAT cycle variations are given in Table 2-11. The parametric performance for the FT8 simple cycle HAT is shown in Figure 2-85 and that for the FT8 I/C in Figure 2-86. Other parametric comparisons are shown in Figure 2-87 and Figure 2-88.

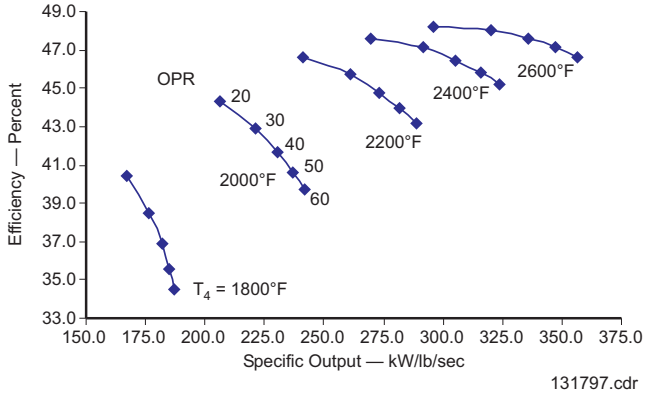

Figure 2-85. FT8 Simple Cycle HAT Performance

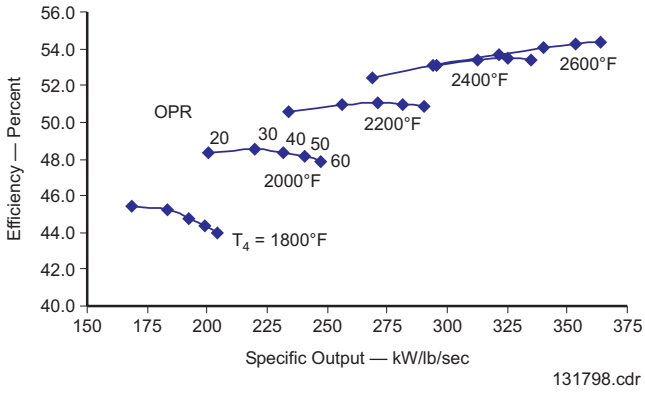

Figure 2-86. FT8 I/C HAT Performance

Table 2-11. Performance of FT8-Based Systems

	FT8 Base	***FT8 HAT***	***FT8 I/C***	***FT8 I/C HAT***
Inlet Flow (lb/sec)	182.7	182.7	283.1	283.1
OPR	19.3	19.3	24.2	24.2
Saturator Exit Temperature (°F)	N/A	297	N/A	296
Saturator Steam Flow (lb/sec)	N/A	33.2	N/A	37.8
Percent Saturation	N/A	18.6	N/A	13.7
Combustor Exit Temperature (°F)	2208	2208	2462	2462
Turbine Cooling (Percent)	18.4	18.4	21.8	21.8
Turbine Exhaust Temperature (°F)	857	886	845	904
Stack Temperature (°F)	857	250	845	250
Gross Gas Turbine Power (MW)	25.2	44.3	57.8	83.7
Gross Efficiency (Percent LHV)	38.2	47	38.9	53.3

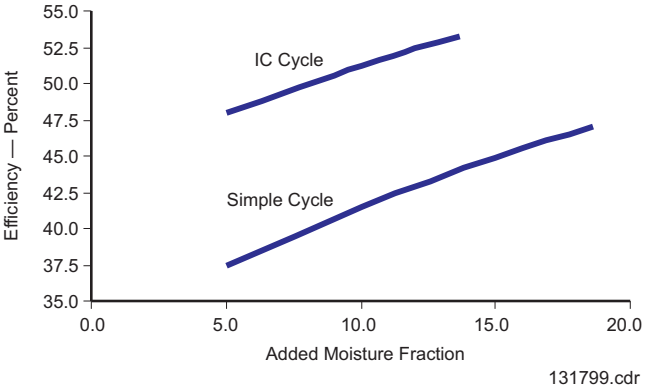

Figure 2-87. FT8 HAT Efficiency as a Function of Added Moisture

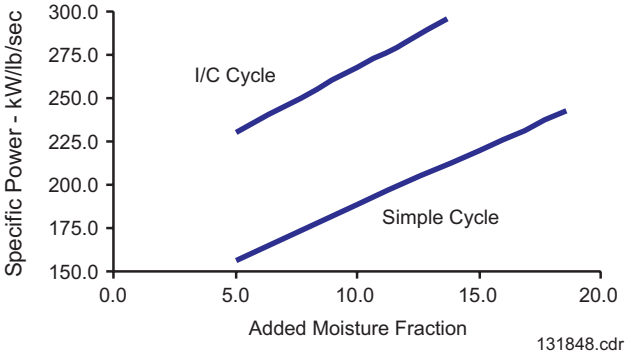

Figure 2-88. FT8 HAT Specific Power as a Function of Added Moisture

2.6.6 Concluding Remarks

The HAT cycle offers the potential of attaining the DOE ATS goal of 60 percent (LHV) in a plant that does not require high-pressure steam boilers or steam turbines. This results in a less expensive powerplant that is simpler to control, operating at off-design conditions more easily and more efficiently. The material, aerodynamic, and cooling technologies necessary to achieve this goal are currently available in aircraft turbines and could be applied to land-based aeroderivative engines with advantage.

Intercooling the compressor improves the HAT cycle efficiency and power density, but is not required to achieve significant improvement over the basic simple cycle engine. The typical twin-spool configuration of aeroderivative engines lends itself to an intercooled design. The additional flow of moisture would require redesign of the turbine gaspath, although it is possible to add as much as 12 to 15 percent moisture (lb H_20/lb in let air) through vane reclassification, thereby retaining the original gaspath.

The addition of moisture has the added benefit of reducing NO_x to levels equal to or below the ATS goals. Single digit NO_x emissions are projected at combustor temperatures well above the 2715°F limit imposed on the FT4000 I/C by NO_x considerations. Because of the high efficiency, the HAT cycle powerplant would also reduce the emissions of CO_2 and other *Greenhouse* gases.

2.7 HUMID AIR NO_X REDUCTION EFFECT ON LIQUID FUEL COMBUSTION

An experimental investigation was carried out at NETL on the humid air combustion process using liquid fuel to determine the effects of humidity on pollutant emissions and flame stability. Tests were conducted at pressures of up to 100 psia (690 kPa), and a typical inlet air temperature of 860°F (733K). The emissions and RMS pressures were documented for a relatively wide range of flame temperatures, from 2440° to 3090°F (1610K to 1970K), with and without added humidity. The results show more than 90 percent reduction in NO_x through a 10 percent humidity addition to the compressed air, compared with the dry case at the same flame temperature. The substantial reduction of NO_x is due to a shift in the chemical mechanisms and cannot be explained by flame temperature reduction due to added moisture, since the comparison was made for the same flame temperature.

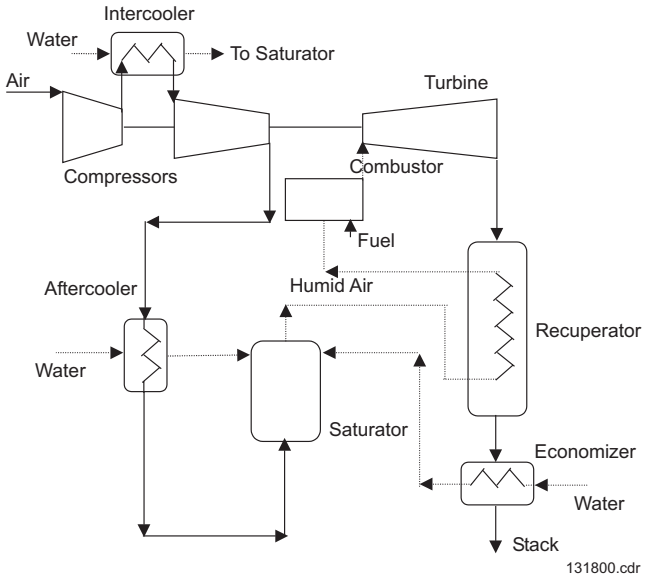

Figure 2-89. A Typical Diagram of the HAT Cycle

The HAT cycle was invented in the 1930s and awarded an U.S. patent in 1940.[1] Over the years several different versions of HAT cycles have emerged. Figure 2-89 shows a typical intercooled HAT cycle, as described by Bhargava *et al*. in 2000.[2] Intercooled compressed discharge goes through an aftercooler to arrive at a saturator to get humidified. The humidified air is then heated up in a recuperator. Afterwards, the hot water vapor-laden air arrives at the combustor and then the turbine.

[1] Martinka, M., U.S. Patent No. 2,186,706, 1940.

[2] Bhargava, A., Colket, M., Sowa, W., Casleton, K. and Maloney, Dan, "An Experimental and Modeling Study of Humid Air Premixed Flames," *Journal of Engineering for Gas Turbines and Power*, Vol. 122, p. 405, July 2000.

The HAT cycle offers many advantages over simple cycles, as well as combined cycles.[1] It produces more power output at higher efficiency, compared with simple cycles, because less work is needed for intercooled compression while more work is done in the turbine. Despite the added cost for a saturator, it reduces capital cost due to the elimination of the steam cycle of a typical combined cycle. The HAT provides flexible operations like quick startup and shutdown as commonly seen in simple cycle turbines, but it also minimizes NO_x emissions through water vapor suppression in the combustion processes. With increasingly stringent environmental requirements on pollutant emissions, production of CO_2, and other *Greenhouse* gases, as well as conservation of energy in the past several decades, there is a significant increase of interest in the HAT cycle.

A number of recent papers in the gas turbine literature have presented studies on the influence of water on NO_x and CO emissions. Lupandin, Dryer, Miyauchi *et al*., and Blevins and Roby have all investigated the subject[2]. However, these studies only dealt with gaseous diffusion flames, premixed gaseous flames, and emulsified fuel combustion. Touchton reported some results on liquid fuel combustion with steam/water injection.[3] Nevertheless, only direct steam/water injection into the combustor was investigated. Direct injection limits the amount of steam/water that can be added due to flame instability, and therefore, does not explore the full benefits of steam addition. Meyer and Grienche investigated the steam effect on a liquid-fired engine with steam and air premixed prior to combustion, but their steam loading was relatively low.[4] The work reported under this program extended the investigations to liquid fuel HAT combustion, with a high steam content in the air before introduction into the combustor. Introduction of humidity to the air before it reaches the combustor has been reported for natural gas fuel, where significant reduction of NO_x was achieved.[5] In this study, partially premixed spray combustion in humid air was examined in a relatively realistic configuration for gas turbine applications with No. 2 diesel fuel. Since liquid fuel combustion generally produces more NO_x emission than lean premixed natural gas combustion, suppression of NO_x production in liquid fuel can have a profound effect in minimizing the adverse impact on the environment.

2.7.1 Experimental Technique

Fuel Nozzle Design

The fuel nozzle used in the tests was a dual fuel axial swirl nozzle with a cylindrical centerbody, as shown in Figure 2-90. Air was introduced in an annular gap between the centerbody and an outer cylinder. Inside the annulus, 16 vanes were installed at an angle to the airflow direction to induce swirling motion in the air stream. Downstream of the vanes, there were 16 radial gaseous fuel spokes to provide distributed fuel injection. Further downstream, 16 pressure swirl liquid fuel injectors were installed. The premixed or partially premixed fuel/air mixture traveled further downstream in the annulus until it reached the nozzle exit plane where the combustor begins. In the nozzle there also was a diffusion flame pilot integrated in the centerbody to mitigate flame instability.

[1] Day, W. and Rao, A., "FT4000 HAT with Natural Gas Fuel," International Gas Turbine Institute, ASME Paper IGTI-Vol. 7, ASME Cogen-Turbo, Book No. 100333, 1992.

[2] Lupandin, V., Romanov, V., Krivutsa, V. and Lupandin, V., "Design, Development and Testing of a Gas Turbine Steam Injection and Water Recovery System," Proceedings of ASME Turbo Expo, 2001-GT-0111, 2001; Dryer, F.L., "Water Addition to Practical Combustion Systems-Concepts and Applications," *Sixteenth Symposium (International) on Combustion*, The Combustion Institute, Pittsburgh, PA, 1976; Miyauchi, Y., Mori, Y., Yamaguchi, T., "Effect of Steam Addition on NO Formation," *Eighteenth Symposium (International) on Combustion*, The Combustion Institute, Pittsburgh, PA, 1981; and Blevins, L.G., and Roby, R J., "An Experimental Study of NO_x reduction in Laminar Diffusion Flames by Addition of High Levels of Steam," ASME Paper No. 95-GT-327, 1995.

[3] Touchton, G.L., "Influence of Gas Turbine Combustor Design and Operating Parameters on Effectiveness of NO_x Suppression by Injected Steam or Water," ASME Paper No. 84-JPGC-GT-3, 1985.

[4] Meyer, Jean-Louis, and Grienche, G., "An Experimental Study of Steam Injection in an Aeroderivative Gas Turbine," ASME Paper No. 97-GT-506, 1997.

[5] Bhargava, A., Colket, M., Sowa, W., Casleton, K. and Maloney, D., "An Experimental and Modeling Study of Humid Air Premixed Flames," *Journal of Engineering for Gas Turbines and Power*, Vol. 122, p. 405, July 2000; Meyer, Jean-Louis, and Grienche, G., "An Experimental Study of Steam Injection in an Aeroderivative Gas Turbine," ASME Paper No. 97-GT-506, 1997; Kendrick, D., Bhargava, A., Colket, M., Sowa, W., Maloney, D. and Casleton, K, "NO_x Scaling Characteristics for Industrial Gas Turbine Fuel Injectors," Proceedings of ASME Turbo Expo, 2000-GT-98, 2000; and Bhargava, A., Kendrick, D., Colket, M., Sowa, W., Casleton, K. and Maloney, D, "Pressure Effect on NO_x and CO Emissions in Industrial Gas Turbines," Proceedings of ASME Turbo Expo, 2000-GT-97, 2000.

It is worth mentioning the multipoint pressure swirl liquid fuel injector incorporated here was made by an external supplier through its macrolamination technology. Figure 2-91 shows a sketch illustrating the macrolamination fuel injector. Macrolamination uses thin etchable metal sheets that are layered and bonded together to create intricate passages. It reduces the part count and the cost to make complicated parts. Liquid fuel nozzles made through macrolamination technology have demonstrated good emission performance in rig tests.[1]

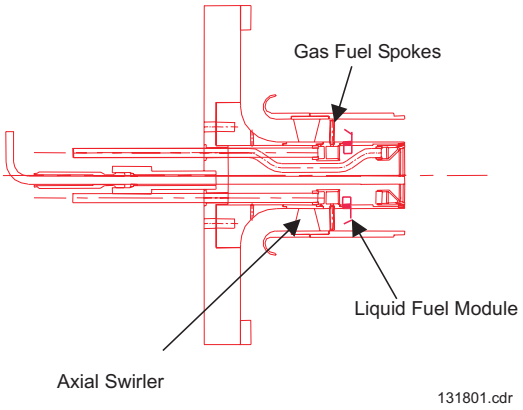

Figure 2-90. Diagram of Axial Swirler Dual Fuel Nozzle

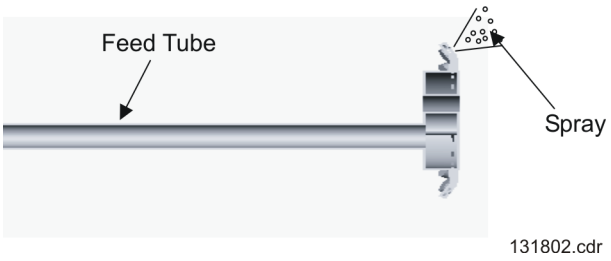

Figure 2-91. Macrolaminate Multipoint Liquid Fuel Injector

The position of the injector relative to the nozzle exit plane is generally determined by balancing two factors: autoignition and mixing. Too far away from the nozzle exit plane may cause autoignition of liquid fuel in the nozzle annulus, yet promote premixing, and therefore, decrease NO_x formation. Too close to the nozzle exit plane reduces premixing and therefore, increases NO_x emission, but reduces the chance for autoignition. Since the main goal of this study is to investigate the humidity effect on NO_x reduction, rather than to optimize the nozzle to reduce dry NO_x emission, the balance mentioned above was shifted towards reducing the chance for autoignition to ensure the success of the experiments. As a result, the liquid injector was positioned close to the nozzle exit plane rather than far away from it. For best flame stability, sprays were directed at 60 degrees away from the main nozzle centerline to ensure enough fuel was distributed towards outside diameter recirculation zone in the combustor. A zero-degree nozzle was also tried and resulted in unstable combustion.

Combustion Test Rig Setup

All the experiments were carried out in the LECTR facility at NETL in Morgantown, West Virginia. The facility has the capability to provide as much as 3 pps (1.4 kg/s) of air at 450 psia (3.1 MPa) and 950°F (783K) and 0.6 pps (0.27 kg/s) of steam. It can independently control air, gas, liquid, and steam flows and inlet temperature and pressure, as well as automatic ramping of these variables. The variable automatic ramping capability is particularly useful for the refractory liner used in the setup to minimize cracking. Figure 2-58 shows a diagram of the experimental setup.

Nonvitiated preheated air and steam generated by a boiler flowed through primary air/steam ports into the plenum. After going through a perforated plate that acts as a flow straightener upstream to fuel nozzle, they provided uniform flow feed to the nozzle. Combustion occurred downstream to the nozzle in a 6-in. (0.15-m) diameter cylindrical refractory lined combustor that best simulates an ideal adiabatic combustion chamber. Due to the favorable refractory liner's physical properties, the need for liner cooling was eliminated. After burning, the combustion products continued to move upward and reached the water-cooled exhaust sampling probe that was located about 12 in. (0.3 m) above the nozzle exit plane. The probe sampled the exhaust in an area-averaged fashion to ensure the extracted gas samples were representative across the combustor exit plane. After passing the sampling probe, the

[1] Mansour, A., Benjamin, M., Straub, D. L. and Richards, G. A, "Application of Macrolamination Technology to Lean, Premix Combustion," Proceedings of ASME Turbo Expo, 2000-GT-0115, 2000.

exhaust moved further upward and reached a plenum and then turned 90-degrees, entering a water quench zone where temperature was reduced before the flow reached a pressure control valve and a stack.

Exhaust samples were transported through heated tubings and were dried before being analyzed. Species analyzed were NO_x, CO, CO_2, O_2, and UHC. All emissions reported here are on a dry basis and have been corrected to 15 percent O_2. The UHC were not reported here because it was only a few parts per million for all cases, except when the CO was high. Excellent fuel/air ratio agreement (generally within 2 percent) was achieved between the emissions-based fuel/air ratio and the metered fuel/air ratio.

The extent of flame temperatures examined for the dry case was determined by CO emission at the lean end and NO_x emission at the rich end. For the dry case fuel ramp stopped when CO level approached 100 ppm or when NO_x approached 430 ppm. The flame temperature range determined by the dry case was also used for the humidified case when steam was added.

For the entire test series presented here, the dynamic pressure was consistently very small. No RMS pressure above 0.3 psi (2.1 kPa) was observed. This may be partly due to the unchoked acoustic boundary conditions or less than perfect mixing in the nozzle, or both.

2.7.2 Results and Discussion

Figure 2-92 reveals the NO_x and CO emissions of diesel fuel combustion as a function of equivalence ratio without steam addition for both the inlet pressure of 50 psia and 100 psia (0.34 and 0.69 MPa). The equivalence ratio is the actual fuel/air ratio divided by the stoichiometric fuel/air ratio. The inlet air temperature was 860°F (733K) and there was 4 percent centerbody natural gas fuel based on total heat of combustion of all the fuels. Both CO curves exhibit U-shaped trends similar to those observed in premixed natural gas combustion.[1] The level of CO at 100 psia (0.69 MPa) is lower than that at 50 psia (0.34 MPa). The lean stability limits moved to lower equivalence ratios as pressure increased. A similar pressure effect was also found in premixed natural gas combustion.[2] The NO_x curves show a near linear dependence on the equivalence ratio for the range tested. This linear relationship can also be observed in most of the data presented in Mansour *et al*. The 100-psia (0.69 MPa) curve displays a steeper slope and substantially higher NO_x value than the 50-psia (0.34 MPa) curve. The absolute value of NO_x is relatively high, compared to well-premixed liquid fuel flame rig data, suggesting the vaporization and mixing of the spray is less than perfect, possibly due to short mixing time in the nozzle. However, the nozzle in Mansour *et al.* is a novel macrolamination nozzle that has yet to be implemented in commercial gas turbines. In the absence of water or steam, the majority of commercial liquid fuel turbine engines produce hundreds of parts per million of NO_x; a level similar to the NO_x produced in the experiments here. One exception is prevaporized and premixed liquid fuel gas turbines. These systems face many operational challenges, including thermal damage to the vaporizing elements and sensitivity to variation in fuel type. The NO_x level here is also significantly higher than those in the lean premixed gas turbine engines (typically 25 ppm). But those systems are natural gas fired and cannot be compared with the system investigated here. Therefore, the noz-

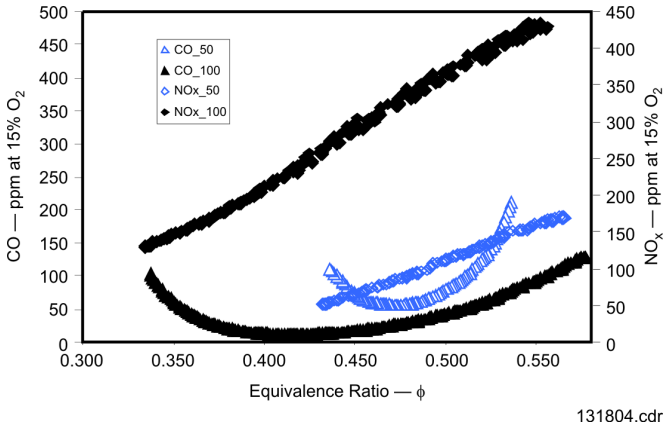

Figure 2-92. Comparison of Measured NO_x and CO of Diesel Fuel Combustion Between 50 Psia and 100 Psia Dry Cases (T_{air} 860ºF and 4 Percent Centerbody Gas Fuel)

[1] Kendrick, D., Bhargava, A., Colket, M., Sowa, W., Maloney, D. and Casleton, K, "NO_x Scaling Characteristics for Industrial Gas Turbine Fuel Injectors," Proceedings of ASME Turbo Expo, 2000-GT-98, 2000.

[2] Mansour, A., Benjamin, M., Straub, D.L. and Richards, G.A, "Application of Macrolamination Technology to Lean, Premix Combustion," Proceedings of ASME Turbo Expo, 2000-GT-0115, 2000.

zle is suitable for the purpose of this investigation, which is to study the NO_x suppression effect of humid air in liquid fuel combustors similar to real engines.

The existence of the centerbody gas pilot of 4 percent fuel in the test contributed a small amount of NO_x to the results. Data without pilot was not acquired during this test series. However, the small effect of pilot on NO_x can be estimated. Assuming the pilot contributes NO_x in a way similar to a premixed natural gas flame, the pilot here would contribute about 6 ppm NO_x.[1] Hence, if we had run cases without the pilot fuel, the NO_x level would be about 6 ppm lower.

The above 100-psia (0.69 MPa) case was then plotted with a humidified case in Figure 2-93 to demonstrate the steam effect on emissions. For the humidified case, steam was 10 percent of the air mass flow rate, the inlet pressure was 100 psia (0.69 MPa), the inlet air temperature was 810°F (705K), which was 50°F (28K) lower than the dry case, and there was no centerbody pilot. As discussed above, the pilot should only account for about 6 ppm NO_x difference; therefore, the difference in NO_x between the two cases was mainly caused by steam addition. For the amount of steam added, typically a higher percentage of steam will bring a higher power output and efficiency to the HAT cycle. Day and Rao [**3**] simulated as high as 25 percent steam addition to a natural gas-fired cycle and 45 percent to a syngas-fired cycle and found major improvement in power output and efficiency. However, high steam addition can increase the difficulty for moisture recovery if it is needed, as well as compressor operations. Fischer *et al*. has found that higher than 10 percent of steam addition may cause compressor surge.[2] They also found that 10 percent steam addition would increase the HAT cycle power by about 30 percent and efficiency by about 15 percent, which are significant. From a NO_x reduction standpoint, the most significant benefits are found at steam loadings on the order of 5 to 10 percent in natural gas.[3] Above 10 percent steam loadings, the NO_x levels are only slightly further reduced but CO emissions begin to increase. Therefore the 10 percent steam content chosen in the tests here is an appropriate level for a practical HAT cycle. As it is shown in Figure 2-93, the addition of steam brought a drastic reduction in the formation of NO_x similar to what was found in premixed natural gas combustion.[4] For the same equivalence ratio, NO_x was reduced more than 95 percent by 10 percent addition of the steam. For example, at an equivalence ratio of 0.47, the NO_x decreases from 323 ppm in the dry case to 15.7 ppm in the humidified case, a 95 percent reduction. With 10 percent humidity addition, the NO_x was reduced to 15 to 35 ppm depending on the flame temperature. These NO_x levels are comparable to those of the lean premixed natural gas fired gas turbines. Also, this shows the NO_x reduction effect of humidity is insensitive to the high dry NO_x level, which indicates wide applicability of this technique to different types of nozzles with different levels of dry NO_x. More importantly, this implies that with HAT it is not necessary to have a perfect mixer to achieve NO_x level below 25 ppm, which potentially eliminates the very destructive acoustic problem commonly associated with lean premixed systems. It is worth further researching on this subject. The CO curve for the steam case also exhibited U-

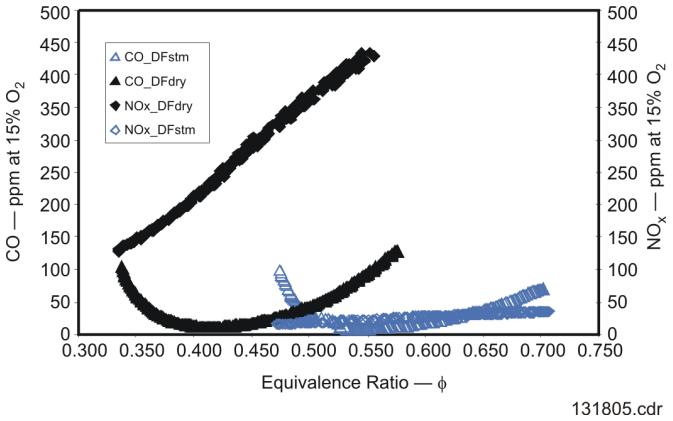

Figure 2-93. Comparison of Measured NO_x and CO of Diesel Fuel Combustion at Different Equivalence Ratios Between Dry and 10 Percent Steam Cases at 100 Psia

[1] Bhargava, A., Colket, M., Sowa, W., Casleton, K. and Dan Maloney, "An Experimental and Modeling Study of Humid Air Premixed Flames," *Journal of Engineering for Gas Turbines and Power*, Vol. 122, p. 405, July 2000.

[2] Fischer, A., Frutschi, H., Haselbacher, H. "Augmentation of Gas Turbine Power Output by Steam Injection," Proceedings of ASME Turbo Expo, 2001-GT-0107, 2001.

[3] Bhargava, A., Colket, M., Sowa, W., Casleton, K. and Dan Maloney, "An Experimental and Modeling Study of Humid Air Premixed Flames," *Journal of Engineering for Gas Turbines and Power*, Vol. 122, p. 405, July 2000.

[4] *Ibid*.

shaped trend similar to that of the dry case. However, the lean stability limit moved to higher equivalence ratio as steam was added. This is due to the fact that steam addition increased the specific heat of the mixture and therefore, reduced the flame temperature for the same equivalence ratio. It is also due to the effect of the pilot in the dry case. The flame temperature reduction with steam addition reduced the *Zeldovich* or *Thermal* NO_x formation mechanism, which partially explains the NO_x reduction effect; however, it cannot explain the entire NO_x reduction observed.

To illustrate this point, the data in Figure 2-93 was plotted against adiabatic flame temperatures. The adiabatic flame temperatures were calculated through NASA CEA equilibrium code. The results are shown in Figure 2-94. It is shown that even at the same adiabatic flame temperature, the 10 percent steam reduced NO_x by 90 percent for all the flame temperatures tested. For example, at a flame temperature of 2600°F (1700K), the NO_x decreases from 223 ppm in the dry case to 19.4 ppm in the humidified case, a 91 percent reduction. This suggests that if, through optimization of the nozzle, a 200 ppm dry NO_x is achieved, it is likely to achieve NO_x below 20 ppm in a HAT cycle at the same flame temperature. This NO_x reduction effect differs completely from the results reported by Touchton in the direct steam/water injection systems where NO_x suppression is exclusively through the *Thermal* mechanism, or lowering peak flame temperature.[1] This strongly suggested that besides the NO_x reduction effect due to lowering the flame temperature through steam addition, the moisture also reduced the NO_x by other mechanisms. Bhargava *et al*. investigated the humid air effect on NO_x reduction in premixed natural gas combustion system and offered following explanation.[2]

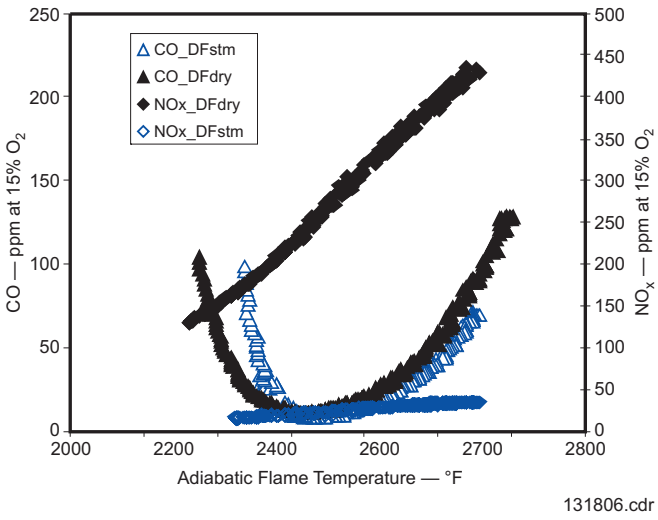

Figure 2-94. Adiabatic Flame Temperature (ºF)

NO_x formation reactions can be categorized into three different groups. They are *Zeldovich*[3] or *Thermal* NO_x mechanism, *N_2O* mechanism, and the *Fenimore*,[4] or *Prompt*, NO mechanism.

Zeldovich mechanism is described by following reactions:

1. $O + N_2 \rightarrow NO + N$

2. $N + O_2 \rightarrow NO + O$.

The overall rates of NO production are controlled mainly by the first reaction, since the second reaction is quicker than the first one. Due to the fact that there is abundance of N_2 available in the combustion system, the rate of the first reaction, and hence, the rate of NO production, is strongly controlled by O concentration. A reduction of O concentration can reduce the rate of the first reaction, thereby reducing NO_x production.

The *N_2O* mechanism consists of reactions involving N_2O that form NO. NO_x formed through this mechanism can be suppressed by the reaction $N_2O + M \rightarrow N_2 + O + M$. A reduction of O concentration can promote the previous reaction and therefore, reduce NO_x production.

[1] Touchton, G. L., "Influence of Gas Turbine Combustor Design and Operating Parameters on Effectiveness of NO_x Suppression by Injected Steam or Water," ASME Paper No. 84-JPGC-GT-3, 1985.

[2] Bhargava, A., Colket, M., Sowa, W., Casleton, K. and Dan Maloney, "An Experimental and Modeling Study of Humid Air Premixed Flames," *Journal of Engineering for Gas Turbines and Power*, Vol. 122, p. 405, July 2000.

[3] Zeldovich, J., "The Oxidation of Nitrogen Combustion and Explosions," *Acta Physicochimica*, URSS, 21, p. 577, 1946.

[4] Fenimore, C. P., "Formation of Nitric Oxide in Premixed Hydrocarbon Flames," *Thirteenth Symposium (International) on Combustion*, The Combustion Institute, 1971.

The key to the *Fenimore* NO mechanism can be described by following reactions:

1. $CH + N_2 \rightarrow HCN + N$
2. $CH_2 + N_2 \rightarrow HCN + NH$
3. $HCN + O \rightarrow CH + NO$.

A reduction of CH/CH_2 will reduce the reaction rate in the first/second reactions and eventually reduce NO. A reduction of O will reduce the reaction rate in the third reaction and therefore, reduce NO.

For the same flame temperature, the humidified case had higher equivalence ratios than the dry case, and therefore, had lower O_2, which reduced the concentration of O atoms. Humidity also promotes the $O + H_2O$ reaction and reduces O concentration. The reduction of O atoms lowered the NO_x formation by all the three mechanisms. In addition, humidity increases OH radical concentration, which promotes the oxidation of hydrocarbon radicals and reduces *Fenimore* NO. These are the reasons why the steam addition reduced NO_x dramatically for the same flame temperature relative to a dry case.

2.7.3 Conclusions

Experimental data was obtained for liquid fuel combustion in humid and dry air at different pressures over a wide range of equivalence. The effect of humidity, pressure, and equivalence ratio on NO_x and CO emissions was evaluated based on the data. Introduction of 10 percent steam in air suppressed NO_x production by more than 90 percent for the same flame temperature. The dramatic suppression of NO_x is attributed to the decrease of O atoms and increase of OH radicals in the humid air combustion.

2.8 TESTS OF HYBRID COMBUSTOR

The low NO_x combustion method using hybrid combustion was conceived at UTRC and related technology was developed and demonstrated subsequently under UTRC, P&W, and Gas Research Institute (GRI) funding. The concept has been described and the development and laboratory demonstrations of technology related to the hybrid combustor are detailed in reports to the GRI and UTRC internal reports.[1] The nearly 10-year development effort has led to design and fabrication of an assembly that fits into the nosecone of the TEN used in the dry low NO_x GG8-2 engine. This study is the first practical application of the hybrid combustion concept in an industrial gas turbine. In this particular application, the hybrid combustor was designed to act only as a low emission pilot (low NO_x and low CO), with pilot flow jetting from the end of the nosecone. It was the objective of the tests reported here to demonstrate the new device under practical engine operating conditions, as well as to investigate its performance under humid air conditions.

The hybrid combustion concept combines three complementary approaches for controlling the formation of NO_x, while maintaining high combustion efficiency and excellent flame stability. Figure 2-95 presents the original hybrid combustion concept, shown for a gas turbine cycle, which features a two-stage combustion process. During this process, the fuel is first catalytically decomposed under fuel-rich conditions (while energy is simultaneously or sequentially extracted); then the partially oxidized fuel is burned to completion by conventional gas-phase combustion. The first stage features a monolithic type of catalytic reactor that provides sufficient chemical reaction and

[1] Colket, M.B., Kesten, A.S., Sangiovanni, J.J., Zabielski, M.F., Pandy, D.R., and Seery, D.J., "Method and System for Combusting Hydrocarbon Fuels with Low Pollutant Emissions by Controllably Extracting Heat From the Catalytic Oxidation Stage," U. S. Patent 5,235,804, August 17, 1993; Colket, M.B., Sangiovanni, J.J., Tredway, W.K., Schmidt, W.R., Knight, B.A., and Snider T.R., "Topical Report on Reactor Fabrication and Catalyst Selection for Hybrid Combustion," GRI, UTRC Report No. 970373-12, October, 1993; and Sangiovanni, J.J., Colket, M.B., Davison, W.R., Lehrach, R.P.C., Welch, E., Knight, B.A., and Snider, T.R., "Hybrid Combustion for Ultra-Low NO_x Emissions," GRI, UTRC Report No. 970373-16, November 1994.

heat transfer rates with minimum pressure loss. The second stage may feature a conventional or advanced combustor that consists of a primary zone in which the main combustion occurs (under lean, rich, or stoichiometric conditions), and a secondary zone into which air is added. Thermal management is accomplished by extracting a portion of the heat of combustion from the first or catalytic stage. Subsequent combustion in the primary zone of the flame then occurs at a substantially lower temperature so as to dramatically reduce NO_x formation by the thermal mechanism in the second stage. To effectively use the thermal energy and to maintain high combustion efficiency, the catalytic reactor must be integrated with a heat exchanger that transfers the thermal energy of the partial fuel oxidation reactions to a secondary fluid. A secondary, but important, benefit of the integrated catalytic reactor/heat exchanger (CRHX) is control of peak temperature in the catalytic reactor, which allows the lifetime of the catalyst to be lengthened. Although the secondary fluid may be air, water, or another medium, the heat that is transferred to this fluid must be used effectively; otherwise, combustion efficiency will be degraded. In the case of the gas turbine, a portion of the heat generated by the catalytic reaction should be transferred to the air that is used in the secondary zone of the flame. Therefore, by principally transferring the heat of catalytic partial oxidation to the secondary combustor air, the primary zone flame temperature is reduced significantly, formation of NO_x by the thermal mechanism is greatly suppressed, and all of the thermal energy from fuel combustion is contained in the exhaust from the flame.

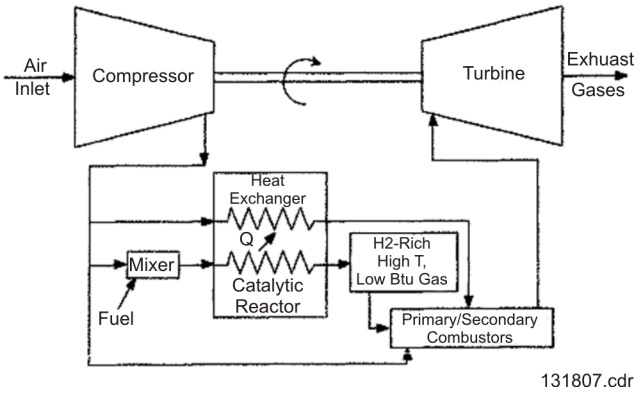

Figure 2-95. Schematic of Hybrid Combustion Integrated in a Gas Turbine

Additional reductions in NO_x formation arise from the fact that large fractions of the fuel are converted to hydrogen and carbon monoxide and thus, fewer CH fragments can be formed during combustion. Since these CH fragments are the precursors to NO_x formation by the *Prompt* mechanism, additional reductions in NO_x formation are realized. Furthermore, since the fuel is converted to lighter and more reactive components, namely hydrogen and carbon oxides, and since the fuel temperature entering the thermal combustor is higher than if it had not been partially oxidized, flame stability is enhanced. Elevating the fuel temperature does not increase NO_x production as in preheated (air or fuel) industrial systems because of the lower heating value of the partially oxidized fuel. Since these latter approaches to reducing NO_x formation depend on the species composition of the partially oxidized fuel from the catalytic reactor, the potential benefits of these approaches depend on the catalyst selectivity and conversion, and the amount of heat transferred to the secondary air. In the present study, the catalyst has been selected to maximize the production of H_2 and CO from the CRHX.

2.8.1 Component Design and Hardware

A cut-away view of an early version of the hybrid combustor pilot installed into the nosecone of the TEN burner is depicted in Figure 2-96. In this original version, the pilot fuel (partially oxidized reaction products) was premixed with secondary air before entering the main burner region. For the hardware tested, the premixing tip was replaced with an air-cooled endcap through which the fuel-rich catalyst products exhausted. Figure 2-96 shows the multiported fuel injection hardware, the CRHX, the adjacent passages with reacting and cooling channels, exit slots for the heated fresh air, and exit slots for the reaction products that are collected together, prior to redistribution near the endcap (not shown).

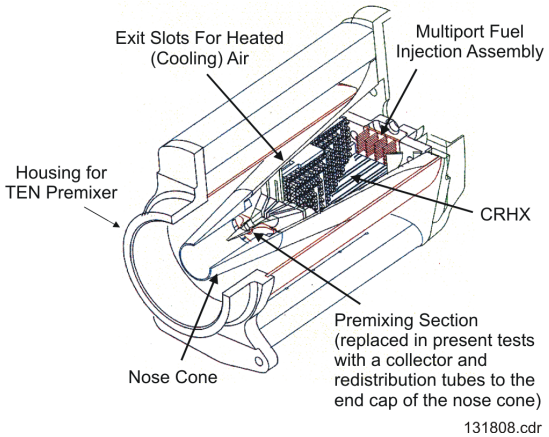

Figure 2-96. Cut-Away Isometric View of the Hybrid Combustor Installed as a Pilot in the TEN Burner

The heart of the hybrid combustor is the integrated CRHX. A side view schematic of the CRHX is provided in Figure 2-97. The device consists of nine parallel plate fin channels. Air flows to the entrance of this reactor and enters each of the nine channels. Fuel is also injected into every other channel through rows of a multiport fuel injection system and sufficient distance is allocated for premixing prior to entrance to the catalyst channel. Airflow splits are controlled through reactor design and minor adjustments after ACd measurements. The ideal equivalence ratio for a dry air system in the reaction channel is four. The fins in the reaction channel are treated with a washcoat and catalyst after the manufacture of the heat exchanger hardware. Upon reaching a temperature above 770ºF, and in the presence of a fuel-rich mixture, the catalyst should autoignite, releasing energy that is transferred partially to the adjacent channels and cooling air. Partially oxidized products with reduced enthalpy exit the endwall of the CRHX, while the heated air exits the sidewalls of the CRHX.

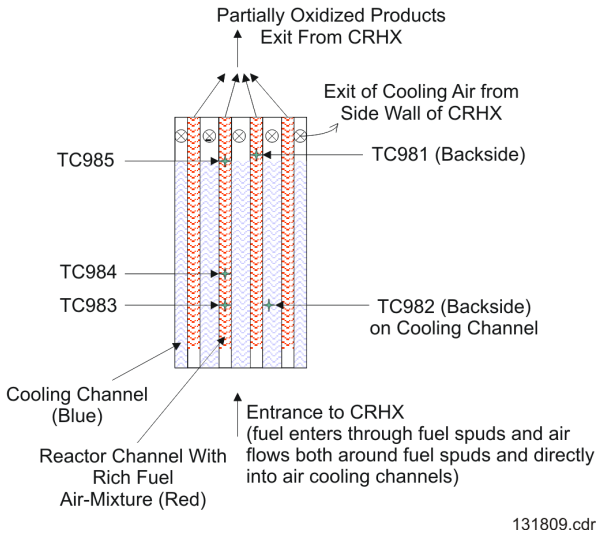

Figure 2-97. Schematic Side View of Catalytic Reactor/Heat Exchanger With Thermocouple Locations Denoted

Photographs of the CRHX and other hardware components, prior to testing, are shown in Figure 2-98 to Figure 2-100. Figure 2-98 shows the hollow nosecone and the internal components properly assembled (and prior to insertion into the nosecone). The slot on the sidewall of the nosecone is not normally a feature of a TEN burner, but is a necessary component of the hybrid combustor system. It is the exit slot for the cooling air from the catalytic reactor. This air exits the series of the slots on the side of the reactor/heat exchanger. The cooling air is trapped between the reactor assembly, its *wings*, and the internal wall of the nosecone, until it forced out of the sidewall of the nosecone. This air originally comes through the backside of the TEN assembly (see Figure 2-96) and flows through air channels adjacent to the reactor channels (see Figure 2-97). At the top of the reactor assembly in Figure 2-98 is the collector and endcap that distributes the pilot gases into the combusting flow field. At the base of the reactor assembly are kidney-shaped holes that allow air to enter at right angles to the trapped heated air and flow along the sidewalls of the reactor assembly to towards the endcap. The backside of the endcap has a series of tiny holes around its circumference that allow the cooling air to flow to its center and cool the endcap with unheated air.



Figure 2-98. Photograph of Hollow Nosecone and Components of Hybrid Burner

Photographs showing separated components of the internal assembly of the hybrid combustion system are shown in Figure 2-99 and Figure 2-100. Two views of each subcomponent are depicted. The multiport fuel injection system can be seen in the fuel distributor and air baffle component. Each row of the pins lines up with the entrance slots to the catalytic reactor for fuel injection into these passages. Adjacent passages receive no fuel and are the cooling heat exchanger channels. At the opposite end of the CRHX, only the fuel-rich reacted gases exhaust and collect prior to redistribution in the endcap.

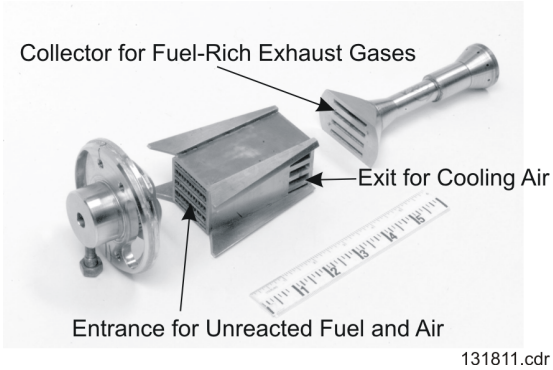

Figure 2-99. Separated Components of the Hybrid Burner

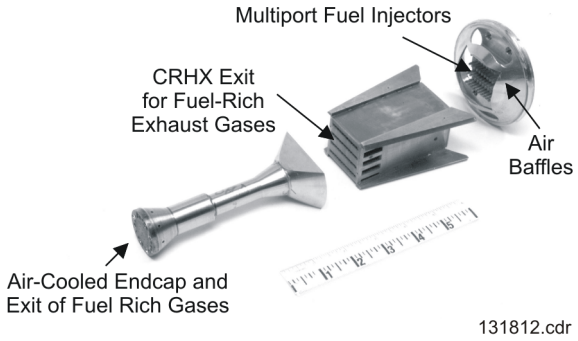

Figure 2-100. Separated Components of the Hybrid Burner

Figure 2-101 and Figure 2-102 are photographs of the exit and entrance of the CRHX. The fuel/air passages are narrower than the air passages. The metal fins in these reaction passages, onto which the catalytic material is placed, are recessed into the reactor to allow space for insertion of the fuel injection pins and premixing of the fuel and air. The air passages are blocked at the end face to allow the cooling air to escape the sidewalls.

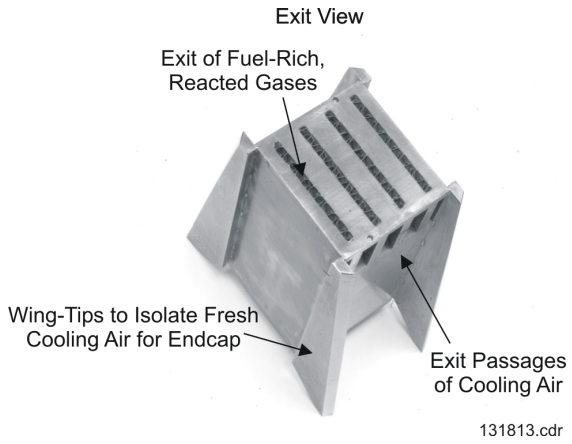

Figure 2-101. Exit View of the CRHX

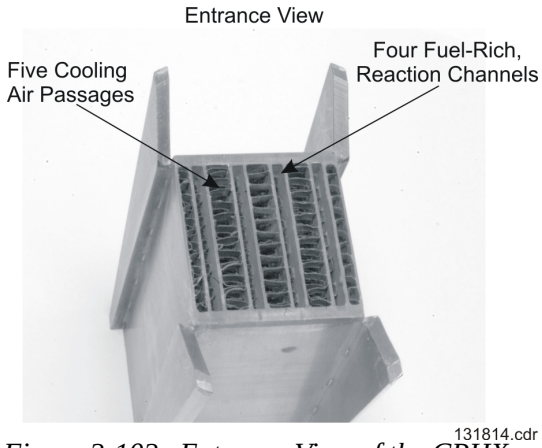

Figure 2-102. Entrance View of the CRHX

Thermocouple beads (TCs) were welded to several locations on the hybrid combustor and the nosecone. Photographs were taken after the experiments to document their locations. Five TCs were placed on the sidewalls of the CRHX, two TCs were placed on the sidewall of the nosecone (TC986 and TC987), and one was embedded in the endcap of the nosecone. Locations of the five TCs on the CRHX are depicted on the schematic shown in Figure 2-97, as well as in Figure 2-99 and Figure 2-100. All but one are placed on the sidewalls of the reaction channels and the fifth (TC982) is located on the sidewall of one of the cooling passages.

2.8.2 Test Description

This series of experiments was the first full-scale demonstration of the hybrid concept using the new hardware and design concepts. After flow tests and baseline combustor tests (without the catalyst *lit*), the first objective of the experiments was to demonstrate self-lighting of the catalytic reactor. Once lit, the performance of the hybrid combustor was examined relative to the goals of reduced NO_x and CO production and enhanced flame stability. Throughout these initial tests, the conditions of the reactor and the endcap were carefully monitored, particularly to avoid overheating of components. Following these initial tests with air, experiments were repeated in the presence

of humid air. A more detailed description of the test series and results are contained in an unpublished report written by Dr. Dan Maloney of the NETL.

The emissions-reduction expectations of these tests are lower than those for a full-scale demonstration in which all of the fuel would be processed through a CRHX. In such cases, NO_x reductions to a factor of three have been demonstrated and experimental measurements always have shown a benefit in CO emissions. Furthermore, prior experimental results show that the lean stability limit is typically reduced by the equivalent of 10 percent. In the present tests, only one of the pilots uses hybrid combustion technology and this pilot consumes only about 5 to 8 percent of the total fuel.[1] Expectations for NO_x reductions can only be based on a reduction of the component of the NO_x that is produced from the centerbody pilot. The objective of this series of experiments was to demonstrate the following:

- CRHX survives the tests
- The catalyst successfully lights off the fuel/air mixture
- NO_x reductions that are significant in magnitude relative to the NO_x generation from the pilot flame.

A complication to the optimum performance of the CRHX was recognized late in the design process. The pressure along the side of the nosecone (at the sidewall exit holes) is significantly higher than the pressure at the exit of the endcap of the nosecone. The driving DP for the flow through the reactor passages, compared to the DP for the flow through the cooling passages, is noticeably larger. Therefore, the cooling flow rates are less than desirable for optimum operation of the CRHX. Practical implications of this constraint are that the CRHX will run hotter than desired and the heat extraction will be less; thus, the NO_x benefit will be mitigated.

2.8.3 Experimental Considerations

In performance of the tests, there were several critical parameters to be monitored. First, the overall equivalence ratio in the mixture for the catalytic reactor should be about four. At an equivalence ratio of four, the overall reaction can be written as $CH_4 + ½O_2 \Rightarrow CO + 2H_2 + 8.5$ kcal/mole.

Thermodynamics inhibits attainment of these reaction products and fractions of the much more exothermic products, CO_2 and H_2O, are also formed, leaving unburned fuel to balance the equation. If the reactor is overcooled, then the strongly exothermic products are favored, but as temperatures increase, CO and H_2 are the preferred products. The CRHX design is based on a trade-off between extracting energy and reducing NO_x emissions and producing large fractions of CO and H_2, or reactive flame gases, for stabilizing the next stage of combustion.

In the following analysis, the parameter describing the mixture strength in the reactor is denoted CR/CR_0, where $CR_0 = 4$, the reference reactor equivalence ratio. Hence, a $CR/CR_0 = 1$ is the *ideal* setting. The reader should recognize that no direct measurement of this parameter was made. Instead, it was computed based on metered fuel flow rate to the reactor, along with the total airflow rates, using cold flow ACd measurements to estimate the fractional air split through the reactor channels.

Other critical parameters were the component wall temperatures. For providing a measurable lifetime for the catalytic material, the preferred maximum CRHX body temperature was 1400ºF. Otherwise, metal temperatures (such as at the endcap) were not to exceed 1500ºF, except for short excursions.

An unusual operating characteristic of the CRHX is related to its fuel-rich operation. As reactor equivalence ratio is beyond the stoichiometric condition where temperatures peak, adding more fuel (or decreasing the airflow) reduces local temperatures rather than the reverse, as is characteristic for overall lean systems.

2.8.4 Flow Control

There are multiple pathways for both the air and fuel. There is no separate control for the different airflow paths. The hardware design and relative pressure drops define the splits between the different pathways. Based on separate cold flow tests, it is estimated that of the total airflow, 95.3 percent passes through the main tangential entry slots (primary air for premixing with fuel), 0.9 percent passes through the fuel rich passages in the CRHX and

[1] There is also a second standard diffusion flame pilot in the combustor sidewall.

reacts with the pilot fuel (hybrid combustion), 3.5 percent directly cools the CRHX and exits the sidewalls of the nosecone, and 0.3 percent cools the endcap at the tip of the nosecone. The estimated flow splits for the hot air shown in Table 2-12 were computed to account for the extra mass, such as fuel, and added to each of the streams and temperature changes.

The fuel flow is split into three paths: Fuel for the main burner that is premixed with the primary air; fuel for the sidewall diffusion flame pilot, and fuel for the hybrid pilot in the centerbody. In contrast to the airflow, there are separate control systems for each of the fuel routes.

Table 2-12. Fractional Mass Flow Splits for Air

	ACd (in.^{2})	***Relative Mass (Cold)***	***Mass Flow (Hot)***
Main Air[1]	3.918	0.944	0.953
Reactor Air	0.06	0.014	0.009
Cooling Air	0.16	0.039	0.035
Tip Cooling	0.012	0.003	0.003
Total Air	4.15	1	1

[1] ACd determined by difference.

2.8.5 Results

The tests were performed over a 2-week period in late January and early February 2001 at the NETL in Morgantown, West Virginia, by personnel (lead by Dan Maloney) from NETL. Med Colket from UTRC was present during the first 2 days of combustor testing with the CRHX to provide guidance in burner control and hybrid combustor expectations.

This section is divided into coverage of catalytic ignition, NO_x reductions, CO emissions, and humid air effects. Throughout these discussions, the relative effects of the centerbody pilot (the hybrid combustor in the nosecone) with and without the piloting fuel injected from the nosecone, are compared. In addition, performance of the burner has been examined with no fuel passing through the CRHX (hybrid combustor), as well as with fuel passing through the nonignited catalyst channels. Variables examined in these studies include total pressure, inlet air temperatures, mass fraction of fuel in the pilots, reactor equivalence ratio, and level of humidity in the air.

Catalyst Ignition

In prior studies with the catalyst selected for these studies, catalytic ignition occurred at about 770ºF (410ºC) for the fuel-rich mixtures of interest in this application.[1] This process is relatively pressure independent. This temperature is well below the base load air temperature for the GG8-2 (840ºF) and thus, the catalyst is expected to self-light with external preheating applied. To test the ability of the catalyst to light the mixture, a series of tests was performed in which the inlet temperature was ramped up slowly, while temperatures of the CRHX were monitored carefully. Figure 2-103 depicts the results of scans from the first (successful) catalyst ignition process. To achieve success during this initial lightoff procedure, temperatures had to be ramped up significantly beyond the expected lightoff point, up to an

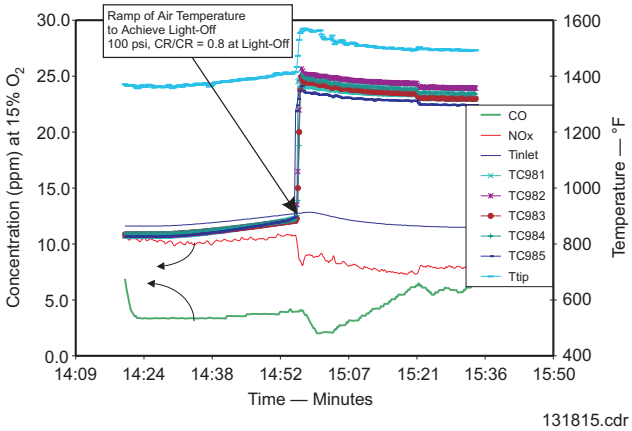

Figure 2-103. Initial Catalyst Lightoff

[1] Colket, M.B., Sangiovanni, J.J., Tredway, W.K., Schmidt, W.R., Knight, B.A., and Snider,T.R., "Topical Report on Reactor Fabrication and Catalyst Selection for Hybrid Combustion," GRI, UTRC Report No. 970373-12, October 1993.

inlet temperature of 910ºF. In subsequent tests, this temperature was reduced substantially, to as low as 760ºF in one test, although typically, lightoff could be achieved in the low 800ºF range. Several factors contributed to the high values initially observed. The process of introducing fuel to the catalyst and slowly ramping the air temperature had two negative features. The added fuel was cold and hence, the CRHX temperature was cooled to temperatures 30ºF below the inlet air temperatures. In addition, the early introduction of the fuel and its unencumbered flow over the catalytic surfaces for an extended period of time, while not ignited, partially deactivated the surfaces. It is also speculated that a long period of shelf storage (the equivalent of 2 years) and rig modifications with the burner in place may have contributed to some deactivation, or surface coverage with foreign materials. Based on subsequent tests, the catalyst could be regenerated by igniting the reactor at higher temperatures (850º to 900ºF) and allowing for some burn-off time.

Figure 2-103 shows several features, characteristic of the reactor system and performance. First of all, when the catalyst ignites, all temperatures along the CRHX rise significantly (500ºF) due to the heat of combustion. The tip temperature rises significantly as well, by nearly 150ºF. The base temperature of the tip was nearly 1400ºF, even without the extra heat added from the hot partially oxidized products. Clearly, insufficient cooling air had been allocated to this component. The temperature of this endcap was a primary constraint to the series of experiments. Shortly after lightoff, the inlet temperature was ramped back down, the overall (main burner) equivalence ratio was reduced to 0.43 from 0.48 and the CR/CR_0 ratio was increased from 0.8 to 0.93 in an effort to keep the endcap (tip) temperature below 1500ºF and the CRHX temperatures under 1400ºF.

The main benefits of the CRHX system are also depicted in Figure 2-103. As the catalyst lights, there is an instantaneous drop in NO_x emissions. CO emissions drop on a slower scale, as there is a 2 to 3 minute delay in the sampling of this species (time required to completely flush the cell used in the infrared detector). The subsequent slower changes in these emissions (waviness) are a result of the other adjustments to the burner system near lean limits when the CO is a strong function of local conditions, especially equivalence ratio.

More time-resolved information of the lightoff process is obtained through an enlarged view of the start-up process. Figure 2-104 depicts a blow-up of both the time and temperature scales. Figure 2-104 clearly demonstrates that TC985 starts the ignition process at first very slowly over a period of 12 minutes (14:42 to 14:54), as it transitions from the coolest TC to the warmest on the CRHX. It heats more rapidly for about a minute, and then dramatically rises (and overshoots) to the final CRHX wall temperature. TC981 follows this thermocouple in its characteristics and once these two have lit, the other TCs rise virtually instantaneously. TC985 and TC981 are both located near the exit of the CRHX, providing strong evidence that the reactor lights-off at the end, then the heat propagates upstream and lights-off the full reactor channel length. This latter process is apparently very rapid, based on the precipitous rise at all the recorded locations at 14:56, or 15 seconds following the very rapid rise for TC985. The decay in the CO profile is also included here (delayed slightly due to the slow instrument response).

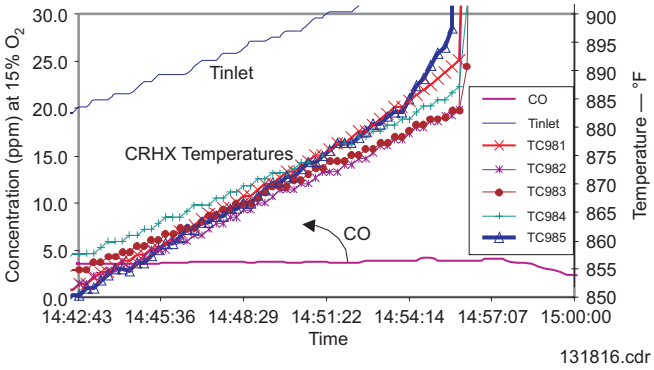

Figure 2-104. Blowup of Initial Catalyst Lightoff

At several times during the 2-week test period, there was a desire to perform experiments with fuel flowing in through the CRHX, but with the catalyst lit. Generally, once the catalyst had been lit during the day, it was difficult to stop and then reintroduce the fuel without immediate lighting of the catalyst. Typically, it was found that if the temperature of the catalyst was reduced to about 750ºF, lightoff could be prevented. By exposing the catalyst to unreacted fuel for a period of time at low inlet temperatures, the catalyst would slowly deactivate and the inlet temperatures could be raised to 800ºF for the comparison tests.

In one case, after an extensive time running without catalyst lightoff, subsequent lightoff occurred much more slowly. Apparently, carbon deposits had formed in the reaction channels and a burnout time was required to reactivate the catalyst. It is also known that rapid carbon growth can occur under selected transient conditions. Conditions when and where carbon deposits are formed have been studied in prior experimental efforts. For normal operation of the CRHX, this should not occur.

Reduction of NO_x Emissions

Several tests were performed to assess the reduction of NO_x emissions. Figure 2-105 shows how NO_x emissions vary as a function of overall equivalence ratio for a series of runs in which there is no pilot fuel and approximately 4 percent and 8 percent in the sidewall pilot, and for runs in which there is approximately 8 percent fuel in the hybrid burner. In the latter case, two series were performed, one in which the catalyst was lit (8 percent lit), and one in which the catalyst did not light (8 percent not lit). For all these runs, the pressure was held at 95 psia, the fuel for the catalyst was set to provide a catalyst equivalence ratio of four ($CR/CR_0 = 1$) and the inlet temperature was 800ºF. This temperature is lower than the base load GG8-2 conditions require, but the lower temperature enabled a slightly wider range of operating conditions when the catalyst was lit (as limited by the end cap temperature) and also enabled constant controllable conditions with the catalyst not lit for comparative experiments. The fractional fuel directed to the pilot is denoted as *approximate,* as the values changed slightly over the course of the experiments. The CR/CR_0 values were set to remain constant, and thus, as the total fuel decreased to access a range of overall equivalence ratios, the percent of total fuel in the pilot increased. All experiments were performed in a consistent manner to facilitate comparisons, although this procedure differs from those in previous tests on piloting effects in which the fuel fraction, rather than the fuel/air ratio for the pilot, would be held constant across an overall equivalence ratio variation.

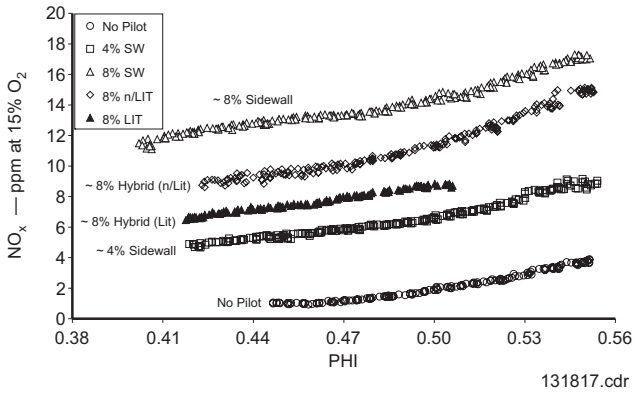

Figure 2-105. Effect of Pilot Level and Catalyst on NO_x Emissions

An immediate observation from Figure 2-105 is that NO_x emissions with no pilot are dramatically lower than for any piloted case. This is consistent with prior studies. For a given amount of pilot, the sidewall pilot produces greater NO_x emissions than for the hybrid pilot (with or without the catalyst lit). The lower emission levels for the hybrid pilot even with the catalyst not lit are presumably due to a combination of the partial premixing and the different location of the pilot. The NO_x generation formed directly from the pilot can be deduced by subtracting the NO_x emissions for the no-pilot runs. Relative to the case in which the hybrid pilot was not lit, the hybrid burner running with the catalyst at $CR/CR_0 = 1$ produces 25 percent less NO_x. This reduction was less than expected for the hybrid burner. The low level of NO_x reduction is believed to be primarily due to the insufficient cooling of the CRHX.

To provide a better assessment of the performance of the catalytic reactor and the hybrid combustor system, a sweep of the NO_x emissions, as a function of the equivalence ratio in the catalyst, was performed. Experiments were performed at 95 psia, 800ºF, and for an overall equivalence ratio of 0.48. The catalyst equivalence ratio was varied between 3.2 and 5.1 and results are shown in Figure 2-106. The ramp was started as the high equivalence ratio went down and then was cycled back up to check for any hysteresis. No significant hysteresis was observed. During the ramp, the fuel to the main burner was adjusted slightly to counteract the change in fuel flowing through the centerbody and to maintain a constant overall equivalence ratio. Temperatures of the reactor are also reported in Figure 2-106. The sequence of increasing temperatures from TCs 982=>981, and TCs 983=>984=>985 demonstrates that heat is still being released along the length of the reactor bed (see Figure 2-97). The specific temperature profile differs from analytical predictions made previously in which the highest temperatures were predicted to occur

at the entrance of the reactor.[1] The predicted high temperatures at the CRHX entrance were a result of full reactant strength and no limitation to reaction (and heat release rates) due to gradients in the reactant concentrations.

NO_x emissions were reduced substantially as the catalyst equivalence ratio was decreased. Considering that the baseline NO_x emission level (no pilot) is 1.5 ppm, the pilot-generated NO_x varied by 60 percent, just because of a change in the catalyst operating conditions. One cause of the reduction is the increased level of reaction in the CRHX and the greater amount of released heat that could be transferred to the cooling air with a decrease in equivalence ratio. The changes in the magnitude of the CRHX temperatures document the higher level of heat release for mixtures closer to stoichiometric levels.

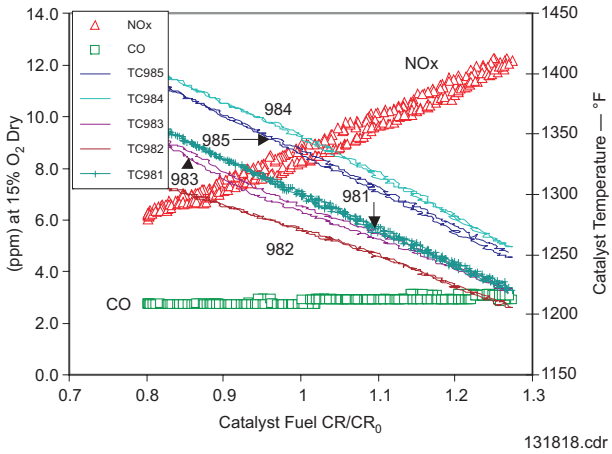

Figure 2-106. Effect of Catalyst Pilot Level on NO_x and CO Emissions and Catalyst Temperature

A portion of the NO_x reduction is due to the slight decrease in the fuel flowing through the centerbody and hence, a reduction in the fraction of fuel in the pilot. For all these flames, the pilot is the primary contributor to NO_x production, so changes in the fueling rate for the pilot will effect NO_x emissions. To assess the relative importance of these two contributors to NO_x production, the data was recast in terms of incremental NO_x production per fuel percentage in the pilot. The data presented in Figure 2-105 and Figure 2-106 are replotted in Figure 2-107 as a function of fuel percentage in the pilot, for an overall equivalence ratio of 0.48. The data created with the sweep in the CR/CR_0 (Figure 2-106) has a slope that is about 50 percent higher than that for the data with the catalyst not lit. This cannot be completely attributed to the effect of the hybrid catalyst, as the sidewall pilot indicates some nonlinearities as a function of the pilot level. Therefore, it is conservatively concluded that the hybrid catalytic system produced a 20 to 25 percent reduction in NO_x emissions. Increased cooling for the CRHX should enhance these reductions.

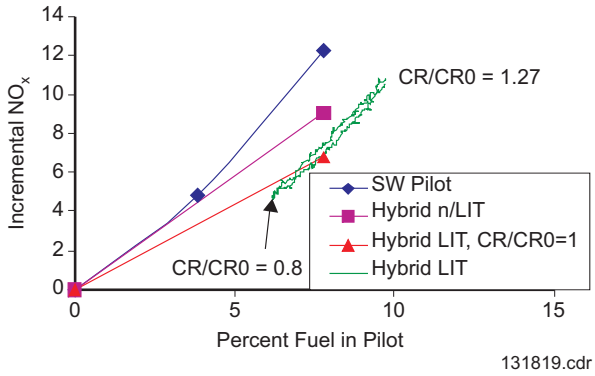

Figure 2-107. Incremental NO_x Emissions from the Pilot

[1] Colket, M.B., Kesten, A.S., Sangiovanni, J.J., Zabielski, M.F., Pandy, D.R., and Seery, D.J.,"Method and System for Combusting Hydrocarbon Fuels with Low Pollutant Emissions by Controllably Extracting Heat From the Catalytic Oxidation Stage," U.S. Patent 5,235,804, August 17, 1993.

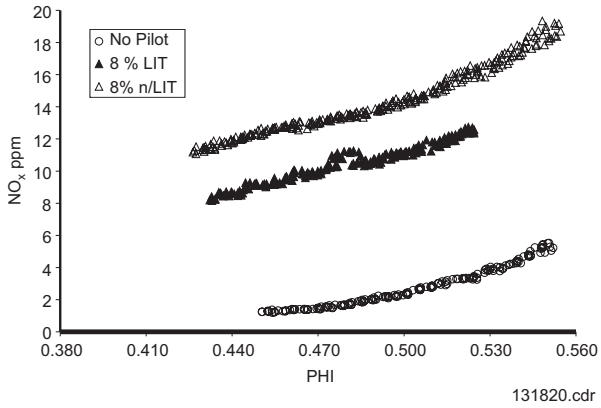

Figure 2-108. Effect of Pilot Level and Catalyst on NO_x Emissions

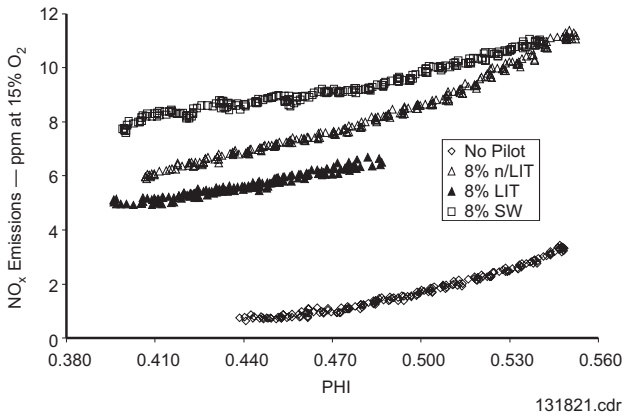

Figure 2-109. Effect of Catalyst, Pilot Level, and Steam on NO_x Emissions

Effects of pressure on NO_x emissions can be seen in Figure 2-108 and Figure 2-109. Generally, the conclusions that the hybrid combustor affords a 20 to 25 percent reduction in NO_x hold true in the pressure range of 50 to 150 psia for the available cooling level. The pressure dependence of NO_x emissions from the pilot versus those from the main premixed flame can be easily discerned from the results shown in Figure 2-110, where data from flames at 50, 95, and 140 psia with no pilot stabilization (**_np*) are compared to data from flames stabilized by the centerbody pilot without the catalyst lit (**_nl*). The very weak pressure dependence for the main flame is consistent with the prior studies of Leonard and Stegmaier.[1]

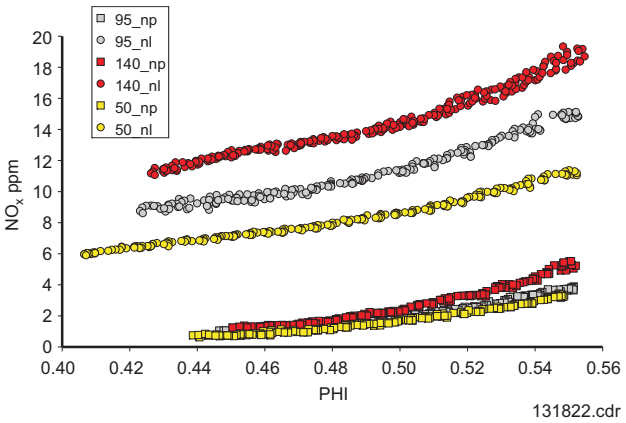

Figure 2-110. Effect of Pressure on NO_x Emissions With and Without the Pilot

CO Emissions and Lean Limits

The effect of the hybrid pilot embedded in the centerbody on CO emissions has been shown in Figure 2-103. More specific comparisons to other conditions are depicted in Figure 2-111 to Figure 2-113 for experiments at 50, 95, and 140 psia. Above a selected overall equivalence ratio, the CO levels are identical, independent of piloting conditions. Under such conditions, the reported concentrations can be defined by equilibrium conditions (assuming a small temperature decay along the burner length). Once defined by equilibrium, the CO emissions should be virtually independent of the piloting method.

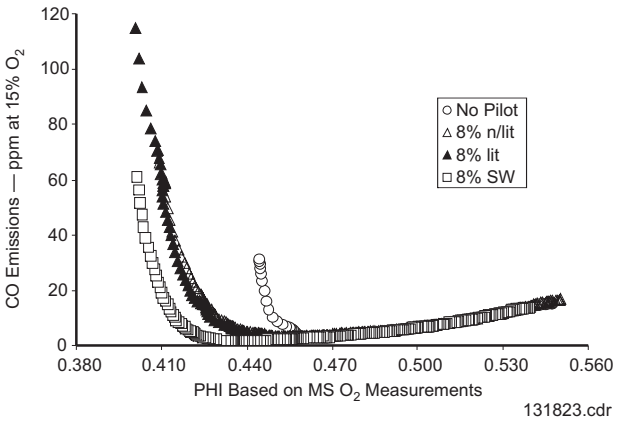

Figure 2-111. Effect of Catalyst and Pilot Level on CO Emissions

Any of the pilots extend this equilibrium line to lower overall equivalence ratios. In such cases, differences are observable.The sidewall pilot is the most successful in extending the lean limit, and this extension is enlarged through the use of higher levels of fuel in the

[1] Leonard G. and Stegmaier, J., "Development of an Aeroderivative Gas Turbine Dry Low NO_x Emissions Combustion System," Transaction of the ASME, Vol. 116, p. 542 (1994).

sidewall pilot. The hybrid pilot in the centerbody (lit) extends the low CO levels to leaner conditions as well, although not as effectively as with comparable fueling levels in the sidewall pilot. In fact, the hybrid, centerbody pilot appears to perform comparably to the sidewall pilot, with the latter at only half the fueling rate (see Figure 2-112). At 50 and 95 psia, the hybrid pilot appears to be only slightly better than the same pilot when the catalyst is not lit. At 140 psia, the hybrid burner apparently has poorer stability characteristics than the hybrid burner with the catalyst not lit. This result is contrary to all previous experiments in the laboratory.[1]

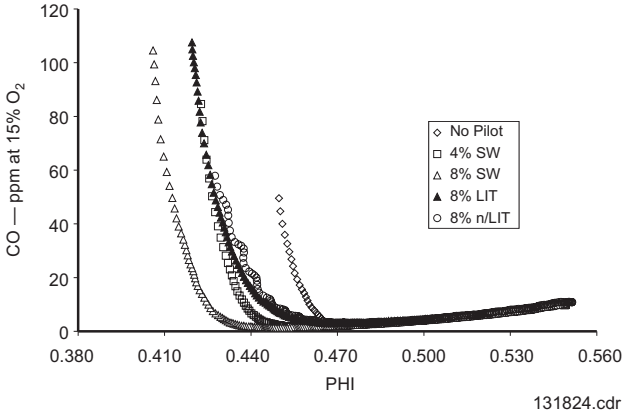

Figure 2-112. Effect of Pilot Level and Catalyst on CO Emissions

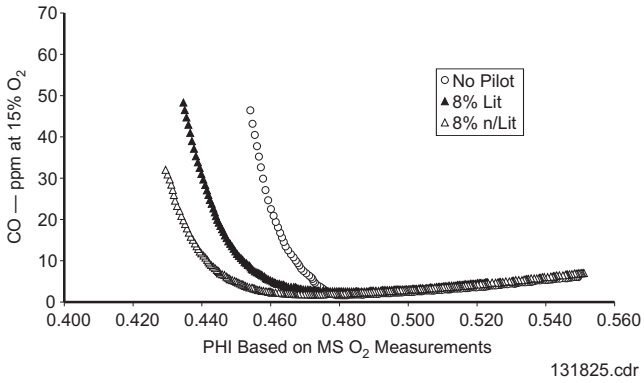

Figure 2-113. Effect of Pilot Level and Catalyst on CO Emissions

Figure 2-114 compares pressure effects on CO emissions for the runs with no pilots and cases in which fuel is flowed through the CRHX, but the catalyst was not lit. An evaluation of the trends indicates that as pressure increases, the stability limits (as indicated by the location of the sharp upturn in the CO emissions) narrow. This trend is not followed for the cases piloted by the hybrid burner without a lit catalyst. It is suspected that a possible error in the flow conditions accounts for the *95_nl* series.

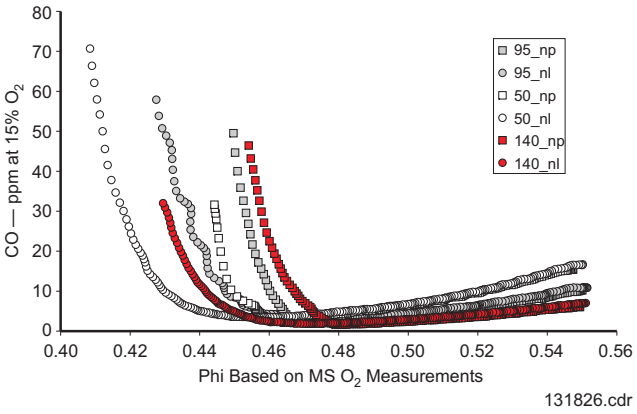

Figure 2-114. Effect of Pressure and Piloting on CO Emissions

Humid Air Effects

Steam was premixed with air as in prior studies on HAT cycle effects. As no prior studies had been performed with humidity in the air for the hybrid combustor, a series of experiments was performed with steam in the air. Maximum amounts of 10 percent steam in the air were arbitrarily selected. Before the experiments, it was expected that the impact on NO_x would be less than in the case with pure air. The explanation is that the overall reaction, $CH_4 + H_2O \Rightarrow CO + 3H_2$ - 49.3 kcal/mole, is substantially endothermic and acts to reduce the temperature rise of the reaction. Therefore, the amount of energy that can be transferred effectively, given otherwise identical operating conditions, is limited.

Figure 2-115 shows NO_x results for two cases with fuel flowing through the CRHX at 50 psia. In addition, the prior results with no steam are included for reference. The case in which the catalyst is not lit (*n/LIT w/10% stm*) appears to yield higher levels of NO_x than for the case in which the catalyst was lit (*LIT w/10% stm*); however, the CO emissions reported in Figure 2-116 indicate that the *equilibrium* CO levels do not match. Therefore, it is assumed that there was an error in the metering system for steam for one of these experiments, and thus, a comparison between lit and not lit results cannot be made.

[1] The small waviness in some of the data sets is due to poor control on the fuel valve at low flow rates.

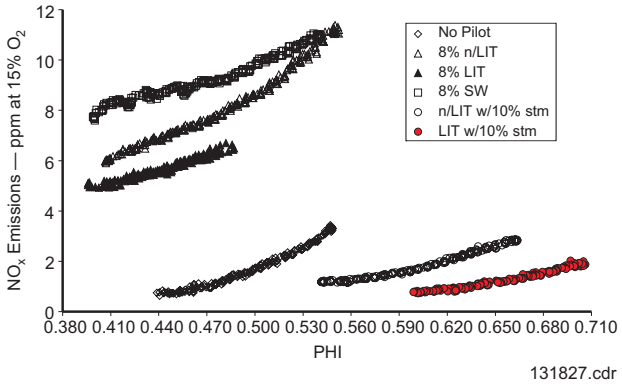

Figure 2-115. Effect of Catalyst, Pilot Level, and Steam on NO_x Emissions

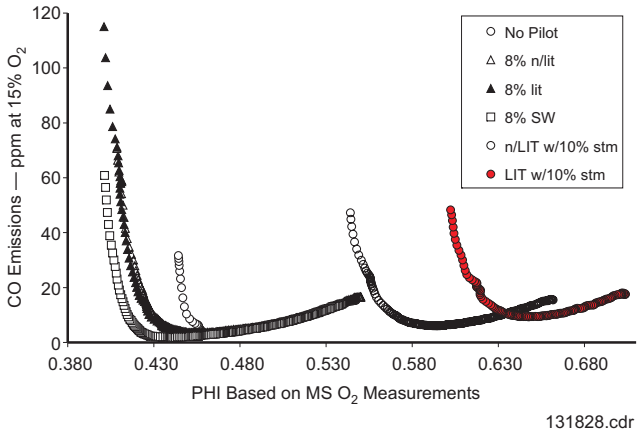

Figure 2-116. Effect of Catalyst, Pilot Level, and Steam on CO Emissions

Results with added steam at 95 psia are shown in Figure 2-117 and Figure 2-118. Data is presented for both 10 percent and 5 percent levels of steam. For reference, prior data sets are included. In this case, the NO_x levels between the sidewall pilot (*SW w/10% stm*) and the hybrid combustor in the centerbody (*LIT w/10% stm*) are virtually identical and lie on top of each other. The threshold for rapid rise of CO (see Figure 2-118) is extended further to lean conditions for the sidewall pilot, consistent with the experiments with no steam.

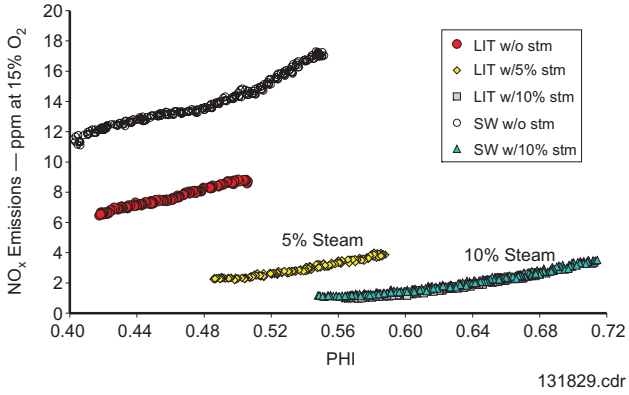

Figure 2-117. Effect of Steam Addition and Piloting on NO_x Emissions

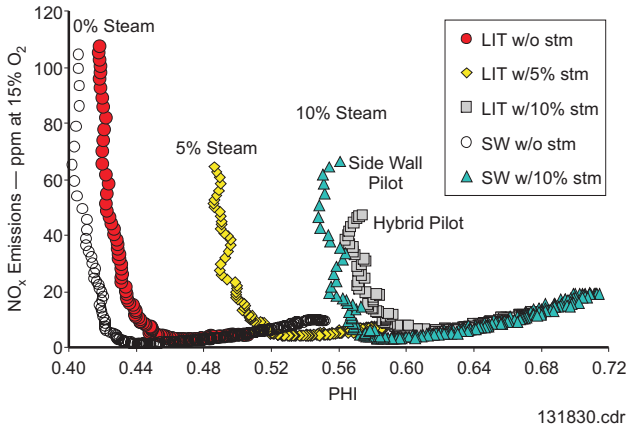

Figure 2-118. Effect of Steam Addition and Piloting on CO Emissions

2.8.6 Component Inspection

After tests at Morgantown at the NETL, the hybrid combustor pilot embedded in the nosecone of the TEN was returned to UTRC for inspection. A photograph (Figure 2-119) of the exterior of the nosecone showing discoloration confirms the experimental result of overheating of the component. The hot air exiting the sidewalls of the nosecone left a swirled streak around the cone, as the adjacent air streams contained premixed fuel.

A close examination of the tip showed further signs of the overheating, as the welds covering the TCs exhibited some distress (Figure 2-120 and Figure 2-121). A similar condition was noted on the opposite sidewall TC (not shown).

The catalytic reactor survived intact. This result was considered a significant success for the experimental study. However, thermal stressing was apparent, based not only on the discoloration (see Figure 2-122 and Figure 2-123), but also on the slight bending of the separation plates at the entrance to the CRHX, as shown in Figure 2-124. No separation of the fins from the adjoining plates was observed, indicating no degradation of the braise or performance of the reactor. The reactor has been cut apart to investigate its interior. Other than the warping at the separation sheets, no damage was observed. The fins remained attached to the separation sheets along the length of the reactor.

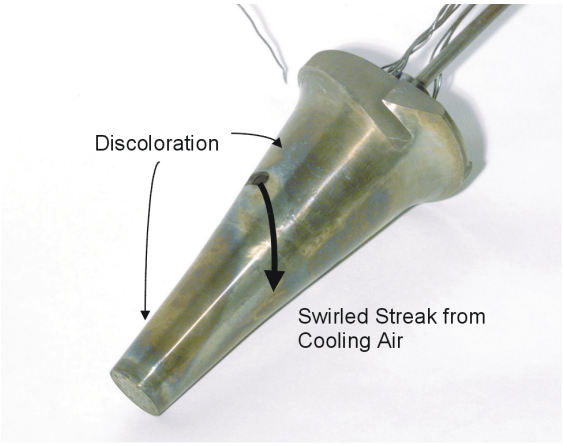

Figure 2-119. Photograph of Nosecone After Testing

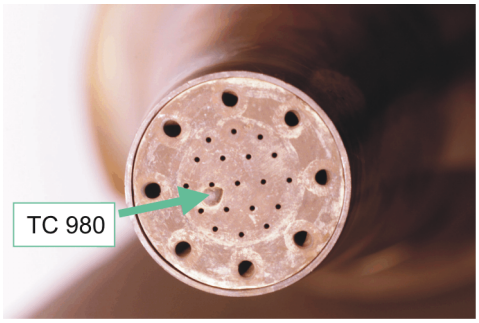

Figure 2-120. Thermal Stress Observed at TC Welds (Endcap)

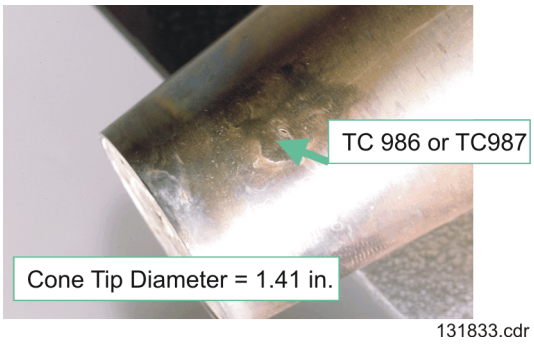

Figure 2-121. Thermal Stress Observed at TC Welds (Sidewalls)

The reactor experienced a host of variable conditions and it is not possible to discern whether the distress occurred over a long period and various sequences of multiple runs, or whether it was the result of short duration tests (or inadvertent excursions) to extreme conditions, well beyond the initial design criteria.

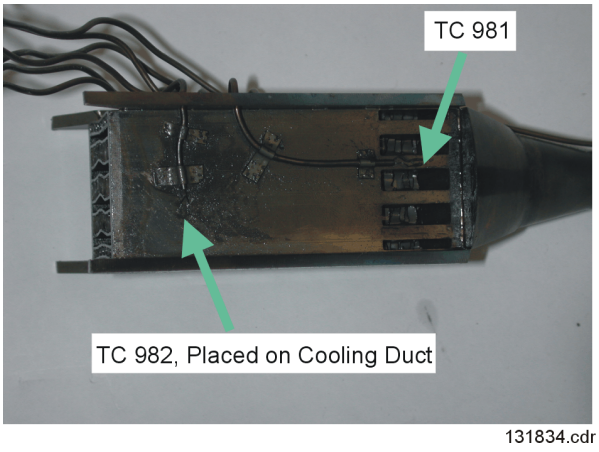

Figure 2-122. Discolored CRHX After Tests

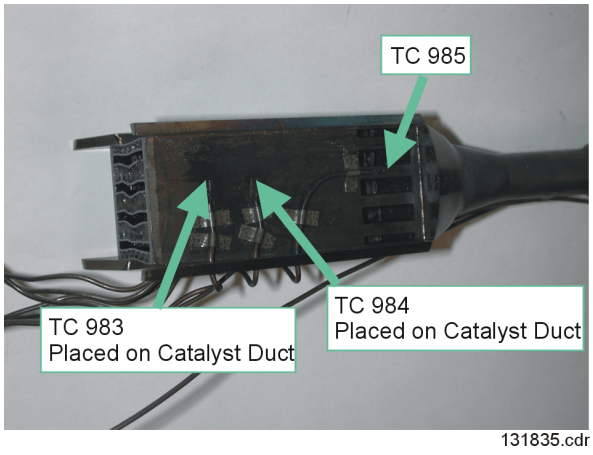

Figure 2-123. Discolored CRHX After Tests

2.8.7 Summary

Experiments using a hybrid burner installed into the nosecone of a TEN have been completed. These tests of a hybrid burner are the first at full-scale conditions. With no steam added to the air, the main successes include the following:

1. The hybrid burner and associated components survived the tests intact
2. Self-lighting of the catalyst was achieved
3. NO_x reduction benefits were demonstrated when the catalyst was lit.
4. CO levels were at least comparable, or lower, with the catalyst lit.

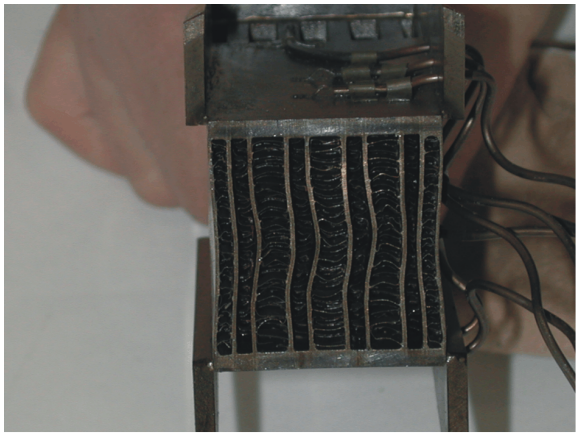

131836.cdr

Figure 2-124. Test-Warped Plates

The benefits to the NO_x and CO levels were not large enough to demonstrate a dramatic improvement, nor were they better than the performance of an alternative sidewall pilot. However, it is recognized that there were constraints to the implementation of this concept in the nosecone and thus, the anticipated and previously demonstrated benefits, such as a factor of three reduction in NO_x, were lower than those theoretically achievable. The principal constraints of this implementation, such as insufficient cooling to the CRHX and to the endcap, prevented exploration of a broad range of operating conditions and led to hardware stress. Catalyst lightoff processes were not fully explored, but the results confirmed prior studies that indicated lightoff occurs around 780ºF. Flowing unreacted fuel along the reactor for an extended period of time tends to deactivate the catalyst and under such circumstances, catalyst lightoff is shifted by about 100ºF.

Addition of 5 percent and 10 percent steam reduces the heat released in the catalyst. No significant differences between the hybrid burner and a separate sidewall pilot were observed, except that the sidewall pilot provided slightly greater stability at the same fueling level, consistent with the results obtained without steam addition.

2.8.8 Recommendations

Based on the results presented above, use of similar hardware in the production hardware TEN burner is not recommended. While cooling of the endcap can be readily modified to resolve the high-temperature problem at the tip of the nosecone, the cooling of the CRHX is insufficient, due in large part to the lower pressure drop driving the cooling airflow. A substantial redesign of the reactor is required, although the general features of the reactor can still be retained.

The substantial successes of catalyst lighting, survival of the hardware, and demonstrated NO_x benefits validate the features of the concept. With proper, or sufficient, CRHX cooling, there are expectations that further benefits (up to a factor of three) can be realized. It may not be ideal to increase the relative mass of cooling air to the burner; however, additional cooling can be achieved by lengthening the reactor. Since temperatures increased along the length of the CRHX, this appears to be the more effective solution. Alternative concepts for piloting should be developed, like the sidewall pilot, or for other burner configurations for either the pilot or the main burner assembly.

Issues of concern for the preferred applications include the inlet air temperature. If inlet temperatures much lower than 850ºF are part of the engine cycle or if the catalyst becomes deactivated, it will be necessary to (electrically) preheat the CRHX. With electrical preheat in place, the reactor should stay lit even to much lower inlet temperatures (the equivalent of 550ºF) based on prior experiments at UTRC.

In any application, a cost benefit analysis should be performed. It is suggested that additional studies be performed to minimize warping of the CRHX.[1] Also, tests need to be performed under full pressure conditions that could not be duplicated in the DOE facilities with the specified flow rates.

2.9 HUMID AIR COMBUSTION WITH A CONVECTIVELY-COOLED LINER

The HAT cycle has been recognized as a unique way to increase gas turbine power output and efficiency while lowering NO_x emissions significantly. Among the many issues relevant to the HAT technology, combustion in moist air is the most critical link in the achievement of low NO_x. A substantial amount of work on the HAT has been done by DOE, UTRC, and P&W, with most experimental work being carried out by the NETL. The experimental investigations at DOE were predominantly done with a relatively idealized combustor liner, which was an uncooled refractory liner. The refractory liner offers an efficient way to investigate many aspects of the combustion process, including emissions. However, it does not offer realistic engine geometry, liner durability information, and acoustic boundary conditions. The acoustic boundary conditions are of particular importance. The most promising way to minimize pollutant emissions is through premixed combustion, which is often complicated by the obstacle of oscillating combustion or dynamics. Oscillating combustion can sometimes affect emissions and break hardware. The acoustic boundary condition, among other things, determines whether the oscillating combustion will occur. Many otherwise good designs became unusable in the engine because of the oscillating combustion. In an effort to move towards real engine configurations, DOE funded the convectively cooled liner study on humid air combustion.

This report summarizes the combustion dynamics and emissions of a combustor that consists of a convectively-cooled liner with near-choke exit. An axial swirler nozzle and a TEN, both 1.97 $in.^2$ ACd, were studied. Comparisons were made with data from different nozzles, as well as from this liner and a refractory liner at different operating conditions. Natural gas was used as the fuel in all cases.

2.9.1 Experimental Technique

Convectively-Cooled Liner Design and Emission Sampling

Figure 2-125 shows the convectively-cooled liner. There are two liner sections downstream of the fuel nozzle. They are an impingement-cooled can and an effusion cooled transition duct. The impingement-cooled can is a cylinder in cylinder design. The outer cylinder was perforated to provide cooling air impingement on the inner can, which is 4.16 in. in inner diameter, but not perforated to eliminate the flame quenching effect that can create higher CO and UHC. Thermocouples and pressure transducers, both static and dynamic, were mounted at various locations to monitor the rig. Water-cooled emission probes were installed at the end of the can, as well as at the exit of the transition duct. The probe sampled the exhaust in an area-averaged fashion to ensure that the extracted gas samples were representative across the sampling planes.

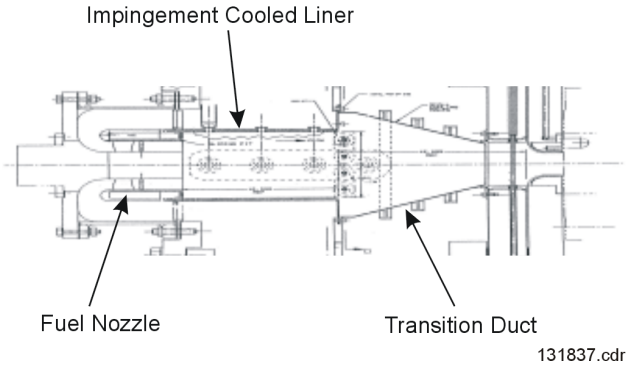

Figure 2-125. A Diagram of the Convectively-Cooled Liner

All the emissions data presented here was sampled at the exit of the transition duct. Exhaust samples were transported through heated tubing and were dried before being analyzed. Species analyzed were NO_x, CO, CO_2, O_2, and UHC. All emissions reported here are on a dry basis and have been corrected to 15 percent O_2. The UHC was not reported here because it was only a few parts per million for all the cases without hardware failures, except when the CO readings were high. Reasonable fuel/air ratio agreement (within 15 percent) was achieved between the emissions based fuel-to-air ratio and the metered fuel-to-air ratio. This number was not as good as the agreement in previous refractory liner tests, which were within 6 percent, with most values within 2 percent. The 15 percent discrepancy may be caused by the nonuniformity in the exhaust flow at the rig exit. Since the air and fuel metering mechanism had not changed from refractory liner to the cooled liner, the metered flows are believed to be accurate.

[1] Perhaps this was observed here since the design limits of the system were pushed

Flow Split

The entire rig with the nozzle was cold flowed at ambient pressure for ACd determination at UTRC. The total ACd, including the nozzle, was 2.97 in^2. The nozzle ACd was 1.97 in^2. Therefore, the nozzle flow split was 66.3 percent of the total flow.

The ambient cold flow rig total ACd, which was 2.97 in^2, was about 15 percent lower than that measured in the cold- and hot-pressured rig at the DOE facility. The discrepancy was significant because it could potentially cause 15 percent error in nozzle fuel-to-air ratio calculation. Since the emissions are a very strong function of nozzle fuel-to-air ratio in premixed combustion systems, this became an important discrepancy. It was decided to use the ambient cold flow rig ACds here for flow split, because the pressured rig test had the pressure transducer measuring the pressure difference between the inlet air plenum and the inside of the combustor. Therefore, the pressurized rig data reflected the ACd from the inlet air plenum to the inside of the combustor. Since the gas from the inside of the combustor had to go through the transition duct exit, which is another flow restrictor to further downstream, the ACd from inlet air plenum to the inside of the combustor must be larger than the ACd for the entire rig. Therefore, it was concluded that ambient cold flow ACds data was accurate and should be used for accurate flow split calculation, instead of the pressurized rig ACds.

Hardware Failures

The experimental portion of this task lasted longer than expected in part, because of a series of hardware failures. There were seal failures; it was found that the humidity in the air destroyed graphoil seals. The air leaked through the broken seals, quenched flames, and created high CO and UHC. Spiratalic gaskets, however, were proven successful and are recommended for humid air combustion tests, or these seals can be welded shut. An increase in sealing surface area also helps. There were also other hardware failures, possibly caused by acoustic pressure waves. The RMS pressure reached as high as 8 psi in the combustor. Good structural integrity has to be maintained for rig design.

The data presented in this report is not associated with any hardware failures. Data compromised by hardware problems are not included in this report.

2.9.2 Results and Discussion

Liner Effect

Figure 2-126 reveals the NO_x and CO emissions as a function of nozzle equivalence ratio for cooled and refractory liners. The inlet air temperature and pressure were about 860ºF and 100 psia, respectively. It is obvious that the NO_x levels were very close for the different liners. The NO_x in the cooled liner was about 4 ppm higher than in the refractory liner for the same equivalence ratios ranging from 0.52 to 0.58. However, the cooled-liner case had significantly lower CO emissions than the refractory-liner case. The CO in the cooled liner was about 14 to 36 ppm lower than in the refractory liner for the same equivalence ratios ranging from 0.52 to 0.58. These facts suggest that NO_x production was determined by front-end flame temperature, while cooling air introduced in the cooled liner downstream of the combustion can oxidize CO significantly.

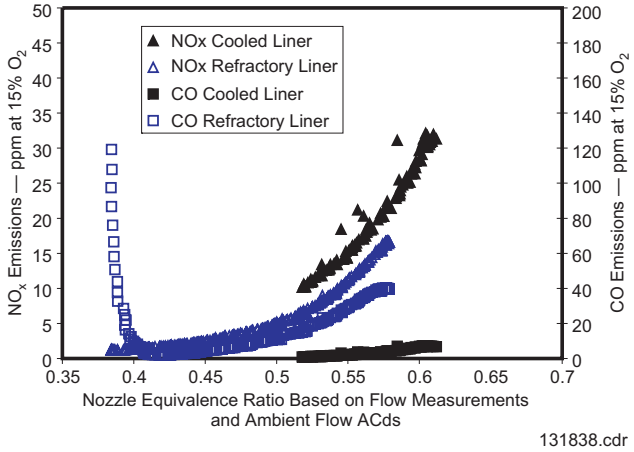

Figure 2-126. Cooled Liner Versus Refractory Liner for the Axial Nozzle

Although not shown here, it was noted that the RMS value of dynamic pressure in the cooled liner for the axial nozzle ranged from 2.7 to 4.4 psia, which was significantly higher than the 1 to 2 psia in the refractory liner. This confirms the need to study lean premixed combustion with realistic acoustic boundary conditions.

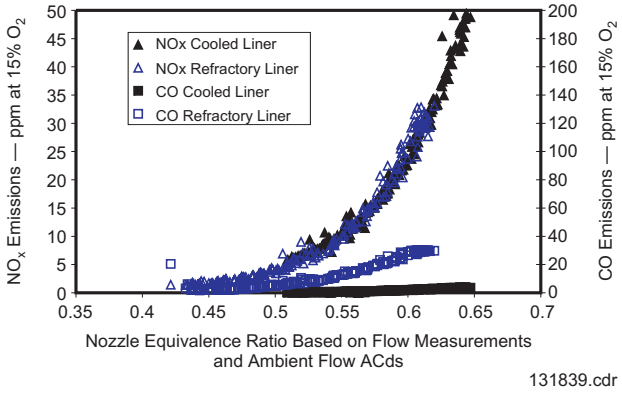

Figure 2-127. Cooled Liner Versus Refractory Liner for the TEN

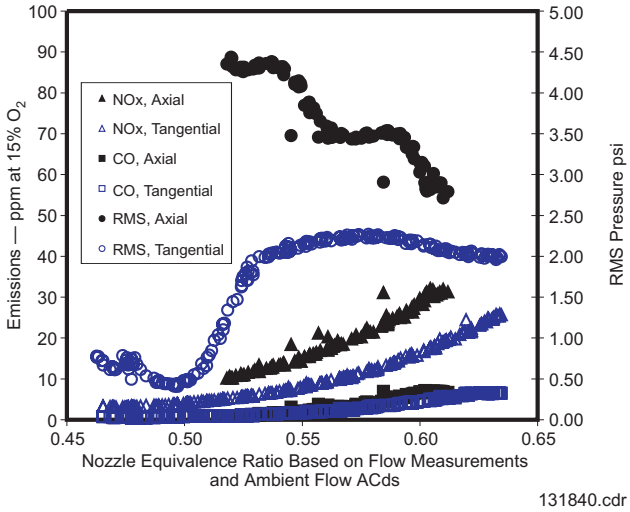

Figure 2-128. Axial Nozzle Versus TEN for the Convectively-Cooled Liner

Figure 2-127 shows the similar data for the TEN. As in the case with the axial nozzle, the NO_x levels were very close for the different liners. The CO in the cooled liner was significantly lower than that in the refractory liner for the same equivalence ratios.

Nozzle Difference

Figure 2-128 shows the NO_x and CO emissions and dynamic pressure as a function of nozzle equivalence ratio for the axial and TEN in the cooled liner. The inlet air temperature and pressure were about 860ºF and 100 psia, respectively. The CO levels were very close for the different nozzles. The NO_x with the axial nozzle was slightly higher than that with the TEN for the same equivalence ratio. This suggests that the TEN may be a better mixer. It was also noticed that the dynamic pressure was significantly higher with the axial nozzle.

Inlet Air Temperature Effect

Figure 2-129 shows the NO_x and CO emissions and dynamic pressure as a function of nozzle equivalence ratio for the TEN in the cooled liner with different inlet air temperatures. The inlet air pressure was maintained at about 173 psia. The CO levels were very close for the different inlet temperatures. The NO_x with higher inlet temperature was higher than with the lower inlet temperature for the same equivalence ratio. To see if this is because higher inlet temperature created higher flame temperature and therefore, higher NO_x, the same data in Figure 2-129 was plotted against calculated flame temperature for the nozzle in Figure 2-130. The adiabatic flame temperatures were calculated through the NASA CEA equilibrium code. As it is shown in Figure 2-130, flame temperature alone cannot account for the effect. This means that the NO_x with higher inlet temperature would be higher than it would with the lower inlet temperature for the same flame temperature. It was also noticed that there was a sudden drop in dynamic pressure as flame temperature was lowered.

Pressure Effect

Figure 2-131 shows the NO_x and CO emissions and dynamic pressure as a function of nozzle equivalence ratio for the TEN in the cooled liner with different inlet air pressures. The inlet air temperature was maintained at approximately 860ºF. The NO_x with higher inlet pressure was higher than it was with the lower inlet pressure for the same equivalence ratio. The CO curves were showing the opposite trend. The CO with higher inlet pressure was lower than it was with the lower inlet pressure for the same equivalence ratio. It was also shown that there was a sudden drop in dynamic pressure as the flame temperature was lowered. At the point of sudden dynamic pressure drop, the 200 psia case showed a sudden increase in NO_x emissions. In the case of 100 psia, the NO_x emissions changed almost continuously.

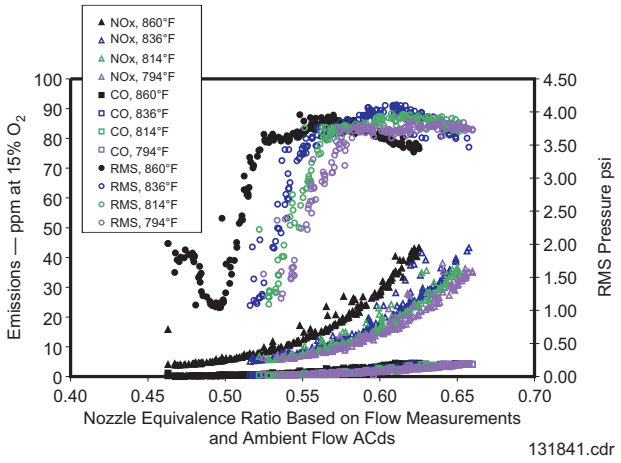

Figure 2-129. Inlet Air Temperature Effect for Convectively-Cooled Liner With TEN

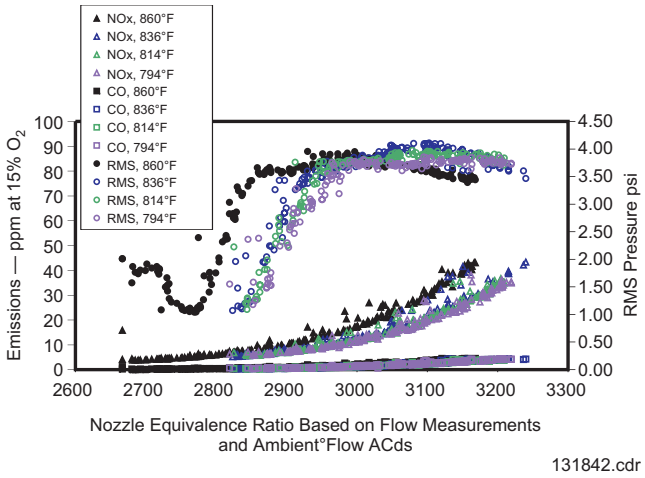

Figure 2-130. Inlet Air Temperature Effect for Convectively-Cooled Liner With TEN

Pilot Level Effect

Figure 2-132 shows the NO_x and CO emissions and dynamic pressure as a function of nozzle equivalence ratio for the axial nozzle in the cooled liner with centerbody diffusion pilot levels. The inlet air temperature and pressure were maintained at approximately 860ºF and 100 psia. The NO_x with pilot was higher than it was without the pilot for the same equivalence ratio. The CO curves were virtually unchanged by the pilot. It was also shown that there was a slight drop in dynamic pressure with the centerbody pilot.

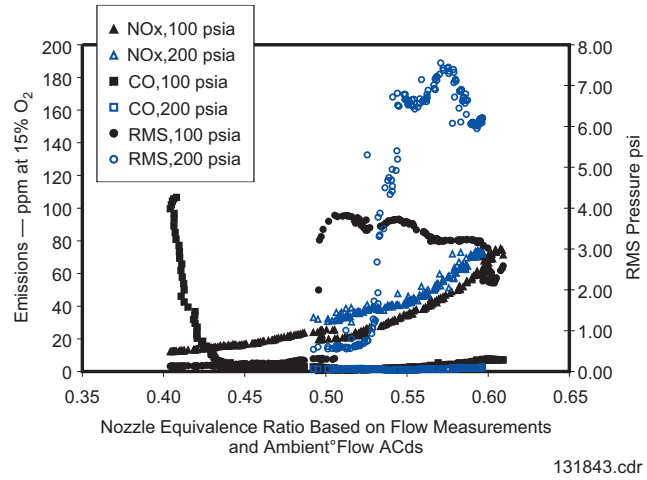

Figure 2-131. Pressure Effect for Convectively-Cooled Liner With Axial Nozzle

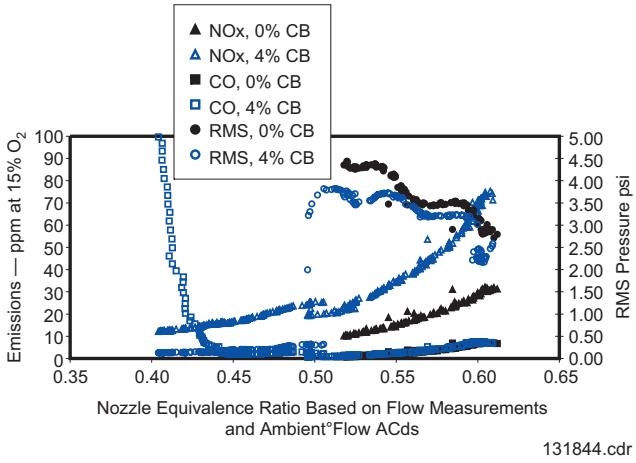

Figure 2-132. Pilot Effect for Convectively-Cooled Liner With Axial Nozzle

Steam Effect

Figure 2-133 shows the NO_x and CO emissions and dynamic pressure as a function of nozzle equivalence ratio for the axial nozzle in the cooled liner, with and without steam addition. The inlet air temperature and pressure were maintained at approximately 860ºF and 200 psia. The percentage of steam is defined on the basis of the combined air and steam flow rate.

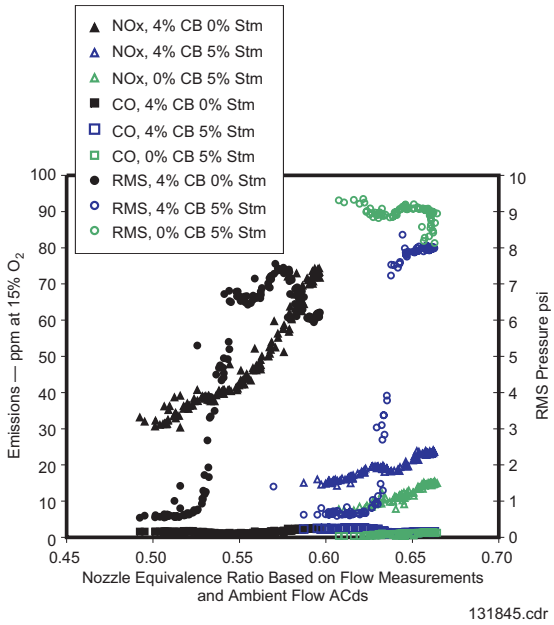

Figure 2-133. Steam Effect for Convectively-Cooled Liner With Axial Nozzle

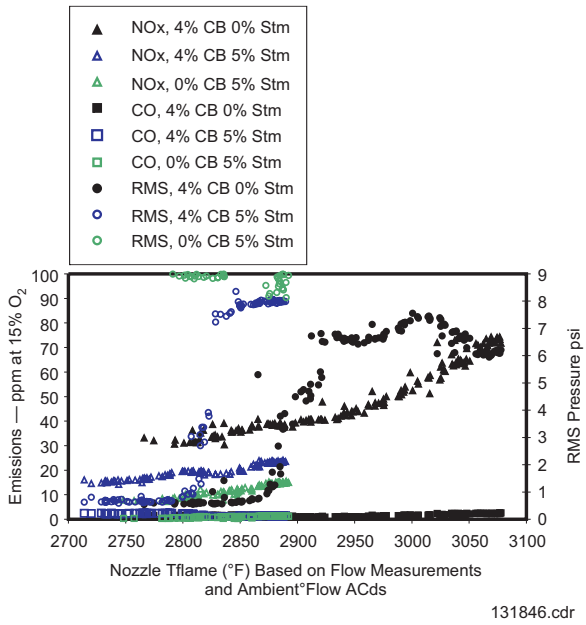

Figure 2-134. Steam Effect for Convectively-Cooled Liner With Axial Nozzle

The addition of steam brought drastic reduction in the formation of NO_x, similar to what was found in the refractory liner. For the same equivalence ratio, more than 75 percent reduction in NO_x emission was achieved by the addition of 5 percent steam. CO curves did not show much difference for the equivalence ratios tested. The flame temperature reduction with steam addition reduced the *Zeldovich* or *Thermal* NO_x formation mechanism, partially explaining the NO_x reduction effect. However, it cannot explain the entire NO_x reduction observed.

To illustrate this point, the data in Figure 2-133 was plotted against adiabatic flame temperatures. The results were plotted in Figure 2-134. It is shown that even at the same adiabatic flame temperature, the addition of 5 percent steam reduced NO_x by 40 to 50 percent depending on the flame temperature. This strongly suggested that in addition to the NO_x reduction achieved through the lowering of flame temperature through steam addition, the moisture also reduced the NO_x by other mechanisms. Bhargava *et al.* investigated the humid air effect on NO_x reduction in premixed natural gas combustion system and offered an explanation.[1]

NO_x formation reactions can be categorized into three different groups. They are *Zeldovich*[2] or *Thermal* NO_x mechanism, N_2O mechanism, and the *Fenimore*,[3] or *Prompt* NO mechanism.

Zeldovich mechanism is described by following reactions:

1. $O + N_2 \rightarrow NO + N$

2. $N + O_2 \rightarrow NO + O.$

The overall rates of NO production are controlled mainly by the first reaction, since the second reaction is quicker than the first one. Due to the fact that there is abundance of N_2 available in the combustion system, the rate of the first reaction, and hence, the rate of NO production, is strongly controlled by O concentration. A reduction of O concentration can reduce the rate of the first reaction, thereby reducing NO_x production.

[1] Bhargava, A., Colket, M., Sowa, W., Casleton, K. and Maloney, Dan, "An Experimental and Modeling Study of Humid Air Premixed Flames," *Journal of Engineering for Gas Turbines and Power*, Vol. 122, p. 405, July 2000.

[2] Zeldovich, J., "The Oxidation of Nitrogen Combustion and Explosions," *Acta Physicochimica*, URSS, 21, p. 577, 1946.

[3] Fenimore, C.P., "Formation of Nitric Oxide in Premixed Hydrocarbon Flames," *Thirteenth Symposium (International) on Combustion*, The Combustion Institute, 1971.

The *N_2O* mechanism consists of reactions involving N_2O that form NO. NO_x formed through this mechanism can be suppressed by the reaction $N_2O + M \rightarrow N_2 + O + M$. A reduction of O concentration can promote the previous reaction and therefore, reduce NO_x production.

The key to the *Fenimore* NO mechanism can be described by following reactions:

1. $CH + N_2 \rightarrow HCN + N$
2. $CH_2 + N_2 \rightarrow HCN + NH$
3. $HCN + O \rightarrow CH + NO$.

A reduction of CH/CH_2 will reduce the reaction rate in the first/second reactions and eventually reduce NO. A reduction of O will reduce the reaction rate in the third reaction and therefore, reduce NO.

For the same flame temperature, the humidified case had higher equivalence ratios than the dry case, and therefore, had lower O_2, which reduced the concentration of O atoms. Humidity also promotes the $O + H_2O$ reaction and reduces O concentration. The reduction of O atoms lowered the NO_x formation by all the three mechanisms. In addition, humidity increases OH radical concentration, which promotes the oxidation of hydrocarbon radicals and reduces *Fenimore* NO. These are the reasons why the steam addition reduced NO_x dramatically for the same flame temperature relative to a dry case.

2.9.3 Conclusions

Experimental data were obtained for natural gas premixed combustion in dry and humid air in a convectively cooled liner with near-choke exit at different pressures over a wide range of equivalence ratios. The effect of liner, nozzle, inlet temperature, inlet pressure, pilot level, humidity, and equivalence ratio on NO_x and CO emissions and dynamic pressure were evaluated based on the data. Introduction of 5 percent steam in air suppressed NO_x production by more than 40 to 50 percent for the same flame temperature. The dramatic suppression of NO_x is attributed to the decrease of O atom and increase of OH radical in the humid air combustion.

3. CONCLUSION

The HAT Cycle Technology Development Program commenced in the 4th Quarter of 1996 and finished in the 4th Quarter of 2001. This program teamed the NETL, P&W, UTRC, and kraftWork. The execution of the program started with bench-top experiments, conducted at UTRC, to extend kinetic mechanisms to the HAT cycle temperature, pressure, and moisture conditions. The fundamental data generated in the bench-top experiments was incorporated into the analytical tools available at P&W to design the fuel injectors and combustors. The NETL then used the hardware to conduct combustion rig experiments to evaluate the performance of the combustion systems at elevated pressure and temperature conditions representative of the HAT cycle. The results were integrated into a kraftWork system analysis to verify that sufficient understanding of the technology had been achieved and prove that large-scale technological readiness and demonstration could be undertaken as a follow-on activity. The optional program extended the experimental combustion evaluations to several specific technologies that can be used with HAT technology.

After 5 years of extensive research and development, we can report that the HAT Cycle Technology Development Program goals have been achieved. Kinetic mechanisms of humid air combustion have been validated and combustor configurations that efficiently burn fuels in high moisture content air while producing low emissions have been identified. With 0 to 10 percent steam addition, emissions achieved during this program for natural gas were:

- Less than 8 ppm NO_x
- Less than 16 ppm CO
- Unburned hydrocarbons corrected to 15 percent O_2 for an FT8 engine operating from 65 to 100 percent power at any day between 0° and 120°F.

For liquid fuel No. 2 Diesel, with 10 percent steam addition, more than 90 percent reduction of NO_x relative to the dry case for the same flame temperature was achieved at 100 psi.

The comprehensive database and understanding of humid air technology generated through this successful program has provided a foundation for future humid air combustion products, including gas turbines. System studies have identified that HAT cycles produce a greater power output at a higher efficiency, in comparison to simple cycles, because less work is needed for intercooled compression and more work is done by the turbine. In its basic simple-cycle configuration, the twin-spool engine FT4000 I/C has an output of 148 MW and an efficiency of 47.5 percent (LHV). The corresponding HAT cycle would have an output of 248 MW and an efficiency of 58.7 percent (LHV); a value quite close to the 60 percent (LHV) goal set by the DOE for the ATS combined cycle. Despite the added cost for parts, such as a saturator, over simple-cycle machines, HAT-cycle machines reduce capital costs, in comparison to combined-cycle machines, since the steam cycle is eliminated. It provides flexible operations like quick startup and shutdown, as commonly seen in simple-cycle turbines. The HAT cycle also minimizes NO_x emissions from both gas and liquid fuel combustion systems, due to water vapor suppression of NO_x in the combustion processes. In conclusion, HAT cycle products can provide significant public benefits by minimizing pollutant emissions, decreasing the production of CO_2 and other *Greenhouse* gases, and enhancing the conservation of energy.

4. REFERENCES

Al-Fawaz, A., Dearden, L., Hedley, J., Missaghi, M., Pourkashanian, Williams, A. and Tap, L., "NO_x Formation in Geometrically Scaled Gas Fired Industrial Burners," *Twenty-Fifth Symposium (International) on Combustion*, The Combustion Institute, Pittsburgh, PA, pp. 1027-1034, 1994.

Argen, N.D., Westermark, M.O., Bartlett, M.A., and Lindquist, T., "First Experiments on an Evaporative Gas Turbine Pilot Plant: Water Circuit Chemistry and Humidification Evaluation," Paper No. 2000-GT-0168, ASME Turbo Expo 2000, May 2000.

Beer, J. and Chigier, N., "Modeling of Combustion Systems," *Combustion Aerodynamics*, Chapter 7, Wiley Press, New York, 1965.

Bhargava, A., Colket, M.B., Sowa, W., Castleton, K., and Maloney, D., "An Experimental and Modeling Study of Humid Air Premixed Flames," AMSE Paper No. 99-GT-8, 1999.

Bhargava, A., Kendrick, D.W., Colket, M.B., Sowa, W.A., Casleton, K., and Maloney, D., "Pressure Effect on NO_x and CO Emissions in Industrial Gas Turbines," Proceedings of ASME Turbo Expo, Paper No. 2000-GT-97, 2000.

Blevins, L.G., and Roby, R.J., "An Experimental Study of NO_x reduction in Laminar Diffusion Flames by Addition of High Levels of Steam," ASME Paper No 95-GT-327, 1995.

Bowman, C.T., "Control of Combustion Generated Nitrogen Oxides Emissions: Technology Driven by Regulations," *Twenty-Fourth Symposium (International) on Combustion*, The Combustion Institute, Pittsburgh, PA, 1992.

Bowman, C.T., Hanson, R.K., Davidson, D.F., Gardiner, W.C., Jr., Lissianski, V., Smith, G.P., Golden, D.M., Frenklach, M., and Goldenberg, M., http://www.me.berkeley.edu/gri_mech, 1994.

Bowman, C.T., and Seery, D.J., *Emissions from Continuous Combustion Systems*, (W. Cornelius and W.G. Agnew, eds.), p.123, 1972.

Carcasci, C., Cosi, L., Fiaschi, D., and Manfrida, G., "Semi-Closed HAT (SC-HAT) Power Cycle," Paper No. 2000-GT-154, ASME Turbo Expo 2000, May 2000.

Colket, M.B., Kesten, A.S., Sangiovanni, J.J., Zabielski, M.F., Pandy, D.R., and Seery, D.J., "Method and System for Combusting Hydrocarbon Fuels with Low Pollutant Emissions by Controllably Extracting Heat From the Catalytic Oxidation Stage," U.S. Patent 5,235,804, Aug. 17, 1993.

Colket, M.B., Sangiovanni, J.J., Tredway, W.K., Schmidt, W.R., Knight, B.A., and Snider, T.R.,"Topical Report on Reactor Fabrication and Catalyst Selection for Hybrid Combustion," Gas Research Institute, UTRC Report No. 970373-12, October 1993

Dahm, W., Driscoll, J., Hsieh, T., "Scaling Characteristics of Aerodynamics and Low-NO_x Properties of Industrial Natural Gas Burners: The Scaling 400 Study," Final Report, Gas Research Institute, 1998.

Day, W. and Rao, A., "FT4000 HAT with Natural Gas Fuel," International Gas Turbine Institute, ASME Paper IGTI-Vol. 7, ASME Cogen-Turbo, Book No. 100333, 1992.

Dryer, F.L., "Water Addition to Practical Combustion Systems-Concepts and Applications," *Sixteenth Symposium (International) on Combustion*, The Combustion Institute, Pittsburgh, PA, 1976.

Fenimore, C.P., "Formation of Nitric Oxide in Premixed Hydrocarbon Flames," *Thirteenth Symposium (International) on Combustion*, The Combustion Institute, 1971.

Fischer, A., Frutschi, H., Haselbacher, H., "Augmentation of Gas Turbine Power Output by Steam Injection," Proceedings of ASME Turbo Expo, Paper No. 2001-GT-0107, 2001.

Fric, T.F., "Effects of Fuel-Air Unmixedness on NO_x Emissions," AIAA 92-3345, 1992.

Gallo, W., Bidini, G., Bettagli, N., and Facchini, B., "The Evaporator Process Simulation and the HAT Cycle Performance," ASME Paper No. 95-CTP-59, ASME Turbo Power Congress.

Glarborg, P., Kee, R.J., Grcar, J.F., and Miller, J.A., "PSR: A Fortran Program for Modeling Well-Stirred Reactors," *Sandia National Laboratories*, SAND86-8209, Livermore, CA, February 1986.

Gore, J., and Faeth, G., *Twenty-First Symposium (International) on Combustion*, The Combustion Institute, pp. 1521, 1986.

Gupta, A., and Lilley, D., "Predictive Techniques," *Flowfield Modeling and Diagnostics*, Chapter 3, Abacus Press, Kent, U.K., 1985.

Hoffman, S., Habisreuther, P., and Lenze, B., "Development and Assessment of Correlations for Predicting Stability Limits of Swirling Flames," *Chemical and Engineering Processing*, 33, pp. 393-400, 1992.

Kee, R.J., Rupley, F.M., and Miller, J.A., "CHEMKIN-II: A Fortran Chemical Kinetics Package for the Analysis of Gas-Phase Chemical Kinetics," *Sandia National Laboratories Report*, SAND89-8009, UC-401, March 1991.

Kee, R.J., and Lutz, A., private communication.

Kendrick, D.W., Anderson, T.J., Sowa, W.A., and Snyder, T.S., "Acoustic Sensitivities of Lean-Premixed Fuel Injectors in a Single Nozzle Rig," AMSE Paper No. 98-GT-382, 1998.

Kendrick, D.W., Bhargava, A., Colket, M.B., Sowa, W.A., Maloney, D.J., and Casleton. K.H., "NO_x Scaling Characteristics For Industrial Gas Turbine Fuel Injectors," Proceedings of ASME Turbo Expo, Paper No. 2000-GT-98, 2000.

Kreith, F., and Bohn, M., *Principles of Heat Transfer*, Harper and Row, Cambridge, U.K., 1986.

Lefebvre, A., *Gas Turbine Combustion*, Taylor and Francis Publishing, 1983.

Leonard, G., and Stegmaier, J., "Development of an Aeroderivative Gas Turbine Dry Low Emissions Combustion Systems," ASME Paper No. 93-GT-288, 1994.

Lupandin, V., Romanov, V., and Krivutsa, V., "Design, Development and Testing of a Gas Turbine Steam Injection and Water Recovery System," Proceedings of ASME Turbo Expo, 2001-GT-0111, 2001.

Maghon, H., Berenbrink, P., Termuehlen, H., Gartner, G., "Progress in NO_x and CO Emission Reduction of Gas Turbines," ASME Paper No. 90-JPGC/GT-4, 1990.

Mansour, A., Benjamin, M., Straub, D.L. and Richards, G.A, "Application of Macrolamination Technology to Lean, Premix Combustion," Proceedings of ASME Turbo Expo, Paper No. 2000-GT-0115, 2000.

Martinka, M., U.S. Patent No. 2,186,706, 1940.

Meyer, Jean-Louis, and Grienche, G., "An Experimental Study of Steam Injection in an Aeroderivative Gas Turbine," ASME Paper No. 97-GT-506, 1997.

Miyauchi, Y., Mori, Y., Yamaguchi, T., "Effect of Steam Addition on NO Formation," *Eighteenth Symposium (International) on Combustion*, The Combustion Institute, Pittsburgh, PA, 1981.

Mongia, R.K., Tomita, Eiji, Hsu, F.K., Talbot, L., Dibble, R.W., *Twenty-Sixth Symposium (International) on Combustion*, The Combustion Institute, Pittsburgh, PA, p. 2749, 1996.

Nguyen, Q.V., Edgar, B.L., Dibble, R.W., and Gulati, A., "Experimental and Numerical Comparison of Extractive and In Situ Laser Measurements of Non-Equilibrium Carbon Monoxide in Lean-Premixed Gas Combustion," *Combustion and Flame*, 100:395-406, 1995.

Peters, N. and Donnerhack, S., "Structure and Similarity of Nitric Oxide Production in Turbulent Diffusion Flames," *Eighteenth Symposium (International) on Combustion*, The Combustion Institute, Pittsburgh, PA, pp. 33-41, 1981.

Rao, A.D., "Process for Producing Power," U.S. Patent 4,829,763, May 1989.

Rao, A.D., and Joiner, J.R., "A Technical and Economic Evaluation of the Humid Air Turbine Cycle," Seventh Annual International Pittsburgh Coal Conference, September 1990.

Reynolds, W.C., "STANJAN, Interactive Computer Programs for Chemical Equilibrium Analysis," Stanford University, January 1981.

Rhine, J., and Tucker, R., "Modeling of Gas Fired Furnaces and Boilers," *British Gas*, McGraw-Hill, London. U.K., 1991.

Robson, F.L., "Phase 1: Advanced Turbine Systems Study-System Scoping and Feasibility Study," DOE Contract DE-AC21-92MC29247, United Technologies Research Center, March 1993.

Rokke, N., Hustad, J., Sonju, O., Williams, F., "Scaling of Nitric Oxide Emissions from Buoyancy-Dominated Hydrocarbon Turbulent-Jet Diffusion Flames," *Twenty-Fourth Symposium (International) on Combustion*, The Combustion Institute, Pittsburgh, PA, pp. 385-393, 1992.

Rosen, P.M., "Evaporative Gas Turbines: A Thermodynamic Evaluation of Their Potential," Report No. ISRN LUTMDN/TMVK -7010-SE, Department of Heat and Power Engineering, Lund Institute of Technology, 1993.

Rutar, T., Martin, S.M., Nicol, D.G., Malte, P.C., Pratt, D.T., ASME Gas Turbine and Aeroengine Congress, Orlando, FL, 1997.

Rutar, T., Martin, S.M., Nicol, D.G., Malte, P.C., Pratt, D.T., "Effects of Incomplete Premixing on NO_x Formation at Temperature and Pressure Conditions of LP Combustion Turbines," ASME Paper No. 97-GT-335, 1997.

Sangiovanni, J.J., Colket, M.B., Davison, W.R., Lehrach, R.P.C., Welch, E., Knight, B.A., and Snider, T.R., "Hybrid Combustion for Ultra-Low NO_x Emissions," Final Report to GRI, GRI-95/0291, November 1994.

Sayre, A., Lallemant, N., Dugue J., and Weber, R., *Twenty-Fourth Symposium (International) on Combustion*, The Combustion Institute, Pittsburgh, PA, pp. 235-242, 1994.

Snyder, T.S., Rosfjord, T.J., McVey, J.B. and Chiappetta, L.M., "Comparison of Liquid Fuel/Air Mixing and NO_x Emissions For a Tangential Entry Nozzle," *International Gas Turbine and Aeroengine Congress and Exposition*, The Hague, Netherlands, June 13-16, Paper No. 94-GT-283, 1994.

Snyder, T., Rosfjord, T., McVey, J., Hu, A., and Schlein, B., "Emission and Performance of a Lean-Premixed Gas Fuel Injection System for Aeroderivative Gas Turbine Engines," ASME Paper No. 94-GT-234, 1994.

Snyder, T.S., Rosfjord, T.J., McVey, J.B., Hu, A.S., and Schlein, B.C., "Emission and Performance of a Lean-Premixed Gas Fuel Injection System for Aeroderivative Gas Turbine Engines," Transactions of the ASME, Vol. 118, January, pp. 38-45, 1996.

Spalding, D., "The Art of Partial Modeling," *Ninth Symposium (International) on Combustion*, The Combustion Institute, Pittsburgh, pp. 833-843, 1962.

Strand, T., "Dry Low NO_x Combustion Systems Development and Operating Experience," ASME Paper No. 96-GT-274, Presented at the International Gas Turbine and Aeroengine Congress and Exhibition, June 10-13, Birmingham, U.K., 1996.

Touchton, G.L., "Influence of Gas Turbine Combustor Design and Operating Parameters on Effectiveness of NO_x Suppression by Injected Steam or Water," ASME Paper No. 84-JPGC-GT-3, 1985.

TurboPower & Marine, "Humid Air Turbine Cycle Public Report," April 1993.

TurboPower & Marine, “Phase 1: Study of Advanced Aero-Derivative Gas Turbine Power Systems,” Collaborative Advanced Gas Turbine Project, December 1993.

Turns, R., and Myhr, F., *Combustion and Flame*, 87, pp. 319, 1991.

Zeldovich, J., “The Oxidation of Nitrogen Combustion and Explosions,” *Acta Physicochimic*a, URSS, 21, p. 577, 1946.